Numerical Simulation of Landslide Impulsive Waves by WC-MPS Method

A Thesis

Submitted to the Faculty of Graduate Studies and Research

In Partial Fulfillment of the Requirements

For the Degree of

Master of Applied Science

in

Environmental System Engineering

University of Regina

By

Kun Guo

Regina, Saskatchewan

August, 2016

UNIVERSITY OF REGINA

FACULTY OF GRADUATE STUDIES AND RESEARCH

SUPERVISORY AND EXAMINING COMMITTEE

Kun Guo, candidate for the degree of Master of Applied Science in Environmental Systems Engineering**,** has presented a thesis titled, ***Numerical Simulation of Landslide Impulsive Waves by WC-MPS Method,*** in an oral examination held on July 25, 2016. The following committee members have found the thesis acceptable in form and content, and that the candidate demonstrated satisfactory knowledge of the subject material.

External Examiner:	Dr. Fanhua Zeng, Petroleum Systems Engineering
Supervisor:	Dr. Yee-Chung Jin, Environmental Systems Engineering
Committee Member:	Dr. Babak Mehran, Environmental Systems Engineering
Committee Member:	Dr. Kelvin Ng, Environmental Systems Engineering
Chair of Defense:	Dr. Abu Bockarie, Faculty of Education

ABSTRACT

Numerical simulation has been widely used and becomes a major approach for solving engineering related problems in the past few decades. Because of the flexibility, efficiency and compatibility of numerical simulation, it has been involved in various engineering and science areas. This approach is capable of interpreting the natural phenomena, and also offering an alternative way of theoretical studies and experiments.

In hydrodynamic simulations, there are two kinds of approaches have been established. The traditional mesh-based methods (e.g., finite element and finite volume method) that have been the dominant methods for decades but not capable of large deformations and fragmentations in the case of free surface flow . Another kind of the major approaches, the mesh-free methods, according to which variables are assigned to particles instead of mesh, are applied to solve both the problems of mash distortion for flowing mesh and the problems of unclear interface for fixed mesh. Mesh-free methods provide a physical system for hydrodynamic problems, and also the effectiveness of this kind of method has been validated/confirmed in many applications. Therefore the mesh-free methods have become a robust tool in the studies on fluid mechanics

In this research, the weakly-compressible moving particle semi-implicit (WC-MPS) method, which is modified and improved by Shakibaeinia and Jin (2010), is applied to simulate the impulse waves generated by landslide. During this study, the complete theory of the WC-MPS model was applied/adopted. The model was modified to simulate the impulse wave for the different landslide cases. This study includes the simulations for the submerged and un-submerged landslide cases, the introduction of different sliding

bed slopes, and also a firsthand comparison between WC-MPS simulation and experiment. After comparing WC-MPS simulation with experimental results for different cases, the applicability of WC-MPS method in simulating the impulse wave generated in/from landslide is confirmed at the end of this study.

WC-MPS is a relatively new process of simulating hydrodynamic problems. However, the developed mesh-free particle method is capable of simulating complex incompressible fluid flow problems characterized by large deformations and fragmentations of boundaries and interfaces. In this thesis, WC-MPS method is used to simulate impulse waves generated by landslides. First, the simulation results are generally compared with previously published papers by other researchers, and then detailed simulation results about the shape of wave, and water velocity around the sliding wedge are compared with an experiment. Based on this study, the WC-MPS method is found to be able to provide a stable and accurate result for the simulation of the impulse wave.

ACKNOWLEDGEMENTS

The author would like to express his sincerest appreciation to his supervisor, Dr. Yee-Chung Jin, for his guidance throughout the whole process of the author's Master program. The advice, encouragement, and financial support from Dr. Yee-Chung Jin are of great importance to the author's research in the last few years. Without the supervision of Dr. Jin, it was impossible for the author to implement this research.

The author would also acknowledge the financial support from the Faculty of Graduate Studies and Research of the University of Regina in the form of Graduate Scholarships.

DEDICATION

I dedicate this thesis to my beloved family and best friends. A special feeling gratitude to my parents, Yuning Song and Runxiang Guo, for all the things they have done for me. Also this thesis dedicated to my wife Shurui Xue, who has been a great source of motivation and inspiration during my tough time, thank you for always being by my side.

A sincere thanks to all the people who encouraged and supported me during my study. I will never let you down.

TABLE OF CONTENT

LIST OF FIGURES

LIST OF TABLES

LIST OF SYMBOLS

C_0 = sound speed in the reference medium

C = the Courant number

C_v = volume concentration of solid materials in water-clay or water-kaolinite mixtures

d = number of dimensions

fi = real value of a physical property i

$\langle f \rangle_i$ = smoothed value of a physical property possessing by particle i

g = gravitational acceleration

$G(r)$ = Gaussian function

H = initial water depth

i = particle i

j = particle j

$k(y)$ = the time step to add inflow particles

K = a constant parameter with the dimension of time in the Cross equation

L = the length of the mixture column in the dam-break problem

M = constant mass of each particle

M_j = mass of the surrounding particle j

n = normalization factor which is used to conserve the physical property in MPS

n_0 = initial particle number density

n^*= temporary particle number density

n'= correction term of the particle number density

$\langle n \rangle_i$ = particle number density (dimensionless)

$\langle n^* \rangle_i$ = particle number density at particle i

N = total number of particles

$\langle N \rangle_i$ = the numbers of particles in a unit volume

p_i = pressure possessing by particle i

p_i^{n+1} = pressure possessing by particle i at the next time step

p_j = pressure possessing by particle j

R_{ij}, or R = the distance between particle i and j

r_e = interaction radius

$\vec{r_i}$ = the position of particle i

$\vec{r_j}$= the position of particle j

T = dimensionless time

u = velocity vector

$u(y)$ = inflow velocity at depth y

u_i = velocity possessing by particle

u_j = velocity possessing by particle

u_n = velocity at current time step

u_{n+1} = velocity at the next time step

u^* = predicted velocity

u' = velocity correction term

x = distance along x axis

x' = dimensionless run-out distance referenced from the initial

$\langle \nabla u \rangle$ = divergence of velocity

$\langle \nabla^2 u \rangle$ = Laplacian of velocity

$U_{average}$ = average flow velocity

$|u|_{max}$ = the maximum flow velocity

$W(R_{ij}, r_e)$ = kernel function (or kernel function, weighting function)

ε = stress tensor

β = threshold coefficient for recognizing free surface particles

$\delta(R_{ij})$ = delta function

Δij = the second invariant of the deformation strain

Δt = time increment

$\Delta\phi_i$ = net change of a physical property at particle i

$\Delta\phi_{i\rightarrow j}$ = diffusion of a physical property from a particle i to its neighbor particle j

$\Delta\phi_{j\rightarrow i}$ = diffusion of a physical property from the neighbor particle j to particle i

Δl = average particle distance, or average particle size

$\Delta\sigma^2$ = variance increase

μ = dynamic viscosity

μ_{eff} = effective viscosity

μ_B= Bingham yield viscosity

μ_0= viscosity at very low shear rates

μ_∞= viscosity at very high shear rates

v = kinematic viscosity

ρ = fluid density

ρ^* = temporary fluid density

ρ' = fluid density correction term

$<\rho>_i$ = fluid density

τ = shear stress

τ_B = Bingham yield stress

ϕ_i = a physical property possessing by a particle i

$<\nabla f>_i$ = the smoothed value of the divergence of a vector $\boldsymbol{fi}$

∇p = pressure gradient

$\nabla \tau$ = divergence of the shear stress term

$\nabla \phi_{ij}$ = the gradient of a property ϕ between particle and particle j

$<\phi>_i$ = the smoothed value of a physical property

$<\nabla \phi>_i$ = the smoothed value of the gradient of a physical property

$<\nabla^2 \phi>_i$ = the Laplacian of a physical property ϕ

CHAPTER 1 INTRODUCTION OF MPS METHOD

1.1 Background

The advancement of computers shows a significant effect on the development of engineering and science. Among all the numerical methods, the major approach to solve fluid flow problems is computational fluid mechanics (CFD). The main feature of numerical method is to describe the physical problem into a discrete form of the mathematical description and solve the problem using computational techniques (Liu & Liu, 2003). With numerical methods, all the details of the problems can be considered at the same time, without the general procedures required in analytical approaches such as assumptions and approximations in mathematical description of the physical phenomena. Comparing to experimental methods, the numerical methods show their advantage in flexibility. Numerical methods are able to provide an alternative and reliable study on physical phenomena without conducting expensive and time-consuming laboratory and field measurements. On the other hand, since numerical methods also provide the knowledge that cannot be obtained directly with other methods, numerical simulations can provide assistance to interpret the phenomena and offer an alternative way to insightfully study the theories or experiments.

After the development of numerical methods, mesh-based methods have been mainly used to simulate fluid flows, such as finite element and finite volume methods. Due to the problem with mesh adaptability and connectivity, the application of the mesh-based methods for complicated phenomena is limited by the existence of large deformations and fragmentations of the boundaries and interfaces. However, large deformations and

fragmentations are common features in fluid flow problems including those related to free-surface flows, and as a result they cannot be avoided. Therefore, researchers developed numerical techniques for tracking and locating the free-surface and the interfaces, such as the marker-and-cell (MAC) method (Harlow & Welth, 1965) and volume-of-fluid (VOF) method (Hirt & Nicols, 1981), in order to make the mesh-based method capable of simulation of interfacial deformations. In the applications, it is found that the main problems of using such methods are the maintenance of sharp or fragmented interfaces (Liu, et al, 2005), and the cells containing the free surface that need complicated treatments (Koshizuka et al, 1998). Furthermore, the problem of numerical diffusion is unavoidable (Koshizuka et al, 1998; Gotoh & Sakai, 2005; Shao & Edmond, 2003) using these methods.

In order to solve this problem, in recent years, people developed a new generation of numerical simulation method, the mesh-free particle (Lagrangian approach) methods. These methods represent the fluid domain by a set of particles moving in the Lagrangian system. The equation of the physical system is expressed with mass, momentum and energy conservation, and each particle possesses a set of field variables such as mass and momentum (Liu and Liu 2003). Since no specific procedure for capturing or tracking of interfaces (e.g. free surface) is needed, and the position of fluid in the application of this method is presented by the particles, these methods are able to simulate the boundary and interface. The advantages of mesh-free Lagrangian methods comparing to mesh-based methods can be summarized as:

- The concise description of large deformations and fragmentations of the free surface,

- No specific procedure forcapturing or tracking of the free surface,
- No problems related to mesh treatments or deformations
- Simplicity of implementation of the computations,

Among all the particle methods, the Smooth Particle Hydrodynamics (SPH) method is one of the earliest and most applied method (Lucy 1977; Gingold & Monaghan 1977), which was originally developed for astrophysical problems and later was extended to solid and fluid mechanics applications (e.g. Monaghan, 1994, 1995, 2005; Dalrymple & Rogers 2006; Lee et al. 2008). The Moving Particle Semi-Implicit (MPS) method (Koshizuka & Oka, 1996) is another particle method originally developed for fluid mechanics applications. In MPS, the spatial gradients and Laplacians are calculated by the weighted averaging of gradients or Laplacians of a physical quantity between the particle of interest and its neighboring particles. The contributions of each particle to a quantity are weighted by kernel function according to their distance from the particle of interest.

1.2 Procedure of Numerical Simulation

Free surface and interfacial flows can be easily found in natural and man-made structures, such as flow in rivers, wave breaking in coastal areas, and flow through hydraulic structures. Some basic insights of free flow can be provided with the applications of theoretical approaches and simple assumptions. Through experimental studies, some detailed information can be provided, but high costs and time consuming would become new issues. Numerical methods provide a strong tool for undertaking a detailed analysis of fluid flow problems including free surface.

All CFD share a similar solution pattern. The standard solution algorithm of numerical simulations can be briefly explained as a flow chart in Figure 1-1. A typical numerical simulation of a computational fluid mechanics problem (CFD) involves:

- Governing equations to mathematically describe the physical problem.
- Boundary conditions and/or initial conditions to define a solution domain.
- Domain discretization technique.
- Numerical discretization technique to turn the partial differential equation (PDE) of the governing equations into the algebraic equations or the ordinary differential equations (ODE).
- Numerical technique to solve the resultant equations.

The physical problem or phenomenon is translated into mathematical representations with certain assumptions and simplifications. These mathematical representations are usually expressed as governing equations accompanied with appropriate boundary conditions (BC) and/or initial conditions (IC). The governing equations are typically a set of ordinary differential equations (ODE), or partial differential equations (PDE). Integration equations and other possible forms of representations of the physical laws are common as well. The boundary conditions and initial condition are defined based on the nature of the problem and the region and time period for which the problem must be solved. According to the technique used for the domain discretization the numerical method can be divided into two classes of mesh-based and mesh-free methods.

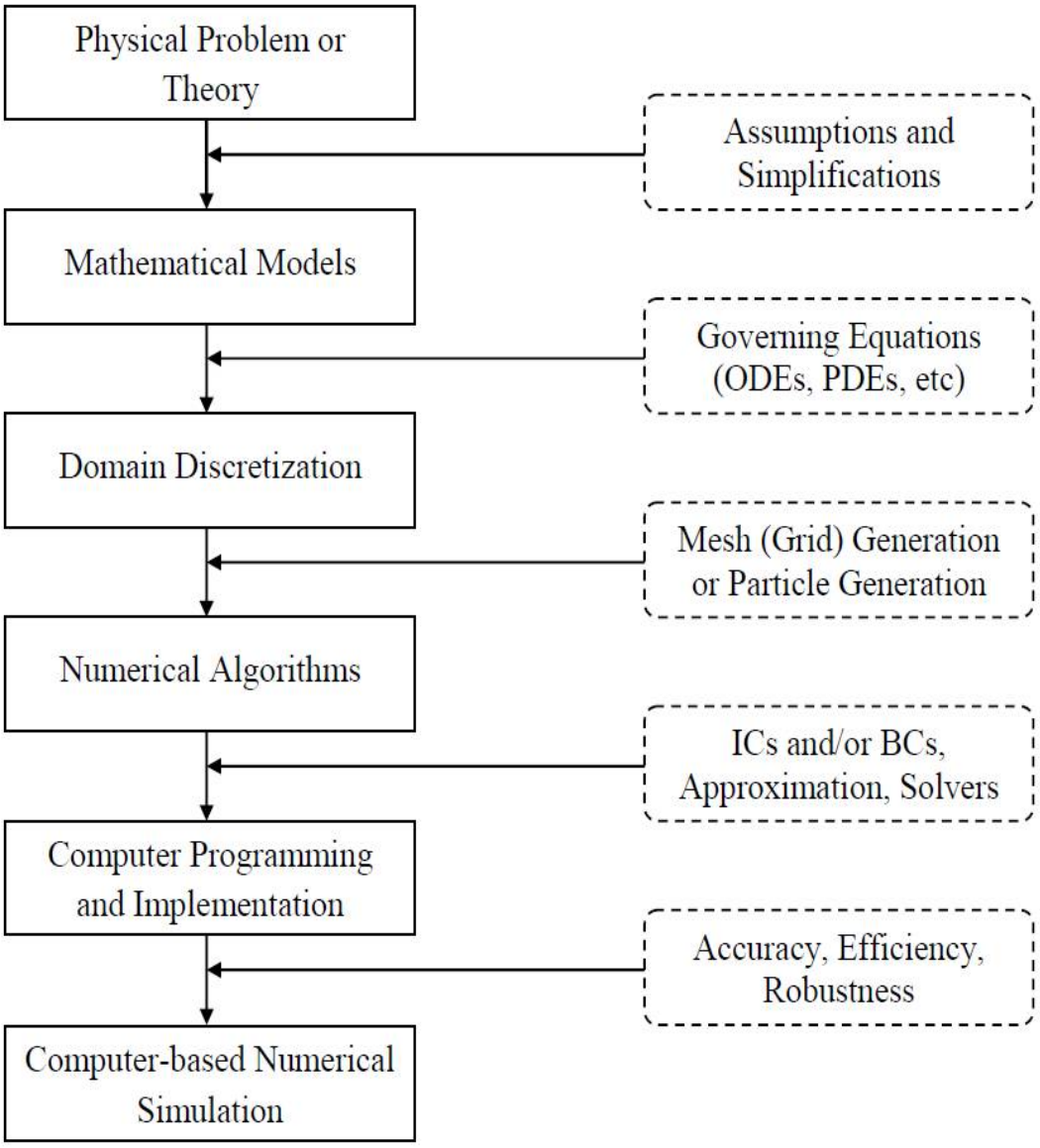

Figure 1-1. Standard solution pattern of numerical simulation (Liu & Liu, 2003)

1.3 Mesh-based Method

Mesh-based method (grid-based method) uses a mesh (grid) system (stationary or adaptive) to represent the domain and to record the field variables, which usually consists a lattice of node points, or grid nodes to represent the geometry of the domain. Field variables are evaluated at these nodes and their relations are determined by some function relationships, these function relationships are called nodal connectivity as well (Liu and Liu, 2003). There are three typical mesh-based methods: The Finite element method (FEM), finite difference method (FDM) and finite volume method (FVM).

Mesh-based methods can be categorized into three groups:

1. Lagrangian mesh-based methods:

The mesh is fixed or attached to the material in the entire computation process and therefore it can move with the material. Since the nodes follow the path of the material, the mesh cells may expand, compress and deform according to the relative movement of the connecting nodes. These methods have the advantages of simpler and faster, because there has no convective terms in the equations; with these methods, it is easy to track the boundaries and interfaces since some of the nods can be placed along with the boundaries and interfaces.

2. Eulerian mesh-based methods:

In the Eulerian mesh-based methods, materials are located and move across the fixed mesh cells, and the nodes remain stationary when the material is moving across the cells during the simulation. During the process of the simulation, the size and shape of the cells remain unchanged in the case of material deformations. Because of this, the Eulerian mesh-based methods can be applied for mesh deformations.

Therefore, these methods are more popular in the computational fluid dynamics (CFD) studies, in which the flow of the fluid dominates. Eulerian mesh-based methods can be applied to deal with the fluid flow problems, but they still have the disadvantages of tracking boundaries and interfaces, and as a result numerical diffusion arising from the advection term is unavoidable (Koshizuka etal, 1998; Gotoh & Sakai, 2005); besides, the methods can only provide the history of variables on the mesh points. Sometimes additional mathematical processes will be introduced to create geometry, such as the marker-and-cell (MAC) method (Harlow & Welth, 1965) and volume-of-fluid (VOF) method (Hirt & Nicols, 1981). On the other hand, the main difficulty in using such methods is the maintenance of sharp or fragmented interfaces (Liu et al, 2005), and the cells containing the free surface need complicated treatments as well (Koshizuka et al, 1998).

3. Combined Eulerian and Lagrangian methods:

There are two approaches of combined Eulerian and Lagrangian methods: the Coupled Eulerian Lagrangian (CEL) (Hans, 1999) and Arbitrary Lagrangian Eulerian (ALE) (Hirt et al, 1974; Benson, 1992). Both approaches are able to track the boundaries and interfaces, but it should be noticed: even with CEL and ALE approaches, the highly distorted mesh can still introduce a severe error in numerical simulations (Hirt et al., 1974; Benson, 1992).

Table 1-1 shows the comparison of Lagrangian and Eulerian methods, and after the development of mesh-based methods, there are still some difficulties in the applications. In hydrodynamic simulations, the mesh-based methods will fail in explosion and high velocity impact problems due to large deformation and fragmentation, highly deformable

boundaries and free surfaces (Liu and Liu 2003).

Table 1-1. Comparison of Lagrangrian and Eulerian Methods

Feature	**Lagrangian Methods**	**Eulerian Methods**
Mesh	Attached to materials	Stationary
Boundaries and Interfaces	Easy	Difficult
Large Deformations	Difficult	Easy
Irregular Geometry	Easy	Difficult

1.4 Mesh-free Methods

Mesh-free methods, comparing to traditional mesh-based methods, have the advantage of simulating hydraulic problems with large deformations and fragmentations on boundaries and interfaces. The problem domain or geometry is represented by arbitrary distributed node points (or particles), rather than the nodes and the mesh in mesh-based methods. In the study by Liu and Liu (2003), they stated that 'Mesh-free methods aim to provide an accurate and stable numerical solution for integral or PDEs with all kinds of possible boundary conditions using a set of arbitrary distributed nodes (or particles) without using any connective mesh' (Liu and Liu, 2003). There are many mesh-free methods, such as Smoothed Particle Hydrodynamics (SPH), Finite Point Method (FPM), Element Free Galerkin Method (EFG), Free Mesh Method (FMM), Moving Particle Semi-implicit Method (MPS), Point Interpolation Method (PIM),

Mesh-free Weak-strong Form (MWS), and Least Squares Mesh-free Method (LSM). Table 1-2 shows the different approximation methods for these mesh-free methods.

Table 1-2. Typical Mesh-free Methods

Methods	Methods of Approximation	References
Smoothed Particle Hydrodynamics (SPH)	Integral representation	Lucy, 1977; Gingold and Monaghan, 1977
Finite Point Method (FPM)	Finite difference representation	Liszka and Orkisz, 1980
Element Free Galerkin Method (EFG)	Moving least square (MLS) approximation Galerkin method	Belytschko et al., 1994, 1996
Moving Particle Semi-implicit Method (MPS)	Finite difference representation	Koshizuka et al., 1995; Koshizuka and Oka, 1996
Free Mesh Method (FMM)	Galerkin method	Yagawa and Yamada, 1996, 1998
Point Interpolation Method (PIM)	Point interpolation, Galerkin method, Petrov-Galerkin method	Liu and Gu, 1999; Wang and Liu, 2000; Gu and Liu, 2001;
Meshfree Weak-strong Form (MWS)	MLS, PIM, Radial PIM, Collocation plus petrov-Galerkin	Liu and Gu, 2002, 2003
Least Square Meshfree Method (LSM)	Moving least square approximation	Kwon et al., 2003

1.5 Mesh-free Particle Methods

According to Mesh-free particle methods (MPM) finite discrete particles is implemented to represent the simulation domain. In mesh-free particle methods, each particle represents either a discrete physical object, or a portion of a continuum domain.

These particles represent the elements of the system and are able to record the state and motion of the system (Liu & Liu, 2003). Particle size can be ranged from the nano scales (extremely small) to the macro, or astronomical scales. Table 1-3 presents some of the major types of mesh-free particle methods.

Comparing to mesh-based methods, mesh-free particle methods have some major advantages. First of all, mesh-free particle methods are based on particles instead of meshes. Hence, there is no requirement of meshes during the simulation process, and the problems of mesh generation and treatment are avoided by the method, which will make the simulation more efficiently. Also because of the particles, deformations and fragmentations can be simulated conveniently. Last but not least, based on the method, the Lagrangian nature is the elimination of convectional terms in governing equations, and thus the numerical diffusion problem is prevented.

Molecular dynamics (MD),as the oldest MPM, was developed by Alder and Wainright (1957) to model the motion of atoms and molecules. The motion of atoms and molecules are defined according to the theoretical physics in the late 1950s, by numerically solving the Newton's equations of motion for interacting particles. It is still wildly used in material science and bio-molecular theories.

Table 1-3. Major Types of Mesh-free Particle Methods (Xie, 2013)

Methods	Scale	References
Molecular Dynamics (MD)	Atomistic	Alder and Wainwright, 1957; Rahman, 1964.
Particle-in-cell Method (PIC)	Macroscopic.	Harlow, 1963; 1964.
Marker-and-Cell (MAC)	Macroscopic	Harlow, 1965
Smoothed Particle Hydrodynamics (SPH)	Macroscopic	Lucy, 1977; Gingold and Monaghan, 1977.
Dissipative Particle Dynamics (DPD)	Mesoscopic	Hoogerburgge and Koelman, 1992.
Discrete Element Method (DEM)	Macroscopic	Cundall, 1987; Owen, 1996.
Moving Particle Semi-implicit Method (MPS)	Macroscopic	Koshizuka et al., 1995; Koshizuka and Oka, 1996
Direct Simulation Monte Carlo Method (DSMC)	Atomistic	Bird, 1994; Pan et al., 1999; 2000; 2002
Lattice Boltzmann Equation (LBE)	Atomistic	Chen and Doolen, 1998; Qian et al., 2000.

Harlow (1963) developed the particle-in-cell (PIC) method, which combined both Eulerian frame and Lagrangian frame. In this method, the movement of particles or fluid elements is defined in a Lagrangian frame and tracked in a continuous phase while properties such as density and currents are calculated simultaneously at Eulerian mesh nodes.

After the particle-in-cell (PIC) method, Harlow introduced the marker-and-cell (MAC) method, which is widely used in computer graphics to model fluid flows. With this method, the velocity field is periodically calculated and marker particles move according to the velocity field to track the flow of the fluid.

Lucy (1977), Gingold and Monaghan (1977) introduced and developed the smoothed particle hydrodynamics (SPH) to address astrophysical problems. This mesh-free Lagrangian method has been widely used in many areas of science such as astrophysics (Monaghan, 1992; Frederic & James, 1999; Monaghan & Lattanzio, 1991; Berczik & Kolesnik, 1993), fluid simulation (Swegle, 1992; Monaghan, 1994; Morris et al., 1997; Colagrossi & Landrini, 2003; Gotoh et al., 2004; Dalrymple & Rogers, 2006; Lee et al., 2008) and solid mechanics (Libersky & Petschek, 1990; Dyka et al., 1997; Randles & Libersky, 2000; Bonet & Kulasegaram, 2000). The SPH was originally developed for astrophysical problems in three dimensional (3D) open spaces owing to the similarities between the movements of the astrophysical particles and the liquid or the gas flow. Therefore, the astrophysical problems can be simulated with the classical Newtonian hydrodynamics. Since then, the SPH had been widely used in various areas of astrophysics, such as modeling of binary stars and stellar collisions (Benz, 1988;

Monaghan 1992; Frederic et al., 1999), collapse and formation of galaxies (Monaghan and Lattanzio, 1991; Berczik and Kolesnik, 1993; Berczik, 2000), supernova (Hultman and Pharayn, 1999) and even the evolution of universe (Monaghan, 1990). However, it was not until the 1990s had the SPH been applied to fluid mechanics (Swegle, 1992; Monaghan, 1994). Since then the application of SPH in fluid mechanic problems had been mushroomed, especially for flow problems with free surfaces (Monaghan, 1994; Morris et al., 1997; Colagrossi and Landrini, 2003; Gotoh et al., 2004; Dalrymple and Rogers, 2006; Lee et al. 2008).

Dissipative particle dynamics (DPD) proposed by Hoogerbrugge and Koelman (1992) is a stochastic simulation to model fluid flows. It aims at solving the hydrodynamic time and space scale problems beyond the capacity of the Molecular Dynamic (MD) method, by modeling the change of dynamics and rheological property of fluids.

Discrete element method (DEM) (or distinct element method) has been developed for simulating the movement and effect of a significant number of small particles by Cundall (1987) and Owen (1996). Although DEM is very similar to molecular dynamics (MD) method, but its applicability in simulating both rotational degrees-of-freedom and complicated geometries is prominent comparing to MD method.

Moving particle semi-implicit method is another Lagrangian approach, which is developed by Koshizuka and Oka (1996) for incompressible free surface flows. One of the similarities of the MPS method to the SPH method is that they both rely on integral interpolations to approximate partial differential equations (PDEs). However, the MPS

method employs a simplified differential operator model for the approximation, while SPH method introduces the gradient of a kernel function. MPS methods have been applied in a wide range of engineering branches such as coastal engineering (Gotoh et al., 2005; Gotoh & Sakai, 2006), environmental engineering (Shakibaeina & Jin, 2009), ocean engineering (Shibata & Koshizuka, 2007; Sueyoshi et al., 2008), structural engineering (Chikazawa et al., 2001), mechanical engineering (Heo, 2002; Sun et al., 2009), bioengineering (Tsubota et al., 2006) and chemical engineering (Sun et al., 2009).

The MPS method is more intuitive and much simpler than SPH to apply. The Current study is focused on the MPS method, and more detailed introductions to MPS and MPS applications are included in the following chapters.

1.6 Scope of the Thesis

As mentioned previously, it has been proved that mesh-free particle method is a robust tool in numerical simulations. There is a significant amount of studies in the past decades, which focus on the applications of mesh-free particle methods to engineering problems, and based on these studies, it is confirmed that mesh-free particle methods have the capability of dealing with CFD problems and related areas.

This study is based on the weakly-compressible moving particle semi-implicit (WC-MPS) method. The original MPS method is proposed by Koshizuka et al. (1995) to study free surface flow problems. The WC-MPS method is modified and improved by Shakibaeinia and Jin (2010). The objective of this thesis is to investigate the impulse wave in landslide by simulating with the WC-MPS method.

Although many numerical studies have been conducted and verified with experimental data on the waves, there has been a lack of investigations on the flow fields. Specifically, the velocity distributions are not obtained due to the difficulty in measuring the unsteady flow field. In order to study the flow field around the sliding block, a Digital Particle Image Velocimetry (DPIV) system is used to capture the water surface profile and velocity distribution (Willert and Gharib 1991, Chen et al., 2013) by using the PIV lab software. The numerical model of this study is based on the WC-MPS.

The aim of this study is to examine the capabilities of the WC-MPS method in simulating the impulse wave caused by sliding structures, including the shape and the height of the wave, and also the velocity and pressure field around the structures.

1.7 Structure of the Thesis

The structure of this thesis can be divided into the following parts:

- An introduction to MPS fundamentals, which explains the theory of the MPS method.
- Discussion of the governing equations in fluid mechanics, and the concept of the WC-MPS method and its application to free-surface flow problems.
- Case study of different types of landslide problems with the WC-MPS method. The results derived with the WC-MPS method are compared with those derived with other numerical simulation methods.
- Simulation of impulse wave generated by landslide with the WC-MPS method. Comparison between the detailed simulation results and the experimental results is made

- A brief conclusion of the proposed study and also recommendations for future works.

CHAPTER 2 FUNDAMENTAL OF MPS

This chapter includes an introduction of the moving particle semi-implicit (MPS) method, a discussion of the improvements and modifications of the MPS method, an explanation of the concept and mathematical fundamentals of the MPS method, and comparison of the discrepancies between the MPS method and SPH method.

2.1 Introduction of Moving Particle Semi-implicit (MPS) Method

The moving particle semi-implicit (MPS) method is a macroscopic, deterministic mesh free particle (Lagrangian) method first developed by Koshizuka & Oka (1995 & 1996) for simulations of incompressible free-surface viscous flows. The method introduces the weighted averaging process to approximate derivatives of a field variable. Through the past years, the MPS method has been applied in a wide range of applied mechanics applications including Nuclear Engineering (e.g., Koshizuka et al., 1999; Xie et al., 2005), Coastal Engineering (e.g., Gotoh et al., 2005; Gotoh and Sakai, 2006), Hydraulics (e.g., Shakibaeina & Jin, 2009, 2010 & 2011), Ocean Engineering (Shibata & Koshizuka, 2007; Sueyoshi et al., 2008), Mechanical Engineering (e.g., Heo et al., 2002; Sun et al., 2009), Bioengineering (e.g., Tsubota et al., 2006) and Chemical Engineering (e.g., Sun et al., 2009). The successful major achievement of MPS methods is the introduction of more accurately modeling to CFD problems with large deformation and fragmentation.

2.2 Improvements and Modifications of MPS

The MPS method was first proposed by Koshizuka et al. in 1995, and used to simulate incompressible viscous flow. In the research, the collapse of a fluid column is analyzed using the MPS method. The calculation result is compared with an experimental result, and shows a good agreement, which means the success of the MPS method.

In 1999, Koshizuka et al. again, used the MPS method to analyse the breaking waves, where the semi-implicit algorithm is used to calculate a two-dement ion, incompressible, and non-viscous flow. In their research, two types of breaking waves, plunging and spilling breakers, are simulated in a tank with a piston on one side to generate waves and a slope on another side, and both generate good results. Also in this research, breaking waves with passive moving float is calculated. This research states that the MPS method is applicable to simulate incompressible flow, and it can be used to simulate fluid-structure interaction as well.

In 2001, Heo et al. did the simulation study on growth of bubble in the transient pool boiling with the application of Moving Particle semi-implicit with mesh-less advection using flow-directional local grid (MPS-MAFL) method. The results give a clear process of the bubble generation in each time step under the high heat flux and shows that the MPS-MAFL method is well-estimates the void fraction under the high heat flux condition.

In 2004, the MPS method was used to analyze the jet breakup in two-dimension incompressible flows by Shibata et al. (2004). In this study, effects of the Weber number and the Froude number on the jet breakup length agrees with the experiment, and The

size distribution of droplets after the breakup agrees with the experiment as well. This study shows a specific advantage of the MPS method: it is free from grid distortion, while the effects from surface tension are still considered.

Ataie-Ashitiani and Farhadi (2005) introduced Euler's equation into the MPS method as the governing equation instead of Navier-Stokes equation to get a stable MPS method of simulating incompressible and inviscid flows. Six kernel functions have been used in total in this research in order to improve the stability of the MPS method. The group studied collapse of water column case conducted by Koshizuka in 1996, and solved the instability problem in Koshizuka's simulation. By applying Euler's equation as the governing equation, the simulation can be stabilized until the water loses momentum. However, Euler's equation is based on the ideal flow, which has no viscosity, and this method can be only used to simulate non-viscosity flows.

In 2006, Harada et al. simulated the drop generation in micro flow. In this case, the original time step of theMPS method is divided into semi-time steps since the extremely high surface tension. From the research, semi-time step helps the simulation become stable and the calculation of droplet size, pitch, and production rate give good results comparing with the experiments.

Also in the year 2006, Wang et al. combined the/a 2D MPS method with fractional Brownian motion (fBm) to generate a 3D model. In their study, they simulated breaking waves by using the MPS method to generate a slice of wave, and then expanded it to 3D by giving motion variation using fBm.

In 2009, Shakibaeinia and Jin replaced the original MPS method with a weakly compressible MPS method. This development increased the efficiency and accuracy of the method and also made the MPS method applicable in the case of open-boundary free surface flow simulation by adding inflow and outflow into the original method. In this study, dam-break, elliptical water bubble, and hydraulic jump formation and free surface open-boundary problems are used to test the feasibility of this new method, and the results shows that the method can be applied to simulate both open-boundary and viscous flows.

In 2010, Park and Jeun (2010) coupled the MPS method with rigid body dynamics, and made the simulation of isothermal multi-phase fluid become feasible. They simulated the collapse of water column and isothermal plunging water jet into a denser fluid pool. The results of their study shows that the coupled method can be used to analyze isothermal multi-phase fluid problems, and it can also increase the stability of simulating single-phase incompressible flows.

In 2011, Sahebari et al. applied the MPS method to simulate the flow over sills. In the research, both sub and supercritical flows are simulated in a rectangular open-boundary channel. The numerical results are compared with experimental results, and show the high similarity.

Also in 2011, Fu and Jin published a paper about modeling flow around a cylinder, in this study, they tested both lower and higher Reynolds number flows around a cylinder and the added the roughness to the wall boundary by adding ghost particles near the wall boundary.

The computational results without adding wall roughness are compared with the results by applying the Volume Finite Method (VFM), and show a good agreement. This study confirmed that the MPS method can be used to simulate both laminar flow and turbulent flow.

Through the past decades, a considerable amount of studies focusing on the improvement of the accuracy and performance of the MPS method have been done by different groups of researchers. These studies proved that MPS is a reliable method in simulating different kinds of fluid flows with or without large deformations and fragmentations.

2.3 MPS Fundamentals

2.3.1 MPS Interpolation

In MPS, the interaction inside the real physical system is represented by the interaction between discrete particles. In this interaction, each discrete particle affects other particles in its vicinity according to a specialized weight function. During the progress, particle properties such as velocity and pressure will be calculated based on those of the neighboring particles. The magnitude of influence between particles is calculated according to a weight function, which is called kernel function. The kernel function is considered to be a smoothing function of physical quantities of the particles, which has an inverse relation with the distance between two particles.

As it is shown in Figure 2-1 and Figure 2-2, The particle *i*, interacts with other particles in its vicinity, *j*, covered with a kernel (weight) function $W(r_{ij}, r_e)$, where $r_{ij}=|\boldsymbol{r}_j \boldsymbol{r}_i|$

is the distance between particle *i* and *j* and *re* is the radius of the interaction area around each particle. The kernel function is considered to be a smoothing function of physical quantities around the particles. A particle interacts with a finite number of adjacent particles located within a distance of *re*.

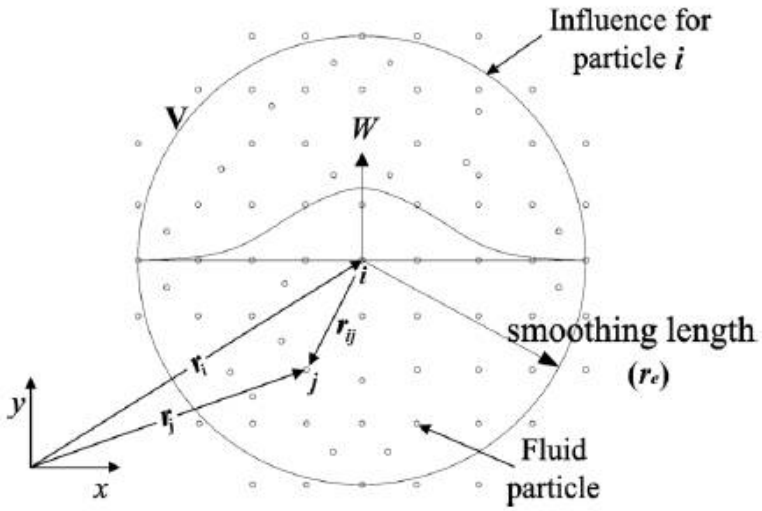

Figure 2-1. Particle Interaction and Kernel Function

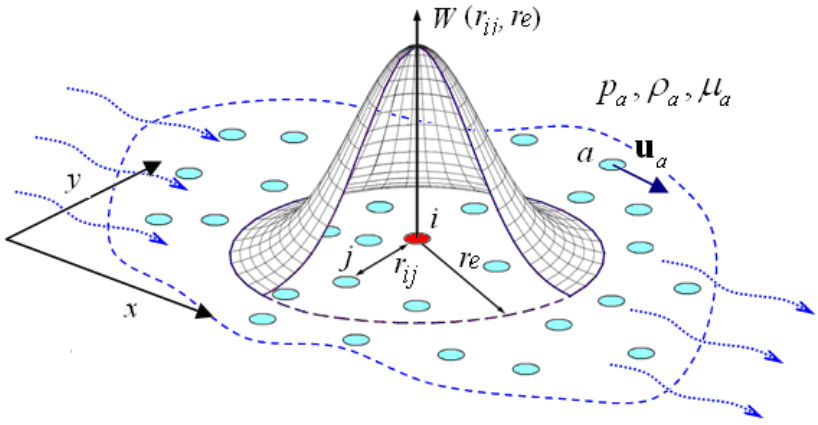

Figure 2-2. Kernel Function in MPS

In MPS, the kernel function is introduced to calculate the smoothed physical properties of each particle by certain particles around it. The smoothed physical property $<\phi>i$ of a certain particle i (i possesses the physical value of ϕi) at coordinate $\boldsymbol{r}i$ will be computed from those of its surrounding particles by

$$\langle\phi\rangle_i = \frac{\sum_{j\neq i}\left(\phi_j W(r_{ij},r_e)\right)}{\sum_{j\neq i} W(r_{ij},r_e)} \tag{2.1}$$

where ϕi is the property possessed by the surrounding particles and itself. In general, the smoothed value $<\phi>i$ of the particle i at coordinate $\boldsymbol{r}i$ is not necessarily the same as its physical property ϕi, or in other words, $<\phi>i$ is the approximation of ϕi. $<\phi>i = \phi i$ only exists as a special case when the kernel function is delta function (Koshizuka et al. 1995). It is obvious that the interaction radius re will determine the size of the neighboring area, and no doubt the numbers of particles will be interacting with a certain particle (or the particle of interest).

To describe the density of particles around a specific particle, Koshizuka et al. (1995) introduced particle number density as a dimensionless parameter defined as

$$\langle n\rangle_i = \sum_{j\neq i} W\left(r_{ij}, r_e\right) \tag{2.2}$$

Therefore, the interpolation of the physical property ϕ can be rewritten as

$$\langle\phi\rangle_i = \frac{1}{\langle n_i\rangle}\sum_{j\neq i}\left(\phi_j\, W\left(r_{ij}, r_e\right)\right) \tag{2.3}$$

The real fluid density ρ can be smoothed as

$$\langle\rho\rangle_i = \frac{\sum_{j\neq i} m_j\, W(r_{ij},r_e)}{\int_v W(r_{ij},r_e)dv} \tag{2.4}$$

where *Mj* is the mass of the neighboring particles *j*, and *dv* is the volume of interaction around particle *i*. The denominator in equation 2.3 indicates the integral of the kernel function within the whole volume. If all the processing particles share the same amount of mass, the smoothed value of fluid density can be simplified as

$$\langle \rho \rangle_i = \frac{m\langle n \rangle_i}{\int_v W(r_{ij}, r_e) dv} \tag{2.5}$$

where *m* is the constant value of mass of each particle.

2.3.2 Kernel Functions

The kernel function is used to measure the influence of the neighboring particles and approximate (or smooth) the physical properties of the particle of interest. Different kernel functions have different kernel effects on the properties of particles. In the MPS methods, two types of kernel functions are mostly used. The first one is the second-order polynomial bell-shaped kernel function, and the second one is the rational kernel function. Both kernel functions are shown in Equation 2.6 and 2.7.

$$W(r_{ij}, r_e) = \begin{cases} 2 - \left(2\frac{r_{ij}}{r_e}\right) & 0 \le \frac{r_{ij}}{r_e} \le \frac{1}{2} \\ \left(2\frac{r_{ij}}{r_e} - 2\right)^2 & \frac{1}{2} \le \frac{r_{ij}}{r_e} \le 1 \\ 0 & \frac{ij}{r_e} \ge 1 \end{cases} \tag{2.6}$$

$$W(r_{ij}, r_e) = \begin{cases} \frac{r_e}{r_{ij}} - 1 & 0 \le \frac{r_{ij}}{r_e} \le 1 \\ 0 & \frac{r_{ij}}{r_e} \ge 1 \end{cases} \tag{2.7}$$

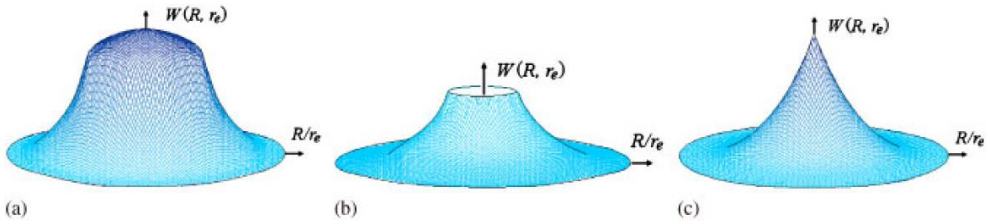

Figure 2-3. Kernel Functions: (a) the/a second-order polynomial bell-shaped kernel; (b) the/a rational kernel; (c) the/a third-order polynomial spiky kernel.

In addition, Atatie-Ashtiani and Farhadi (2006) studied another six different kernel functions, from different researchers. These six kernel functions also can be generally summarized in to two groups: bell-shaped kernel and rational kernel. Table 2-1 shows the kernel functions studied by Atatie-Ashtiani and Farhadi.

In MPS applications, using the bell-shaped kernel function leads to particle clustering, because two particles approach so close to each other that repulsive force does not increase sufficiently to avoid their clustering. The rational kernel function solves this problem by increasing repulsive force to infinity when two particles are too close, but the infinity value for particle distance of zero can lead to instability in the model even if just two particles approach too close. Therefore, Shakibaeinia & Jin (2010) developed a third-order polynomial spiky kernel function, which is defined as

$$W(r_{ij}, r_e) = \begin{cases} \left(1 - \frac{r_{ij}}{r_e}\right)^3 & 0 \le \frac{r_{ij}}{r_e} < 1 \\ 0 & \frac{r_{ij}}{r_e} \ge 1 \end{cases} \tag{2.8}$$

This kernel function solves the problems mentioned above: when two particles approach each other, the function value and hence the repulsive force will increase

rapidly to decrease, the chances of particle clustering. Moreover, for zero particle distance, the spiky function has a certain value that solves the problem with the infinity value. The accuracy of this kernel function has been investigated comparatively using the elliptical bubble test case.

Because of the advantage of the third-order polynomial spiky kernel function, this kernel is also used in this study.

Table 2-1. Kernel Functions Studied by Atatie-Ashtiani and Farhadi (2006)

Kernel Functions	**Formula**	**Reference**
1	$W(R_{ij}, r_e) = \begin{cases} \frac{r_e}{R} - 1 & 0 \le R \le r_e \\ 0 & R \ge r_e \end{cases}$	Koshizuka et al. (1995)
2	$W(R_{ij}, r_e) = \begin{cases} e^{-\left(\frac{R}{\alpha r_e}\right)} & 0 \le R \le r_e \\ 0 & R \ge r_e \end{cases}$	Belytschko et al. (1996)
3	$W(R_{ij}, r_e) = \begin{cases} 1 - 6\left(\frac{R}{r_e}\right)^2 + 8\left(\frac{R}{r_e}\right)^3 - 3\left(\frac{R}{r_e}\right)^4 & 0 \le R \le r_e \\ 0 & R \ge r_e \end{cases}$	Belytschko et al. (1996)

4	$$W(R_{ij}, r_e) = \begin{cases} \frac{2}{3} - 4\left(\frac{R}{r_e}\right)^2 + 4\left(\frac{R}{r_e}\right)^3 & 0 \le R \le \frac{r_e}{2} \\ \frac{4}{3} - 4\left(\frac{R}{r_e}\right) + 4\left(\frac{R}{r_e}\right)^2 - \frac{4}{3}\left(\frac{R}{r_e}\right)^3 & \frac{r_e}{2} \le R \le r_e \\ 0 & R \ge r_e \end{cases}$$	Belytschko et al. (1996)
5	$$W(R_{ij}, r_e) = \begin{cases} \frac{r_e}{R} - 1 & 0 \le R \le r_e \\ 0 & R \ge r_e \end{cases}$$	Koshizuka et al. (1998)
6	$$W(R_{ij}, r_e) = \begin{cases} \frac{40}{7\pi {r_e}^2}\left(1 - 6\left(\frac{R}{r_e}\right)^2 + 6\left(\frac{R}{r_e}\right)^3\right) & 0 \le R < \frac{r_e}{2} \\ \frac{10}{7\pi {r_e}^2}\left(2 - 2\frac{R}{r_e}\right)^3 & \frac{r_e}{2} \le R < r_e \\ 0 & R \ge r_e \end{cases}$$	Shao and Lo (2003)

2.4 MPS Discretization

As mentioned above, the inter-reactions between particles are used to transfer the problem from the real physical system into MPS. Therefore, spatial derivatives in governing equations are needed in MPS method. This section will introduce and describe the basics of the discretization in MPS

2.4.1 Gradient and Divergence Discretization

In MPS methods, the gradient of any property $\nabla\phi_{ij}$ between particle i and j at position r_i and r_j can be defined as

$$\nabla\phi_{ij} = \frac{\phi_j - \phi_i}{|\vec{r_j} - \vec{r_i}|^2}(\vec{r_j} - \vec{r_i})$$

(2.9) where $r_{ij} = |\vec{r_j} - \vec{r_i}|$. According to Equation 2.1, the smoothed value of gradient at particle *i* can be derived by the kernel function $W(r_{ij}, r_i)$ as

$$\langle\nabla\phi\rangle_i = \frac{d}{\langle n\rangle_i}\sum_{j\neq i}\left(\frac{\phi_j - \phi_i}{{r_{ij}}^2}(\vec{r_j} - \vec{r_i})W(r_{ij}, r_e)\right) \quad (2.10)$$

where *d* is the number of space dimension. Since the study only considers the incompressible fluid, the particle density remains the same as the initial particle density n^0. Then, Equation 2.10 can be written as

$$\langle\nabla\phi\rangle_i = \frac{d}{n^0}\sum_{j\neq i}\left(\frac{\phi_j - \phi_i}{{r_{ij}}^2}(\vec{r_j} - \vec{r_i})W(r_{ij}, r_e)\right) \quad (2.11)$$

Same as gradient, the divergence of vectors between particle *i* and its neighbor particle *j*, f_i and f_j, can also be defined as

$$\langle\nabla f\rangle_i = \frac{d}{n^0}\sum_{j\neq i}\left(\frac{f_j - f_i}{{r_{ij}}^2}(\vec{r_j} - \vec{r_i})W(r_{ij}, r_e)\right) \quad (2.12)$$

2.4.2 Laplacian

In MPS, the Laplacian term is proposed by Koshizuka et al. (1995) for the diffusion model. In diffusion model, Laplacian term is approximated with the weighted averaging value of the diffusion of the physical property from a particle to its neighboring particles$\nabla\phi_{i\to j}$. When solving a diffusion problem with a delta function being the initial profile in an unlimited space, a Gaussian function (2.13) will present the analytical solution

$$\mathrm{G}(r) = \left(\frac{1}{\sqrt{4\pi\nu t}}\right)^{d} e^{\frac{r^2}{4\nu t}} \tag{2.12}$$

where d is the dimension of the problem space and ν is the kinematic viscosity. Therefore, if a physical property ϕi possessed by a particle i is treated as a delta function, the solution of the diffusion can be derived/obtained through the superposition of Gaussian functions. During this calculation, part of the physical property is maintained by the particle i and the remains will be distributed to the neighboring particles through a weight function. The Laplacian term can be derived from the divergence of a gradient vector as follows:

$$\Delta\phi = \nabla^2\phi = \nabla\nabla\phi = \frac{1}{r^2}\frac{\partial}{\partial r}\left(r^2\frac{\partial\phi}{\partial r}\right) = \frac{1}{r^2}\left(2r\frac{\partial\phi}{\partial r} + r^2\frac{\partial^2\phi}{\partial r^2}\right) \tag{2.13}$$

Based on the Taylor series expansion of physical property ϕ on the particle j in a vicinity of particle i,

$$\phi_j = \phi_i + r_{ij}\frac{\partial\phi_{ij}}{\partial r_{ij}} + \frac{1}{2}{r_{ij}}^2\frac{\partial^2\phi_{ij}}{\partial {r_{ij}}^2} \tag{2.14}$$

Equation 2.14 can be rewritten as

$$\frac{\partial^2\phi_{ij}}{\partial {r_{ij}}^2} = \frac{2}{{r_{ij}}^2}\phi_{ij} - \frac{2\partial\phi_{ij}}{r_{ij}\partial {r_{ij}}^2} \tag{2.15}$$

By substituting Equation 2.15 into Equation 2.13,

$$\nabla^2\phi_{ij} = \frac{1}{{r_{ij}}^2}\left(2r_{ij}\frac{\partial\phi_{ij}}{\partial r_{ij}} + {r_{ij}}^2\left(\frac{2}{{r_{ij}}^2}\phi_{ij} - \frac{2\partial\phi_{ij}}{r_{ij}\partial r_{ij}}\right)\right) = \frac{2\phi_{ij}}{{r_{ij}}^2}$$

(2.16)

By introducing the weighted averaging of Equation 2.16 into the MPS approximation of Laplacian formula,

$$\langle \nabla^2 \phi \rangle_i = \frac{2d}{n^0} \sum_{j \neq i} \left(\frac{\phi_{ij}}{{r_{ij}}^2} W(r_{ij}, r_e) \right) \tag{2.17}$$

According to the research by Koshizuka et al. (1995), in the MPS Laplacian formula, the term r_{ij} is replaced with λ as a weighted averaging of ${r_{ij}}^2$, then Equation 2.17 can be written as

$$\langle \nabla^2 \phi \rangle_i = \frac{2d}{n^0 \lambda} \sum_{j \neq i} \left(\phi_{ij} W(r_{ij}, r_e) \right) \; ; \; \lambda = \langle {r_{ij}}^2 \rangle_i = \frac{\sum_{j \neq i} \left({r_{ij}}^2 W(r_{ij}, r_e) \right)}{\sum_{j \neq i} \left(W(r_{ij}, r_e) \right)} \tag{2.18}$$

According to the probability theory, the central limit theorem (CLT) states that a large number of identical independent random variables (particles) with finite mean and variance, will be approximately normally distributed (Rice, 1995). The analytical solution of the diffusion problem in an infinite space with a delta function as the initial profile will result in a normal (Gaussian) distribution (Koshizuka et al., 1995). It should be noted that using a Gaussian function to transfer a physical property from a particle to other particles leads to a variant increase of λ. The λ added to the MPS diffusion formula causes the increase of variance $(\Delta\sigma^2)$ to be equivalent to the increase of variance in analytical solution.

$$\lambda = \Delta\sigma^2 = \frac{\sum_{j \neq i} \left({r_{ij}}^2 W(r_{ij}, r_e) \right)}{\sum_{j \neq i} \left(W(r_{ij}, r_e) \right)} \tag{2.19}$$

By employing the integral to calculate λ,

$$\lambda = \frac{\int_v W(r,r_e) r^2 dv}{\int_v W(r,r_e) dv} \tag{2.20}$$

Therefore, for two dimensional space, Equation 2.20 can be written as

$$\lambda = \frac{2\pi \int_0^{re} W(r,r_e) r^3 dr}{2\pi \int_0^{re} W(r,r_e) r dr} \tag{2.21}$$

As Equation 2.21, λ can be calculated in three dimensional space as

$$\lambda = \frac{4\pi \int_0^{re} W(r,r_e) r^4 dr}{4\pi \int_0^{re} W(r,r_e) r^2 dr} \tag{2.22}$$

Take kernel function 1 in Table 2-1 for example, λ can be calculated as (Koshizuka et al. 1995)

$$\lambda = \frac{31}{140} {r_e}^2 \tag{2.23}$$

Also for Equation 2.18, the MPS Laplacian for vector **f** on the particle *i* can be obtained as

$$\langle \nabla^2 \mathbf{f} \rangle_i = \frac{2d}{n^0 \lambda} \sum_{j \neq i} \left(\mathbf{f}_{ij} W\left(r_{ij}, r_e\right) \right) \tag{2.24}$$

2.5 Comparison between MPS and SPH

MPS and SPH are both mesh-free particle methods, since the similar theory, they both employ a finite number of particles to discretize the continuum domain to solve the fluid flow problems. However, they use different numerical procedures to solve the governing equations (Tokura, 2014).

2.5.1 Approximation of a Physical Property or Function

Regarding to equation 2.1 (quoted below), the smoothed physical property of certain particle *i* can be written as

$$\langle \phi_i \rangle = \frac{\sum_{j \neq i} \left(\phi_j W(r_{ij}, r_e) \right)}{\sum_{\neq i} W(r_{ij}, r_e)} \tag{2.1}$$

However in SPH method, the kernel approximation of function ϕ for the particle *i* establishes from the identity (Liu & Liu, 2010):

$$\phi_i = \int_v \phi \delta(r_{ij}) dv \tag{2.25}$$

where $\delta(r_{ij})$ is the Dirac delta function given by

$$\delta(r_{ij}) = \begin{cases} 1, & r_i = r_j \\ 0, & r_i \neq r_j \end{cases} \tag{2.26}$$

In order to implement the particle discretization, the delta function is replaced by the kernel function (or smoothing function) *W*(*Rij*, *re*) with the finite spatial dimension in the SPH method, and subsequently the approximation of the function <ϕ>*i* can be obtained as

$$\langle \phi \rangle_i = \int_v \phi_j W(r_{ij}, r_e) dv \tag{2.27}$$

when implementing at the discrete particles, equation (2.21) is converted into the discrete form as

$$\langle \phi \rangle_i = \sum_{j \neq i} \frac{m_j}{\rho_j} \phi_j W(r_{ij}, r_e) \tag{2.28}$$

Based on the facts above, MPS considers the influence of the surrounding particles to the desired property, the contribution of the surrounding particles is not directly encountered; while in SPH it accounts for the direct contribution of the surrounding particles to the desired property. One thing need to be mentioned is only the kernel function $\mathrm{W}(r_{ij}, r_e)$ in MPS is the delta function in SPH, the value of physical property will be the same ($\langle\phi\rangle_i = \phi_i$).

2.5.2 Kernel Approximation of Derivatives

As equation 2.12 (quoted below), the approximation for the spatial derivative in MPS can be written as

$$\langle\nabla f\rangle_i = \frac{d}{n^0}\sum_{j\neq i}\left(\frac{f_j - f_i}{{r_{ij}}^2}(\vec{r_j} - \vec{r_i})W(r_{ij}, r_e)\right) \tag{2.12}$$

In SPH, the approximation is defined by substituting f_i with∇f_i, which is

$$\langle\nabla\vec{f}\rangle_i = \int_v[\nabla\vec{f_j}]\,W(r_{ij}, r_e)dv \tag{2.29}$$

Based on Liu & Liu (2010), by applying the divergence theorem, equation 2.29 can be written as

$$\langle\nabla\vec{f}\rangle_i = -\int_v \vec{f_j}\nabla W(r_{ij}, r_e)dv \tag{2.30}$$

The discrete form of equation 2.30 can be obtained by following the same procedure similar to the approximation of the physical property function as follow (Liu & Liu, 2010):

$$\langle \nabla \vec{f} \rangle_i = -\sum_{j \neq i} \frac{m_j}{\rho_j} \vec{f}_j \nabla W(r_{ij}, r_e) \tag{2.31}$$

From the equations, it is obvious that the spatial gradient in SPH is calculated from the values of the function and the derivatives of the smoothing function *W*, instead of the derivatives of the function itself (Liu & Liu, 2010).

CHAPTER 3 FREE SURFACE FLOW MODELING WITH WC-MPS

In this chapter, the original MPS formulations and algorithms for modeling of incompressible viscous free-surface flow are explained. The governing equations of the system and solution algorithm are given. Then the MPS formulations for approximation of the derivatives, the method of pressure calculation the boundary treatment techniques and the turbulence model are explained.

3.1 Governing Equations

The motion of an incompressible viscous fluid flow is described by the continuity and momentum equations. In the Lagrangian system, they can be written as

Continuity:

$$\frac{D\rho}{Dt} + \rho(\nabla \mathbf{u}) = 0 \tag{3.1}$$

Momentum:

$$\rho \frac{Du}{Dt} = -\nabla p + \mu \nabla^2 \mathbf{u} + \mathbf{f} \tag{3.2}$$

where $\mathbf{u}$ is the flow velocity, ρ is the density, p is the pressure , μ is the dynamic viscosity, and $\mathbf{f}$ represents the body forces (per unit volume). Needless to say that, in the Lagrangian system, there is no convective acceleration term in the left hand side of the momentum equation. The movement of each particle is tracked down by using $\frac{D\mathbf{r}}{D\mathrm{t}}$, with $\mathbf{r}$

being the position vector. In MPS method, the temporal derivatives are approximated by time splitting method.

3.2 MPS Solution Procedure

3.2.1 Time Splitting and Prediction-Correction Process

In MPS, each step of a complete calculation includes two pseudo steps: prediction and correction. As with the method, the velocity at the next time step will be predicted at first, and then corrected. In the prediction step, velocity is predicted using explicit parts of source terms. The pressure is added during the correction step implicitly. The value of the physical properties such as **u**, **r**, ρ and n in a new time step (k+1) can be achieved from the summation of their prediction value, and their correction value as

$$\begin{aligned} \mathbf{u}^{k+1} &= \mathbf{u}^{*} + \mathbf{u}' \\ \mathbf{r}^{k+1} &= \mathbf{r}^{*} + \mathbf{r}' \\ \rho^{k+1} &= \rho^{*} + \rho' \\ n^{k+1} &= n^{*} + n' \end{aligned} \tag{3.3}$$

where k, (*) and ($'$) represent the step of calculation, the prediction and the correction values respectively. The time derivative of velocity in momentum can be written as

$$\frac{D\mathbf{u}}{Dt} = \frac{\mathbf{u}^{k+1}-\mathbf{u}^{k}}{\Delta t} = \frac{\mathbf{u}^{k+1}-\mathbf{u}^{*}}{\Delta t} + \frac{\mathbf{u}^{*}-\mathbf{u}^{k}}{\Delta t} = \frac{\mathbf{u}'}{\Delta t} + \frac{\mathbf{u}^{*}-\mathbf{u}^{k}}{\Delta t} \tag{3.4}$$

Also for the density, the time derivative of density in momentum can be written as

$$\frac{D\rho}{Dt} = \frac{\rho^{k+1}-\rho^{k}}{\Delta t} = \frac{\rho^{k+1}-\rho^{*}}{\Delta t} + \frac{\rho^{*}-\rho^{k}}{\Delta t} = \frac{\rho'}{\Delta t} + \frac{\rho^{*}-\rho^{k}}{\Delta t} \tag{3.5}$$

Based on equation 3.4, the momentum equation (equation 3.2) can be rewritten as

$$\mathbf{u}' + (\mathbf{u}^* - \mathbf{u}^k) = \Delta \mathrm{t}\left(-\frac{1}{\rho}\nabla p\right) + \Delta t(v\nabla^2\mathbf{u} + \mathbf{f}) \tag{3.6}$$

where v is the kinematic viscosity, and

$$\begin{cases} \mathbf{u}^* = \mathbf{u}^k + \Delta t(v\nabla^2\mathbf{u} + \mathbf{f})^2 \\ \mathbf{u}' = -\Delta t\frac{1}{\rho}\nabla p^{k+1} \end{cases} \tag{3.7}$$

As it is mentioned above, each calculation step includes prediction and correction steps. In equation 3.7, the predicted velocity $\mathbf{u}^*$is calculated by employing the viscous and body force terms, and the correction term $\mathbf{u}'$is calculated by using the pressure gradient term. Therefore, the velocity for the new time step can be calculated by adding the prediction velocity to the correction velocity $\mathbf{u}^{k+1} = \mathbf{u}^* + \mathbf{u}'$.

In the same approach, the continuity equation can be written as

$$\begin{cases} \frac{1}{\rho}\frac{(\rho^* - \rho^k)}{\Delta t} = -\nabla\mathbf{u}^* \\ \frac{1}{\rho}\frac{\rho'}{\Delta t} = -\nabla\mathbf{u}' \end{cases} \tag{3.8}$$

At the end of each time step, particles are moved based on their new velocity

$$\mathbf{r}^{k+1} = \mathbf{r}^k + \Delta t\mathbf{u}^{k+1} \tag{3.9}$$

This process is repeated for every fluid particle at each time step and progresses until the pre-set time point. The whole calculation for a complete time step can be simply viewed in Figure 3-1. From the algorithm, it is obvious that as long as the velocity at the next time step of each particle is obtained, the new position of each particle will be determined through the new velocity, thus, the movement of the fluid is completed for the current time step.

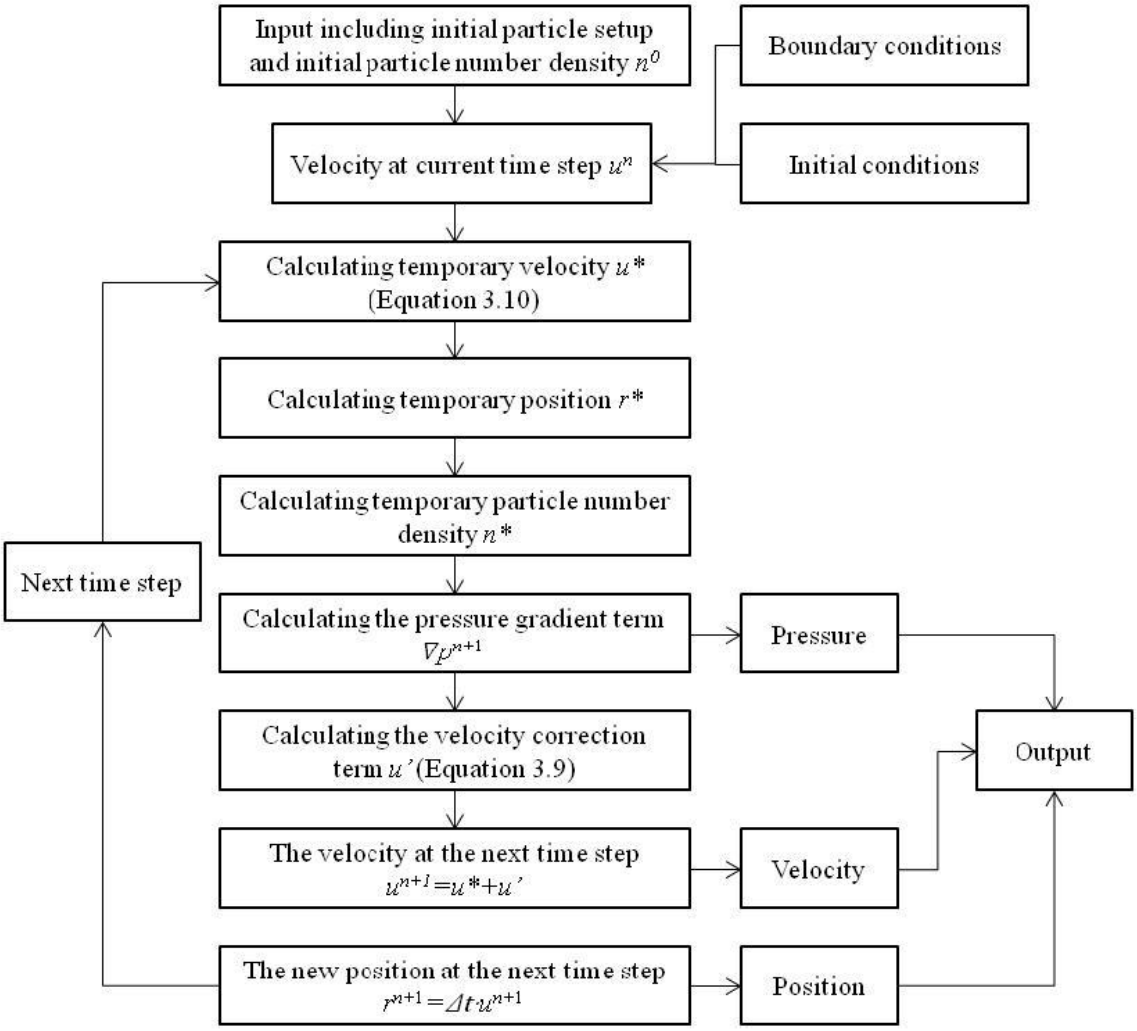

Figure 3-1. Simulation Procedure of MPS Method

3.2.2 Modeling of Incompressibility and Pressure Calculation

3.2.2.1 Fully Incompressible Method

In original MPS method, the incompressibility model is derived from the continuity equation because of the density of the simulated fluid does not change. For a fully incompressible fluid, $\frac{D\rho}{Dt}$ equals zero. In MPS method, the particle density refers to the

density of the simulated fluid, so the continuity equation also can be used for the constant particle number density. Therefore, for the cases in which the calculated particle number density from the prediction step (n^*) varies from the initial particle number density (n^0), it will be implicitly corrected as follow (Shakibaeinia & Jin, 2010)

$$n^0 = n^* + n' \tag{3.10}$$

By substituting the density ρ with n^0 and ρ' with n' in equation (3.8), the following equation will be achieved

$$\frac{1}{n^0}\frac{n'}{\Delta t} = -\nabla u' \tag{3.11}$$

Similar, by substituting the equivalent of velocity correction value from right hand side of equation (3.7) into equation (3.11), a Poisson equation for pressure calculation can be derived as

$$\nabla^2 {p_i}^{k+1} = \frac{\rho}{\Delta t^2}\frac{n'}{n^0} = \frac{\rho}{\Delta t^2}\frac{n^0 - {n^*}_i}{n^0} \tag{3.12}$$

Since n^* is associated with the temporary position of the particles in the prediction step, the value of n^* varies for every particle. In order to obtain the pressure field, discretization of the left hand side of equation (3.12) is needed by using the Laplacian equation (2.24), and eventually results in a linear symmetric $N \square N$ matrix (N denotes the fluid particles). To solve this matrix, an iterative numerical solver is required, such as the conjugate gradient method. As Koshizuka et al. (1998) mentioned in their research, to solve the PPE, it take as much as two third of the CPU calculating time at each time step, for a case only contains 2418 particles, which means when the number of the particles increases rapidly, especially in large scale flow modeling problems, generating and solving the PPE matrix will slow down the simulating process sharply.

3.2.2.2 Weakly Compressible Method

Shakibaeinia and Jin (2010) proposed to introduce the equation of state in their MPS model to improve simulation efficiency. In this model, an explicit relation replaces the Poisson equation. To achieve a fluid with this specific feature, the compressibility value of that fluid should be kept very small, so the method is given the name of weakly compressible MPS method. The concept of weakly-compressible is originally from SPH method and is common among SPH models (Monaghan 1994, Bonet and Lok 1999, Dalrymple and Rogers 2006, and Violeau and Issa 2007).

In the research of Monaghan (1944), he used the equation of state which is described by Batchelor (1967) in his SPH method by replacing the fluid density by particle number density, the equation of state can be described as

$$p_i^{k+1} = \frac{\rho_0 {c_0}^2}{\gamma}\left(\left(\frac{\langle n^* \rangle_i}{n^0}\right)^{\gamma} - 1\right) \tag{3.13}$$

where γ is coefficient and the typical value is 7 (Monaghan 1994, Shakibaeinia and Jin 2010), c_0 is the sound speed in the reference medium. In most simulations, a much lower artificial sound speed is used. According to Dalrymple & Rogers (2006), the Mach number should be smaller than 0.1 to maintain the density fluctuation less than 1% of reference density. In order to make Mach number less than 0.1, the artificial sound speed must be at least ten times higher than the maximum fluid velocity. Because of this feature in pressure calculations, this method is called weakly compressible MPS method (WC-MPS). By employing equation 3.13 into equation 2.11, the pressure gradient equation becomes

$$\langle \nabla \mathrm{p} \rangle_i = \frac{d}{n^0} \sum_{j \neq i} \frac{p_j - p_i}{{r_{ij}}^2} (\vec{r_j} - \vec{r_i}) W(r_{ij}, r_e) \quad (3.14)$$

3.2.3 Viscous Term

By applying the MPS Laplacian formula (equation 2.24) into equation 3.6, the MPS approximation of viscous term $v\nabla^2\mathbf{u}$ can be described as

$$\langle v\nabla^2\mathbf{u} \rangle_i = \frac{2dv}{n^0\lambda} \sum_{j \neq i} \left((\mathbf{u}_j - \mathbf{u}_i) W(r_{ij}, r_e) \right) \quad (3.15)$$

3.3 Boundary Conditions

3.3.1 Free Surface

As it is mentioned above, the one of the most significant advantages for particle method is that the method can treat problems with large deformations and fragmentations. To track the free surface during the simulation process, when the particle reaching the free surface, since there has no particles outside the region, the number of particles in the searching radius will decrease, which means the particle number density will also decrease. In this case, a special treatment is required to identify the free surface particles.

To identify the free surface particles, Koshizuka et al. (1998) defined the following condition

$$\langle n^* \rangle_i \leq \beta n^o \quad (3.16)$$

where β is the threshold coefficient, and should be less than 1. In this research, Koshizuka et al. (1998) found that the simulation results are almost the same when β value is between 0.8 and 0.99. Therefore, 0.96 is used in their study.

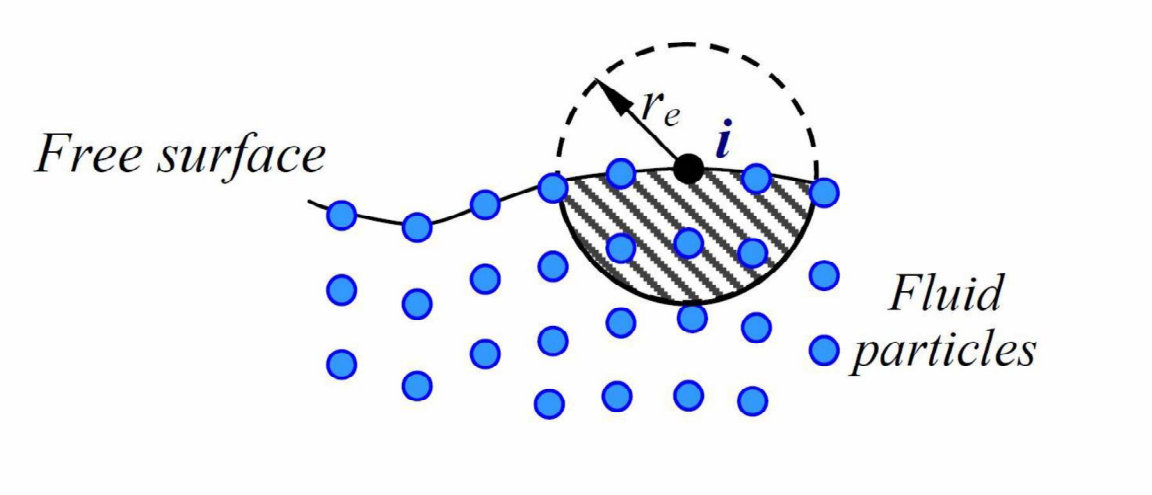

Figure 3-2. Free Surface Particle Recognition (Shakibaeinia and Jin, 2010)

3.3.2 Solid Boundary

When a particle reaches the solid boundaries, such as walls and beds, the particle density will also decrease, which is similar to the free surface. However, this will cause the error in the process of weighted averaging. Because of the flow patterns near solid boundaries are different from the flow near free surface, the treatment of free surface cannot be applied.

In current study, the method used to eliminate particle density deficiency near solid boundaries are introduced by Koshizuka et al. (1998). In this method, solid boundaries are made by wall particles (one layer), ghost particles (located outside the solid boundaries) are introduced, and the number and location of these ghost particles are

fixed. By introducing ghost particles, the boundary values are interpolated to the fluid particles during the calculation.

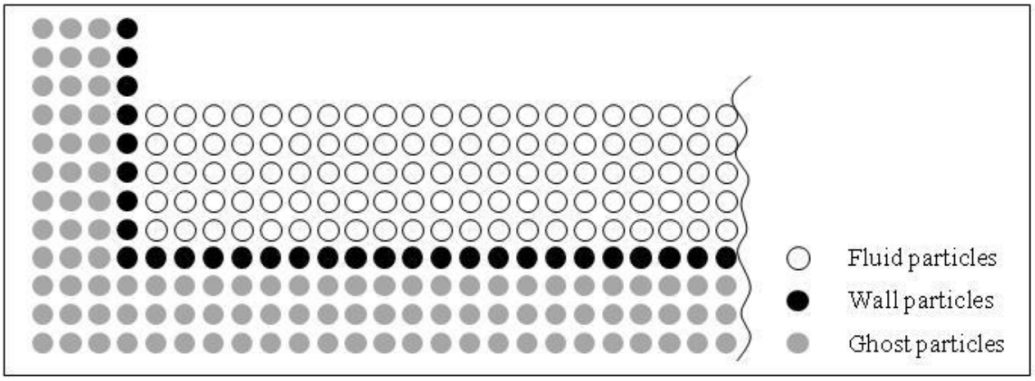

Figure 3-3. Solid Boundary Condition

The normal velocity of ghost particles is equal to zero, and there are two different boundary conditions for calculating tangential velocity of ghost particles: free-slip boundary condition and no-slip boundary condition. For free-slip boundary condition, the tangential velocity of ghost particles are equal to the fluid particles, and for no-slip condition, the velocity of ghost particles are opposite of the tangential velocity of fluid particles.

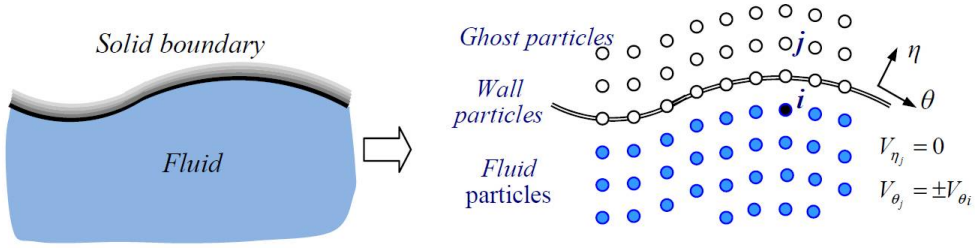

Figure 3-4. Normal $(V_{\eta j})$ and Tangential $(V_{\theta j})$ Velocities for Ghost Particles

CHAPTER 4 CASE STUDIES OF LANDSLIDE IMPULSE WAVES

4.1 Introduction

Impulse waves are generated by the impact of rockfalls, slumps, glacier breakdowns, or avalanches onto reservoirs, lakes, rivers, estuaries, oceans, and bays. The impulse waves are much larger compare to underwater-generated tsunami or wind-induced waves, the height of impulse waves are significantly exceed the vertical extensions of common water waves. Impulse waves may cause severe disaster due to the consequent runup and inundation resulting in the loss of lives and destruction of property (Pugh and Harris 1982). Destructive impulse wave events occurred in various parts of the world, such as in Lituya Bay, Alaska (Miller 1960), Yanahuin Lake, Peru (Plafker and Eyzaguirre 1979), Vaiont Reservoir, Italy (Vischer and Hager 1998), and many lakes and fjords. The huge rockslide on Vaiont Reservoir in 1963 caused an impulse wave to overtop the thin arch dam by roughly 100 m resulting in a tremendous flood with almost 3,000 casualties in the downstream located village of Longarone. In general, dams, buildings, and ships in the relative proximity of possible landslide impacts are inherently endangered by the risk of nearfield generated gravity water waves. Relative heights and comparative lengths of impulse waves typically range between the intermediate and the shallow-water regimes of the gravitational water wave spectrum (Dean and Dalrymple 1991). The generation and propagation of landslideinduced impulse waves was experimentally investigated by Wiegel (1955), Kamphuis and Bowering (1970), and Huber (1980). A computational approach toward the prediction of impulse waves was first presented by Noda (1970).

Further numerical studies were conducted to solve the nonlinear shallow water equations as applied to the complex dynamics of extremely unsteady flow, e.g., Abbott et al. (1978), Sander (1990), and Heinrich (1992).

To study the physical model parameters in terms of prototype events, the analysis of the characteristics of historical landslide generated impulse waves and their influence parameters are shown in table 4-1, which includes the most destructive submerged and un-submerged landslide generated waves. Table 4-1 includes the date, the location, the slide material, and the governing parameter Vs,α, h, the slide run-up height R, and number of fatalities, the data are from Slingerland and Voight (1979), Fritz (2002), Ward and Day (2003), and Panizzo et al. (2005).

Table 4-1. Some Historical Submerged and Un-submerged Landslide Generated Impulse Wave in AL=Alaska, IT=Italy, IN=Indonesia, JP=Japan, NW=Norway, P=Peru, PNG= Papua New Guinea, and USA=United States of America from Slingerland and Voight (1979) (S&V 1979), Fritz (2002), Ward and Day (2003) (W&D 2003), and Panizzo et al. (2005) (P et al. 2005). (Heller, 2007)

date, location	material	parameters	effects	reference
		V_s [m^3], α [°], h [m]	R [m], fatalities	
22.02.1756, Tjelle (NW)	granite gneiss	15×10^6, > 25, > 200	46, 38	S & V (1979)
21.05.1792, Shimabara (JP)	volcanic debris	500×10^6, 10, 64	10, > 15,000	S & V (1979)
27.08.1883, Krakatau (IN)	pyroxene/basalt	-, -, -	35, 36,000	Fritz (2002)
13.03.1888, Ritter Island (PNG)	basalt/andesit	5000×10^6, 10 - 15, 1000	20, > 100	W & D (2003)
04.07.1905, Disenchantment Bay (AL)	glacier ice	29×10^6, 28, 80	35, 0	S & V (1979)
07.04.1934, Tafjord (NW)	gneiss	$2 - 3 \times 10^6$, 60, > 200	62, 41	S & V (1979)
13.09.1936, Ravnefjell (NW)	gneiss	1×10^6, 25, < 60	74, 73	S & V (1979)
09.07.1958, Lituya Bay (AL)	schist	31×10^6, 40, 122	524, 2	S & V (1979)
22.03.1959, Pontesei reservoir (IT)	silt/clay debris	5×10^6, ≈ 5, 47	-, 1	P et al. (2005)
09.10.1963, Vaiont reservoir (IT)	limestone	240×10^6, 0 - 40, 50	270, ≈ 2000	S & V (1979)
18.03.1971, Yanahuin Lake (P)	limestone	0.1×10^6, 45, 38	30, 400 - 600	S & V (1979)
18.05.1980, Mount St. Helens (USA)	rock	430×10^6, -, -	200, 0	Fritz (2002)

From the study, the historical studies of impulse waves can be summarized as:

- Documented human death exceeds 60,000 (disasters in Table 4-1)
- Properly monitored field data are difficult to obtain because of the unexpected and disastrous nature of the slides (Kamphuis and Bowering 1972)
- No detailed information of close field wave height
- Limited data for far field wave height
- Most cases happened unexpected with no reaction time
- Possible landslide triggers are precipitation, changes in surface levels of water bodies adjacent to slopes (e.g. Vaiont case), seismic activity (e.g. Lituya Bay case), volcanic eruptions (e.g. Mount St. Helens case), erosion, or failure of natural dams (Schuster and Wieczorek 2002)

In order to avoid the disaster and the loose of lives, it is worth and necessary to study the impulse wave caused by landslide. By doing the simulation, the potential threats can be predicted and preventive action can be applied in advance.

In this chapter, different landslide cases from other researchers are studied by using WC-MPS method. Results are compared to testify the capability of MPS method in modeling impulse waves, which are generated by landslide. For landslide cases, based on the position of landslide, there are two categories: submerged landslide and un-submerged landslide; also based on the sliding material, it can be divided into two different groups: deformable landslide and non-deformable landslide. For deformable

landslide cases, the shape of materials used to slide down along the slope bed to generate impulse waves is able to change, such as soils and sands. For non-deformable landslide cases, the shape will not change, like solid wedges.

4.2 Case Studies

4.2.1 Deformable Landslide Cases

In this part, three different deformable landslide cases are studied. Water surface (shape of impulse waves) and shape of deformable materials during the simulation process are compared.

4.2.1.1 Biscarini's Case

According to the study made by Biscarini (2009), a comparison between a full Navier-Stockes mathematical model based on FLUENT 6 (Biscarini, 2009) and an experimental result from Firtz (2001) are made. In the experiment, the measurements have been made in a rectangular water wave channel with water depth of 0.45m and a hill slope angle of 45^{o} (shown in Figure 4-1). The test used an artificial granular material of 87% barium-sulfate ($4.5t/m^3$) compounded with 13% polypropylene ($0.91t/m^3$), the impact velocity is set to 6.68m/s, and Froude number F equals to 3.18.

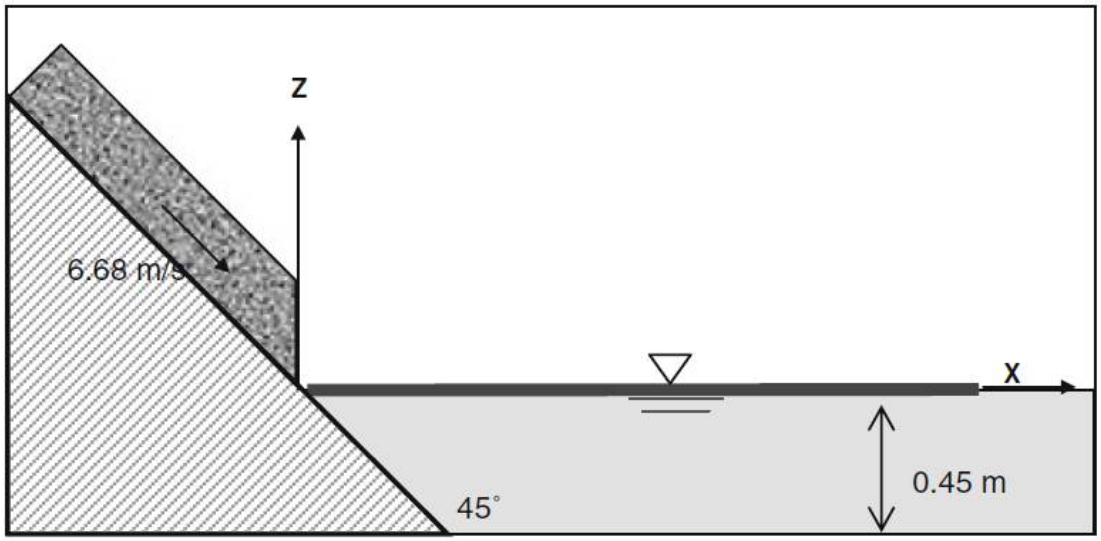

Figure 4-1. Geometrical Scheme for Biscarini's Case (Biscarini, 2009)

To test the capability of MPS model for simulating impulse wave generated by deformable landslide, this case is redid by WC-MPS method, and the simulation results of impulse waves in different time steps are shown in Fig 4-2.

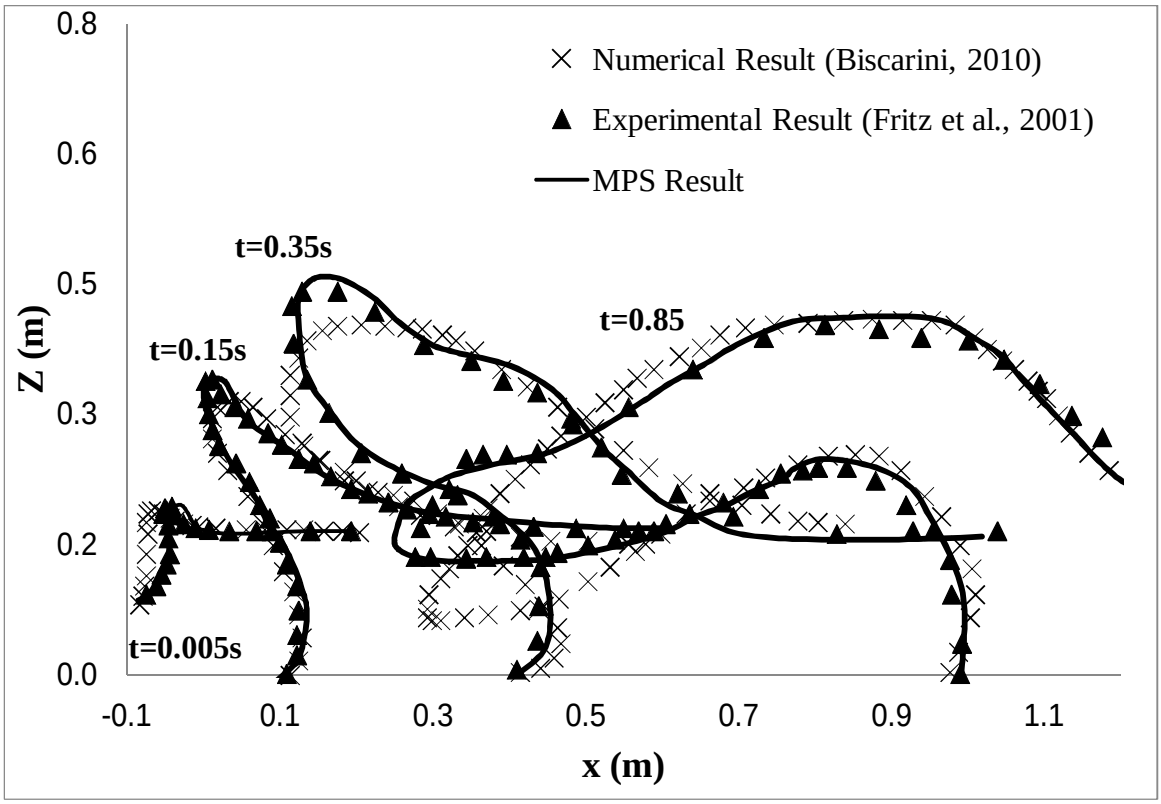

Figure 4-2. Comparison Result of Biscarini's Case

From the results, it is obviously that the simulation results from WC-MPS method is more like the experimental results, which means the WC-MPS method has the capability of simulating the impulse wave generated by deformable landslide.

4.2.1.2 Capone's Case

This is a submerged deformable landslide case did by Capone et al. (2015). In their research, the experiments of Rzadkiewicz et al. (1997) were tested by SPH method. The experiment consists in a triangular mass of sand to slide along a slope of 45^{o}. The bulk of slide is 0.65m in height and length. In SPH simulation, the water density is $1000kg/m^3$, viscosity is 0.001Pa.s, and the density of sand is set to $1950kg/m^3$. The same data is used

in WC-MPS simulation. The purpose of doing this case is to test the capability of WC-MPS to simulate deformable landslides and their interactions with the water. The geometrical scheme of this case is shown in figure 4-3, and the comparison results of water surface are in Figure 4-4 and Figure 4-5.

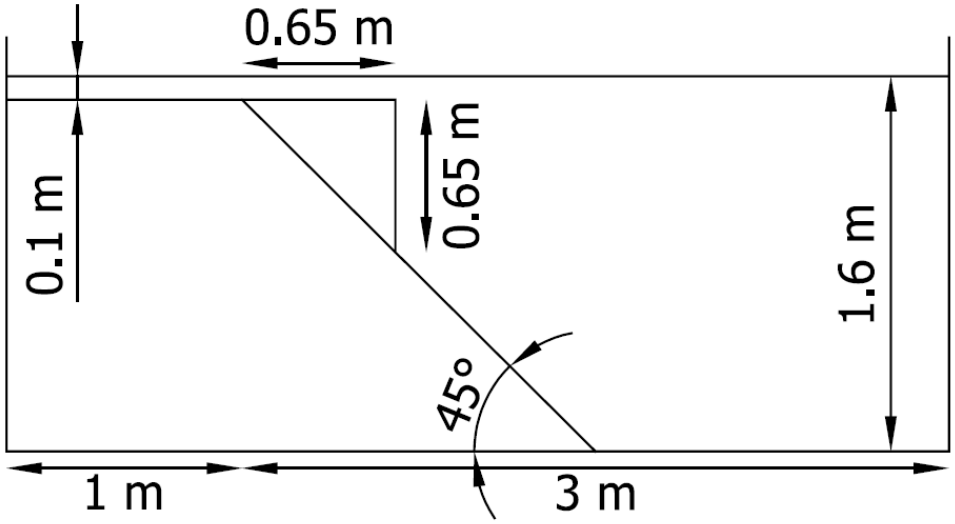

Figure 4-3. Geometrical Scheme for Capone's Case (Capone et al., 2015)

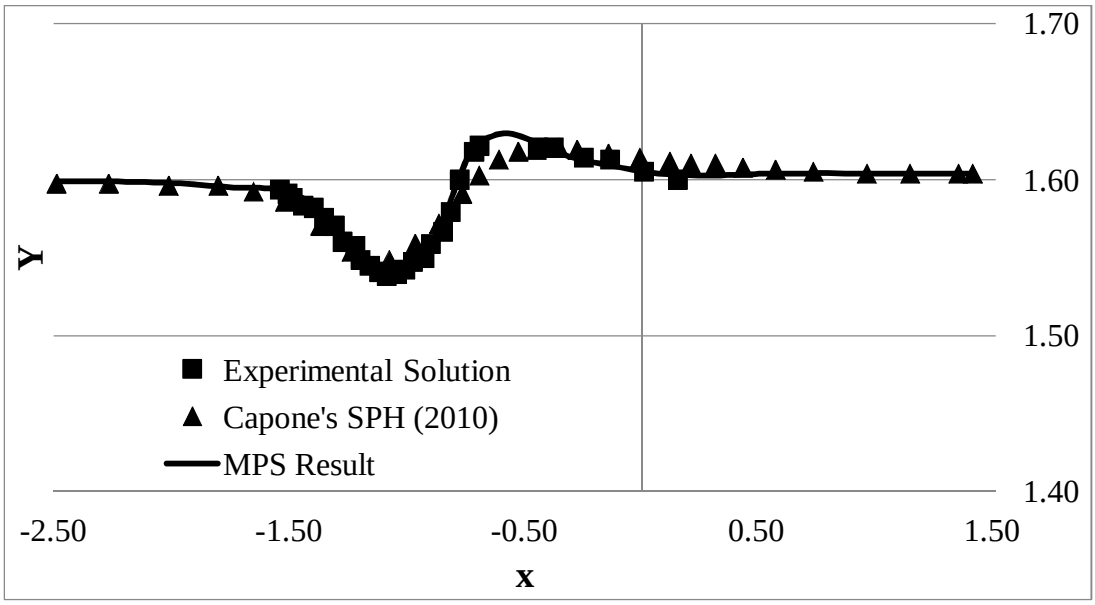

Figure 4-4. Comparison Result of Water Surface at 0.4s

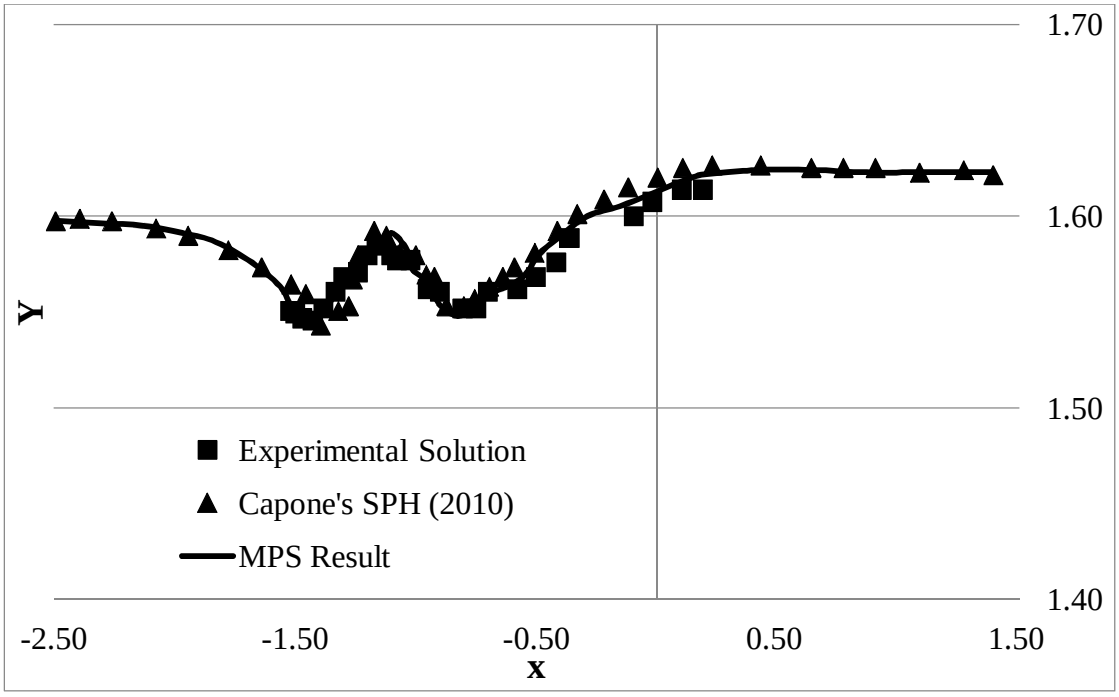

Figure 4-5. Comparison Result of Water Surface at 0.8s

4.2.2 Non-deformable Landslide Cases

As it is mentioned above, in none-deformable landslide cases, the sliding structure is a solid wedge, therefore, the shape and all the other properties of the sliding structure will remain the same for the whole process.

4.2.2.1 Heinrich's Submerged Case

In 1992, Heinrich used both experiment and a two-dimensional hydrodynamic program Nasa-Vof 2D to study the generation, propagation, and run-up on the shore of water waves created by landslides. According to Heinrich (1992), experiments were carried out in a 20m long channel, 0.55m wide and 1.5m deep. The experiment generates water waves by allowing a box to slide freely down a slope bed with a 45 degree slope. The shore was modeled by a second incline with a 15 degree slope, and the intersection of two inclines was 1m above the bottom of the channel. The box was triangular in cross section (0.5 m x 0.5 m) and was as wide as the flume. The geometrical top of the box was parallel to the still water surface during the experiment, and 0.2m under water surface at initial condition. Lead weights were loaded into the box to increase its fall velocity down the slope. The box, equipped with four rollers, slid into the water under only the influence of gravity, and was abruptly stopped as it reached the bottom by a 5-cm high rubber buffer. The geometrical scheme is shown in Figure 4-6.

To measure the height of impulse wave, three electrical contact-type gauges were installed outside of 4-m range of the camera. They were located 4 m, 8 m, and 12 m from the left side of the set up and could determine wave height with an error of ±3 mm.

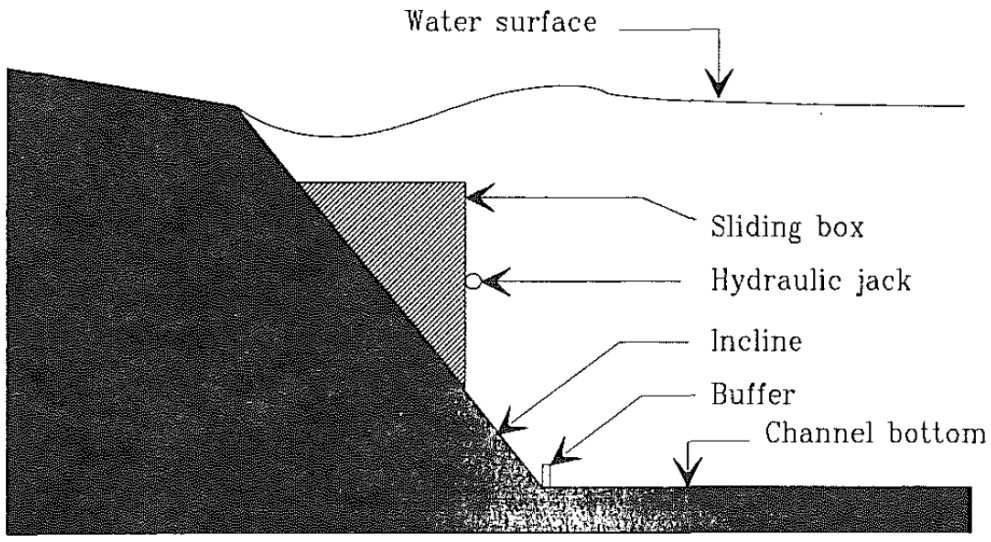

Figure 4-6. Geometrical Scheme for Heinrich's Case (Heinrich, 1992)

To test the capability of using MPS method to simulate impulse waves generated by non-deformable landslide, a model based on WC-MPS method is created to improve Heinrich's case, and a comparison between Experimental result, Nasa-VOF 2D simulation result and MPS result is made. Based on Heinrich's research, wave height are measured by three gauge at specific locations, and the initial water depth is 1.2m from bottom. The comparison results of impulse wave between three different methods are shown in Figure 4-7, Figure 4-8, and Figure 4-9.

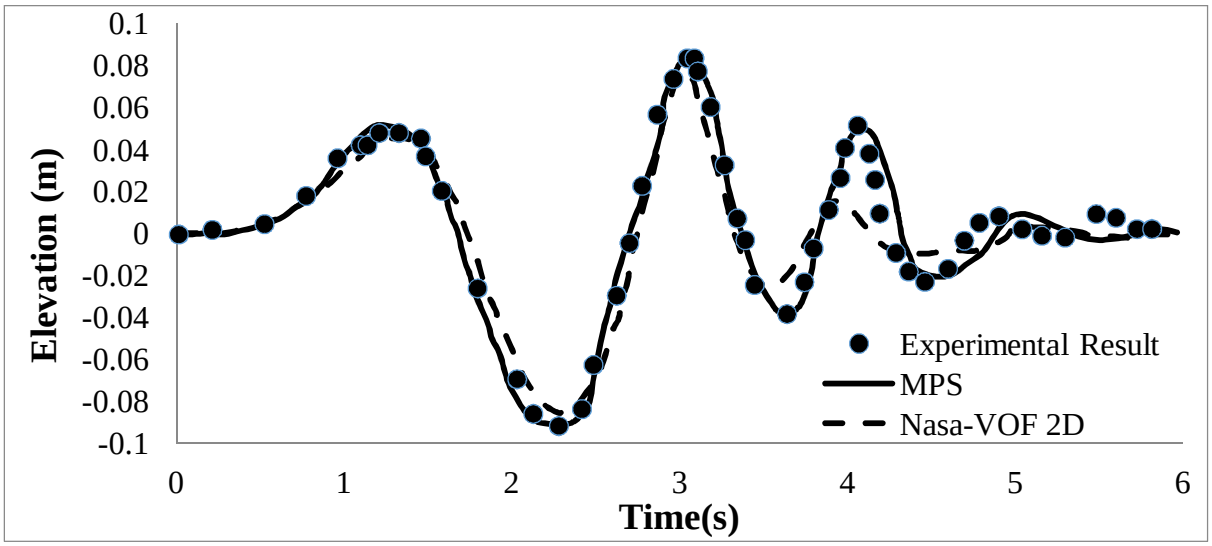

Figure 4-7. Comparison Result of Heinrich's Submerged Case at 4m

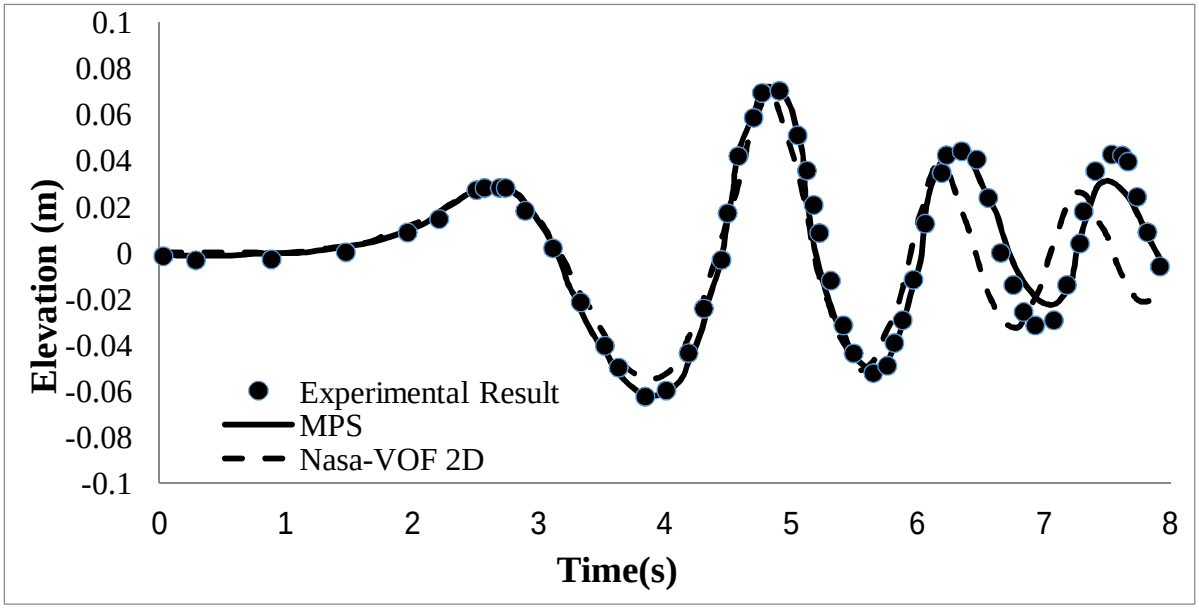

Figure 4-8. Comparison Result of Heinrich's Submerged Case at 8m

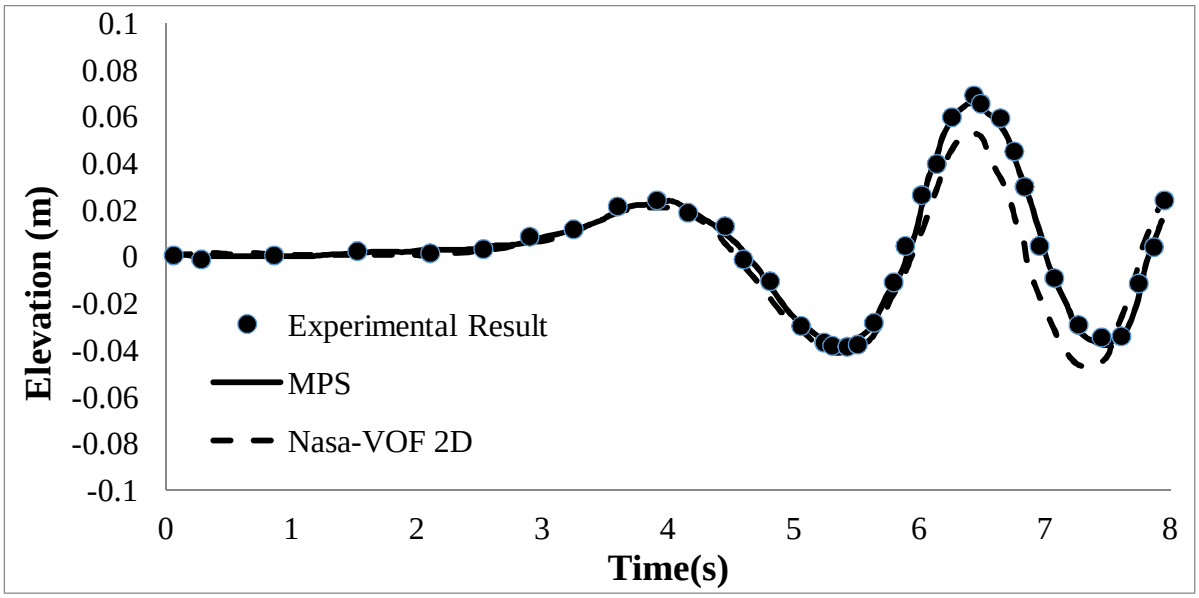

Figure 4-9. Comparison Result of Heinrich's Submerged Case at 12m

From the figures above, the simulation results from WC-MPS method show a better agreement with experimental results, which means the WC-MPS method is capable for simulating the impulse waves generated by submerged, non-deformable landslide.

4.2.2.2 Heinrich's Un-submerged Case

Similar to the previous submerged case, Heinrich's un-submerged case used the same wedge, however the initial water depth is reduced to 0.4m, and the sliding slope is remain 45 degree. The wave gauges in this case are also located at 4m, 8m, and 12m away from the left side of the setup, and the bottom of the wedge is initially just above the still free-surface. In this case, the comparison is also between experimental, Nasa-Vof2D, and MPS results.

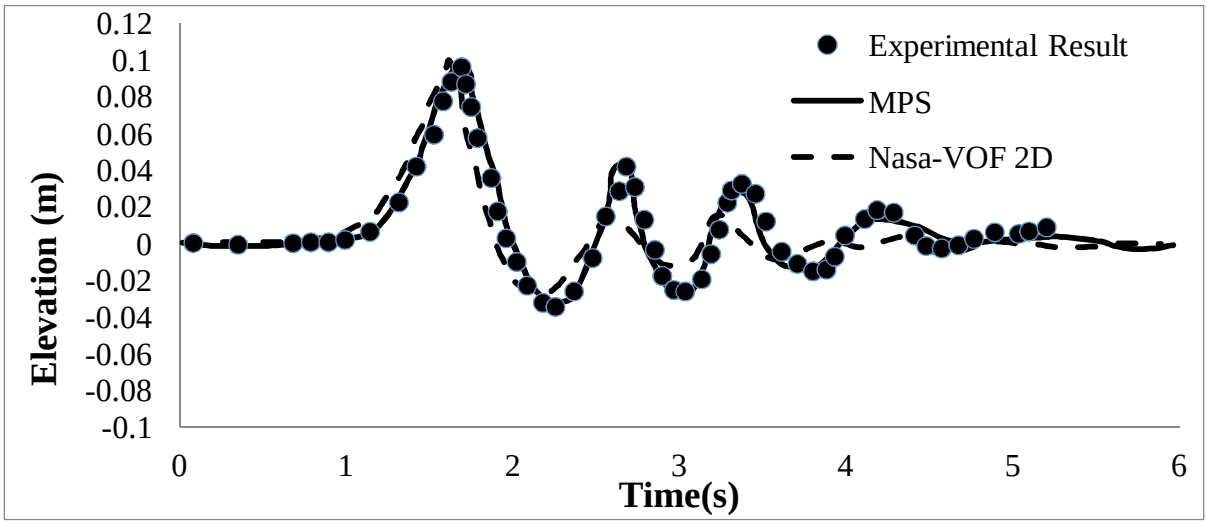

Figure 4-10. Comparison Result of Heinrich's Un-submerged Case at 4m

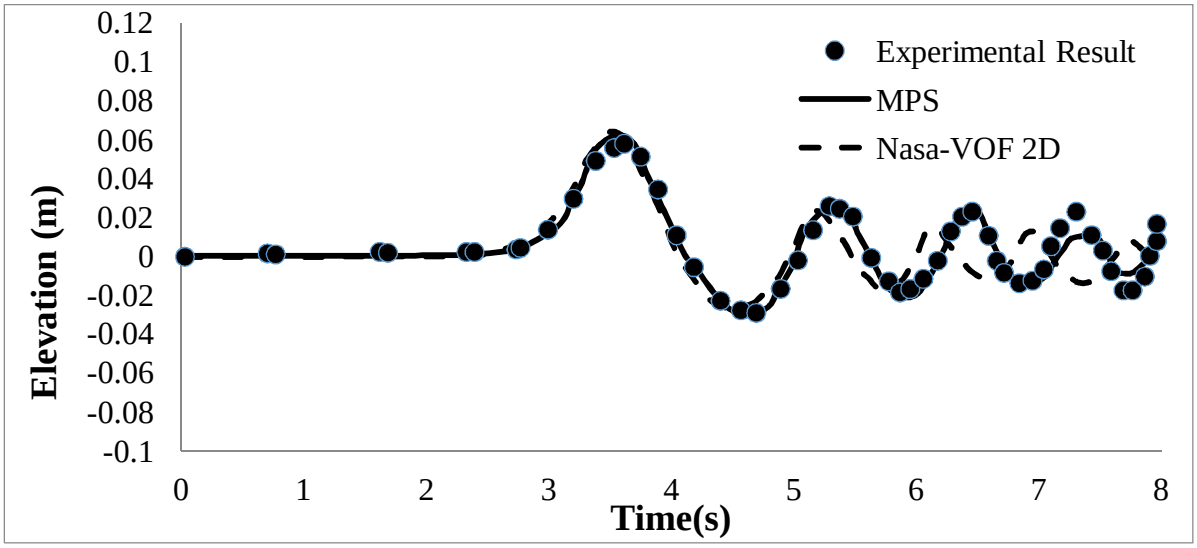

Figure 4-11. Comparison Result of Heinrich's Un-submerged Case at 8m

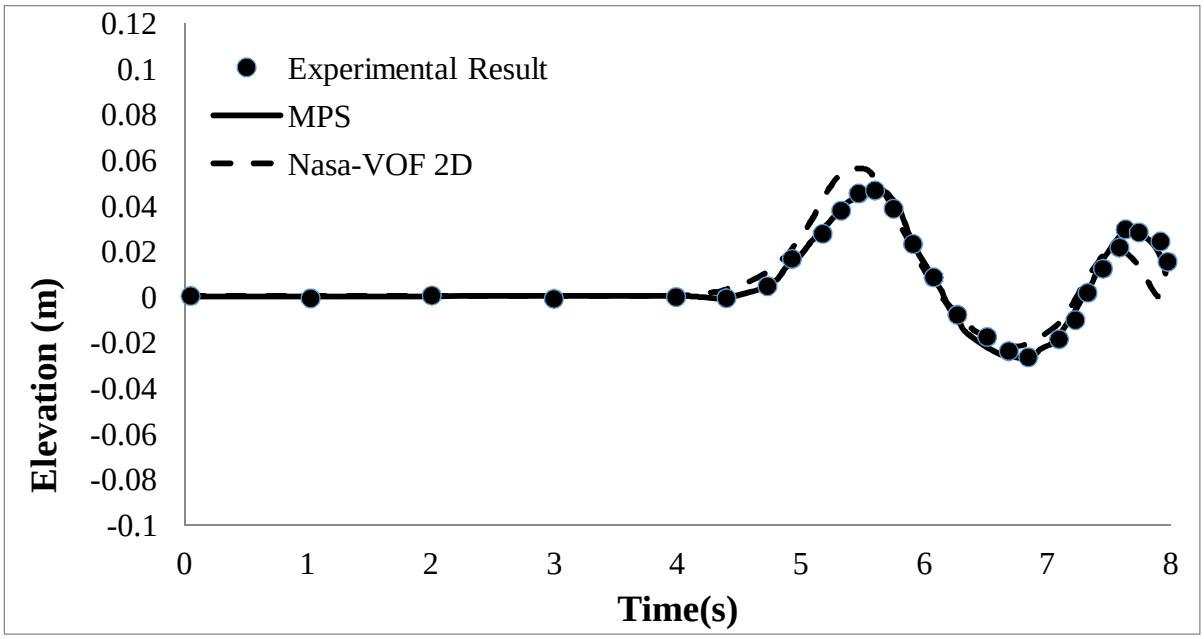

Figure 4-12. Comparison Result of Heinrich's Un-submerged Case at 12m

From the results, it is easy to see that MPS is a good method for simulating the impulse wave in un-submerged non-deformable landslide cases.

4.2.2.3 Watts' Case

Another chosen case to study the impulse wave generated by non-deformable landslide is introduced by Watts (2000). In this case, an underwater landslide was modeled as a right triangle initially at rest on a straight incline $\theta = 45^{o}$ from horizontal. The water tank is 0.101m wide, 9.14m long, and 0.66m high. One resistance wave gauge was positioned above the middle of the initial landslide location at x/h=0, and another was located at x/h=4.25. The solid wedges have different size based on their density, however, they are all 0.099m wide. The top domain of the wedge is parallel to the initial water surface, and the right side on the wedge is horizontal to the initial water surface.

Three different densities are tested for this case in MPS method and compared with Watts' experimental result. The geometrical scheme is shown in Figure 4-13.

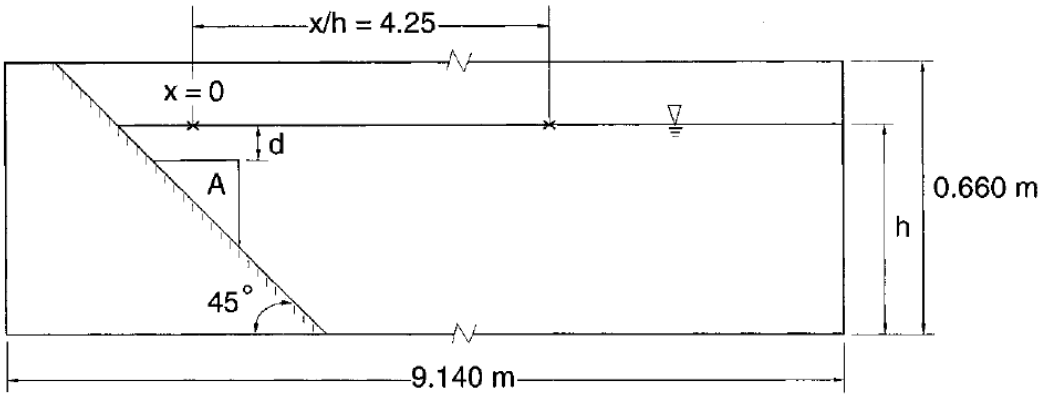

Figure 4-13. Geometrical Scheme of Watts' Case

For MPS simulation, three different size of wedges are used, and the weight of wedges are 440g, 784g, and 987g. According to Watts (2000), the comparison of water amplitude is made between MPS simulation results and Watts' Experimental results, at both *x/h*=0, and *x/h*=4.25 locations. The comparison results are shown in Figure 4-14, and 4-15.

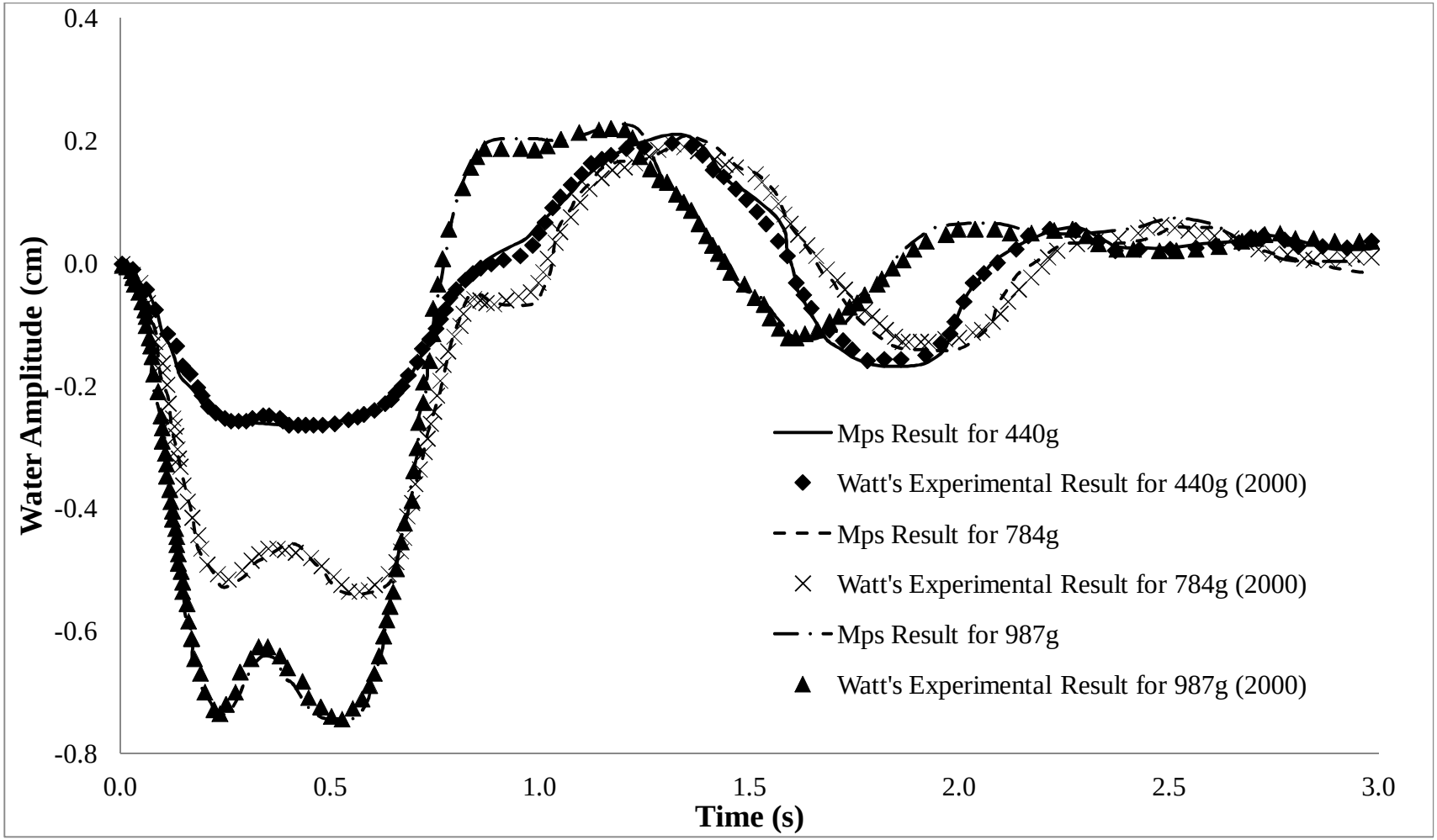

Figure 4-14. Comparison Result of Watts' Case at x/h=0 with Different Density Wedges Released with Initial Submergence d=74mm

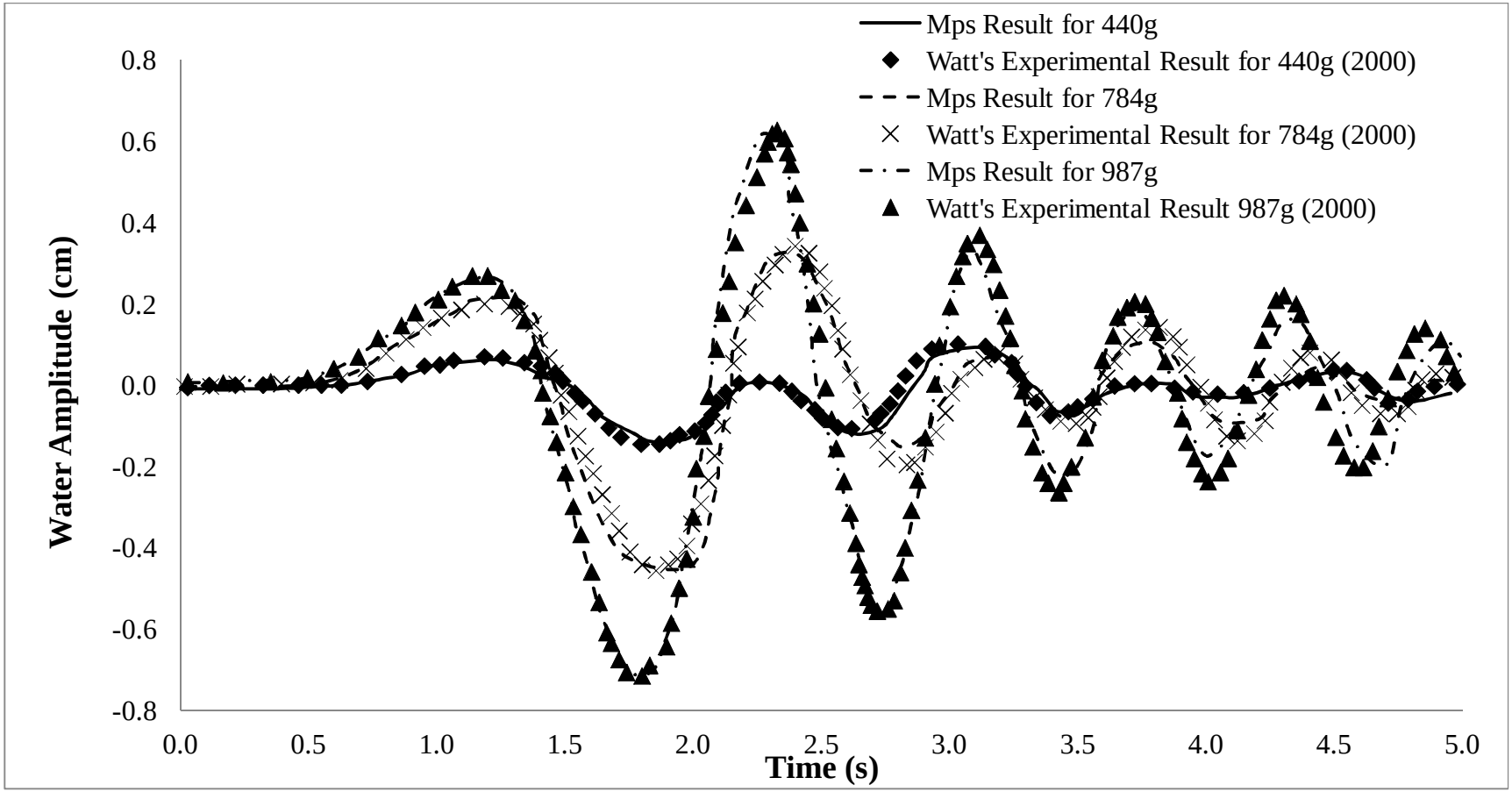

Figure 4-15 Comparison Result of Watts' Case at x/h=4.25 with Different Density Wedges Released with Initial Submergence d=74

From these figures, MPS method shows the amplitude of impulse wave generated by different materials in non-deformable landslide cases are simulated well.

4.3 Summary

In this chapter, WC-MPS method is applied in different landslide cases to prove the capability of simulating the impulse waves. From these case studies, it is obviously to draw the conclusion that WC-MPS method is a reliable tool for simulating the impulse wave generated by different kinds of landslide cases. The simulation results from WC-MPS method, is more accurate in simulating the impulse waves, which will give a better result compare to the other methods used by the authors in their researches.

CHAPTER 5 MODELING OF LANDSLIDE IMPULSE WAVE WITH WC-MPS METHOD

5.1 Introduction

In this chapter, WC-MPS method is used to simulate impulse waves and the properties of water field, such as velocity, in three landslide cases. The simulation results are compared with the experimental results. The simulations are focused on non-deformable landslide cases, including above water releasing (un-submerged), close to water releasing (submerged), and under water releasing (submerged). Both water surface and water velocity are modeled (simulater?) in this application.

The objective of this chapter is to study the impulse wave generated by non-deformable landslide, and evaluates the simulation result with experimental data in order to prove the capability of WC-MPS method in this area.

Compare to previous studies from other researchers, the velocity analysis of the water field around the sliding structure is introduced in this chapter, which is never been studied in this detail previously.

5.2 Experimental Setup

5.2.1 Close to Water Releasing (Submerged) Case

The MPS simulation configuration is based on Dai, Y.C. 2015 “Experiment of Solid Structure Sliding along 45 Degree Slope Bed”, unpublished report. The geometrical scheme is shown in Figure 5-1. The length of the slope bed is 60cm, and the water tank is

6cm wide. The tank is filled with water with the initial water depth of 75cm. The triangular shaped wedge is used in this experiment, the wedge is 5.8cm wide, 10cm long, and 10cm high, with the weight of 359g. There are wheels at the bottom of the wedge to avoid the surface friction.

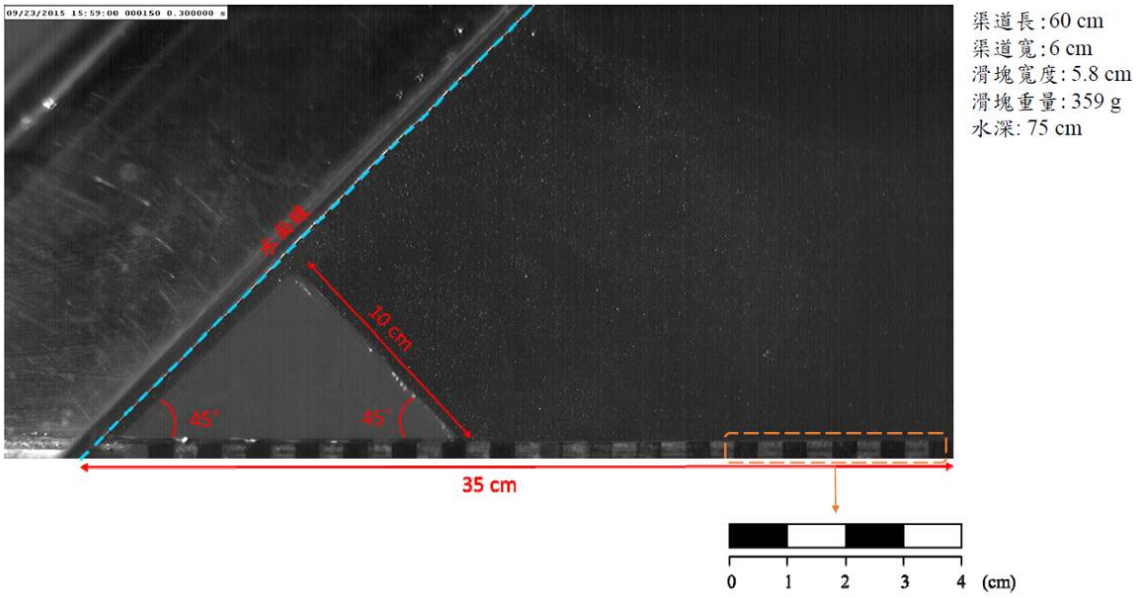

Figure 5-1. Geometrical Scheme of Close to Water Releasing Case (Dai, 2015)

At the beginning, the wedge is placed 0.3cm under the water surface along the slope bed, hold by a string. After cutting the string, the wedge slides along the slop bed due to gravity, no additional force is applied to the wedge. The experiment snapshots are taken by a high speed camera to show the impulse wave, and the velocity of water is studied as well.

5.2.2 Under Water Releasing (Submerged) Case

Similar to close to water releasing case, this case is also submerged. Instead of 0.3cm under water surface before releasing, the wedge is placed 5cm under water surface. All the other conditions are the same as close to water releasing case. Shape of impulse wave and water velocity is also studied in this experiment.

5.2.3 Above Water Releasing (Un-submerged) Case

As it is mentioned in the previous chapter, landslide can be defined into two categories: submerged and un-submerged. Both close to water releasing and under water releasing cases are submerged. In order to fully study the property of impulse wave and water field velocity generated by non-deformable landslide, an un-submerged case is needed. In this experiment, the wedge is placed along the 45 degree slope bed right above the water surface. The other conditions are also the same as close to water releasing case, which is described in 5.2.1.

5.3 Results and Comparisons

5.3.1 Close to Water Releasing (Submerged) Case

In this case, the MPS simulation is conduct in a two-dimensional domain; the particle size is set to 0.005m, which gives the total particle number of 187,562 during the simulation. A series of experimental snapshots of the impulse wave of this case is

provided in Figure 5-2 up to 0.9s after releasing the wedge. Parameter t_0 is the initial time for cutting the string.

From the snapshots, the development of impulse wave can be viewed clearly, and the MPS simulation of impulse wave will be compared with the experimental data.

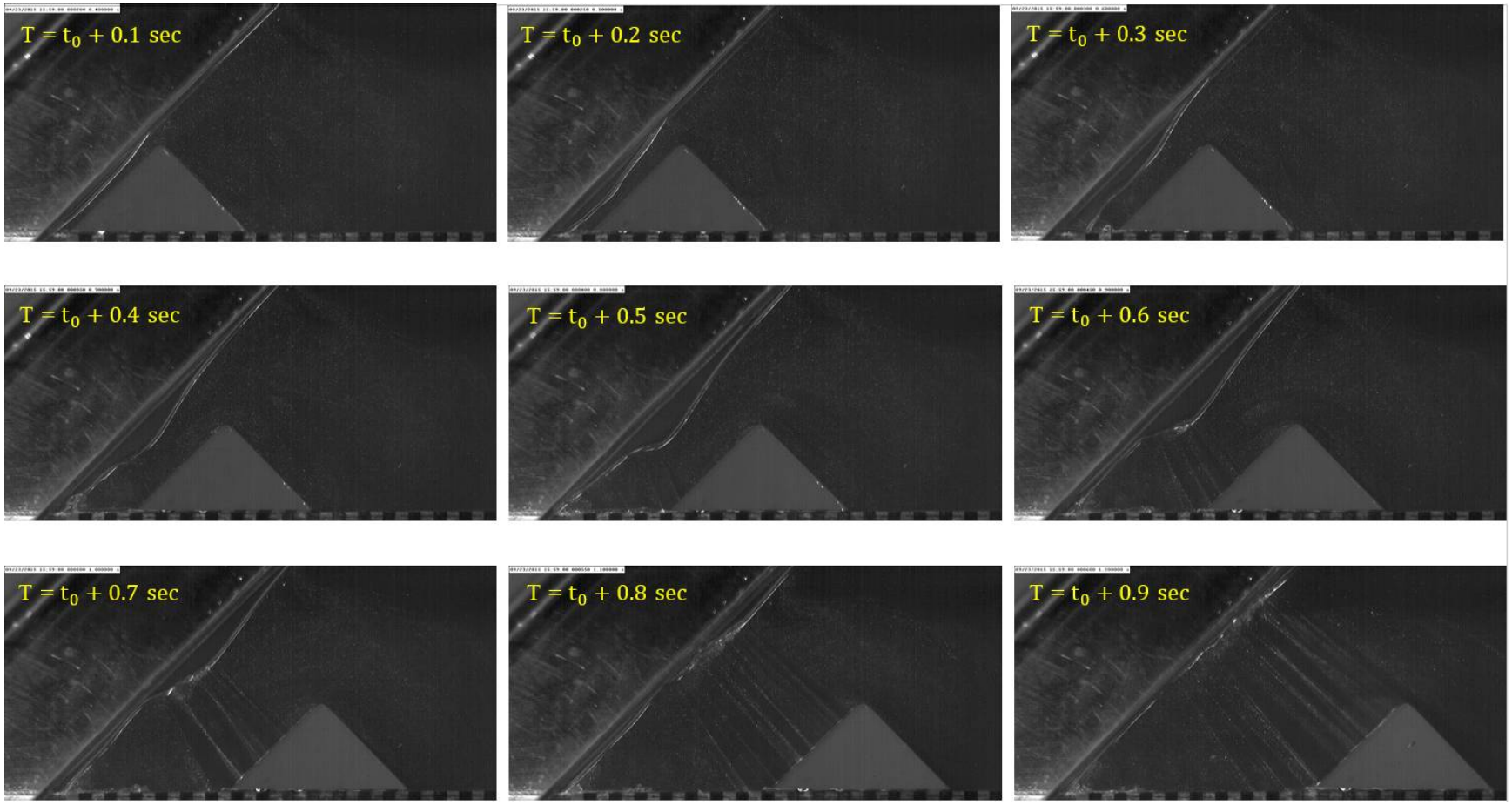

Figure 5-2. Experimental Snapshots of Impulse Wave for Close to Water Releasing Case

To compare the water surface between MPS simulation method and Experimental data, a geometrical scheme of coordinate is shown in Figure 5-3, all the water surface comparisons are based on this coordinate.

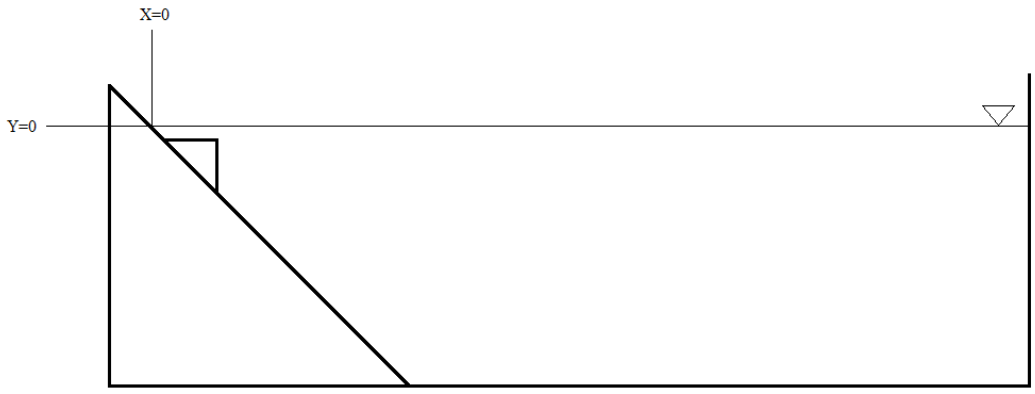

Figure 5-3. Coordinate for Water Surface Comparison

The comparison of impulse wave between MPS simulation results and experimental data are from 0.1s to 0.9s after releasing the wedge, with the time step of 0.1s. The comparison results are shown in Figure 5-4.

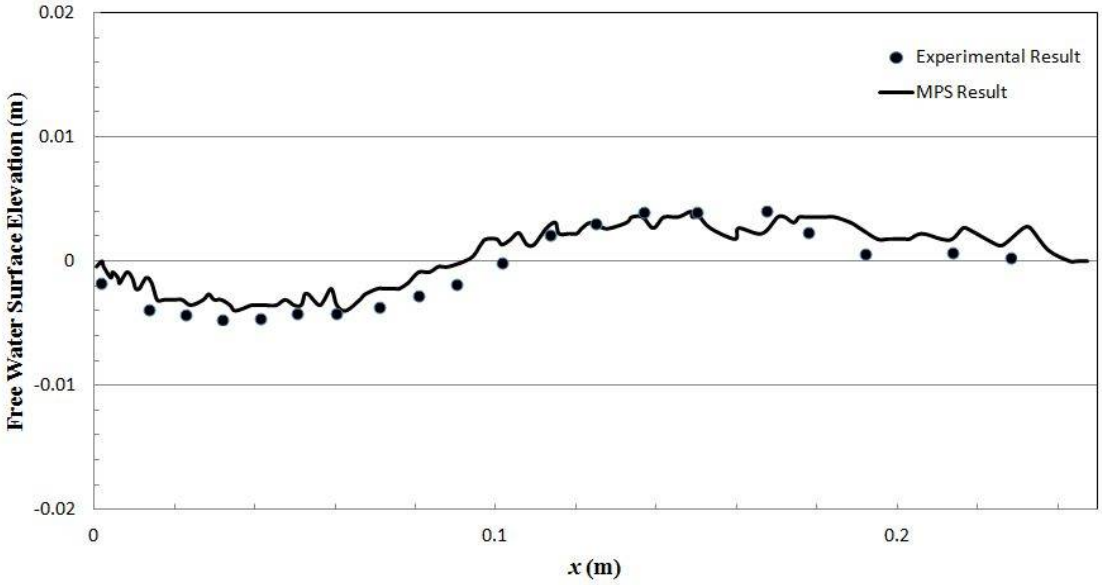
0.02
0.01
0
-0.01
-0.02
Free Water Surface Elevation (m)
0
0.1
0.2
x (m)
Experimental Result
MPS Result

(a) t=0.1s

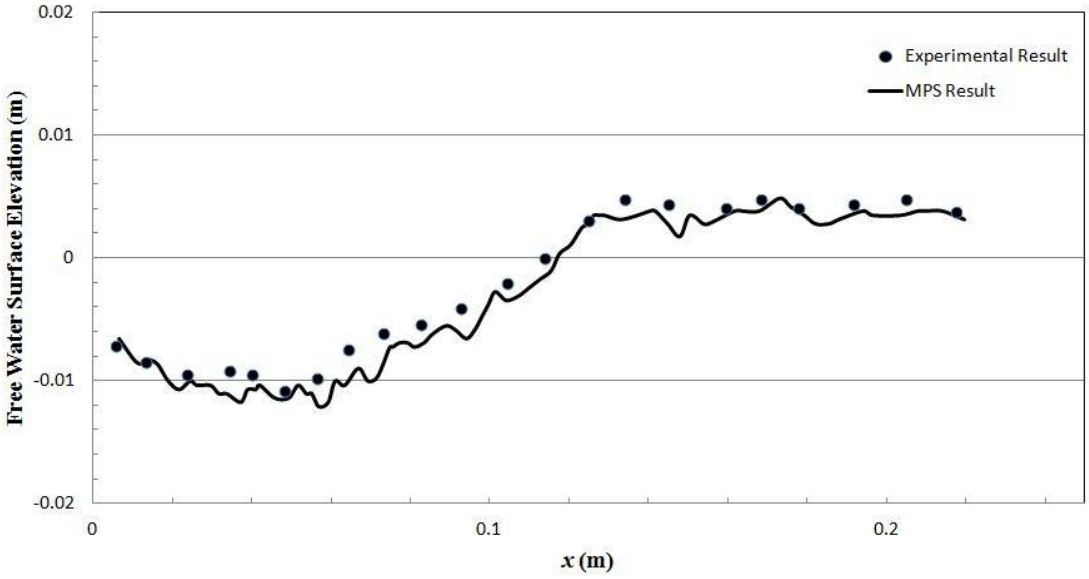
0.02
0.01
0
-0.01
-0.02
Free Water Surface Elevation (m)
0
0.1
0.2
x (m)
Experimental Result
MPS Result

(b) t=0.2s

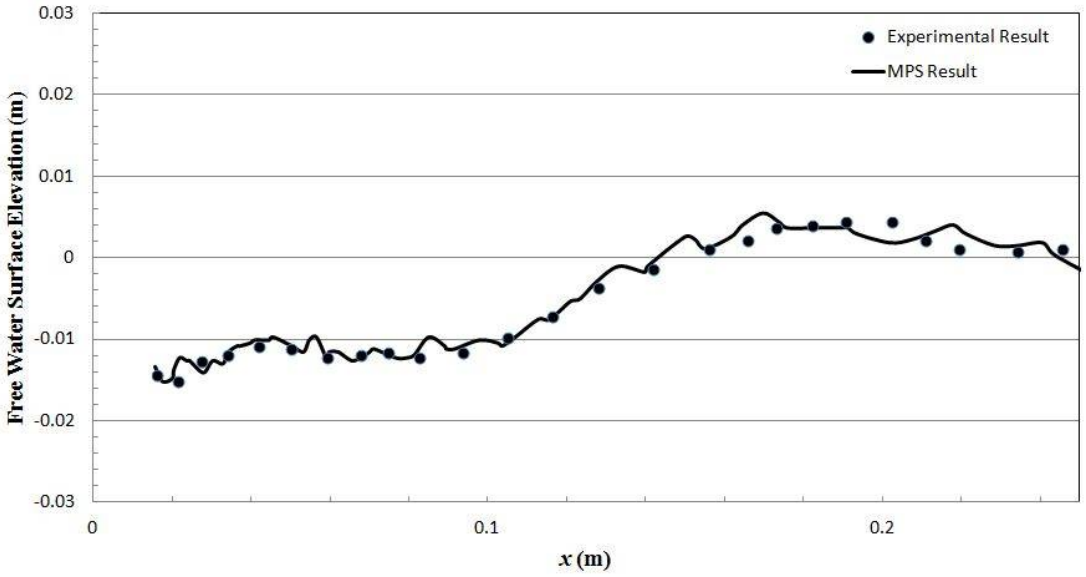
Experimental Result
MPS Result
Free Water Surface Elevation (m)
0.03
0.02
0.01
0
-0.01
-0.02
-0.03
0
0.1
0.2
x (m)

(c) t=0.3s

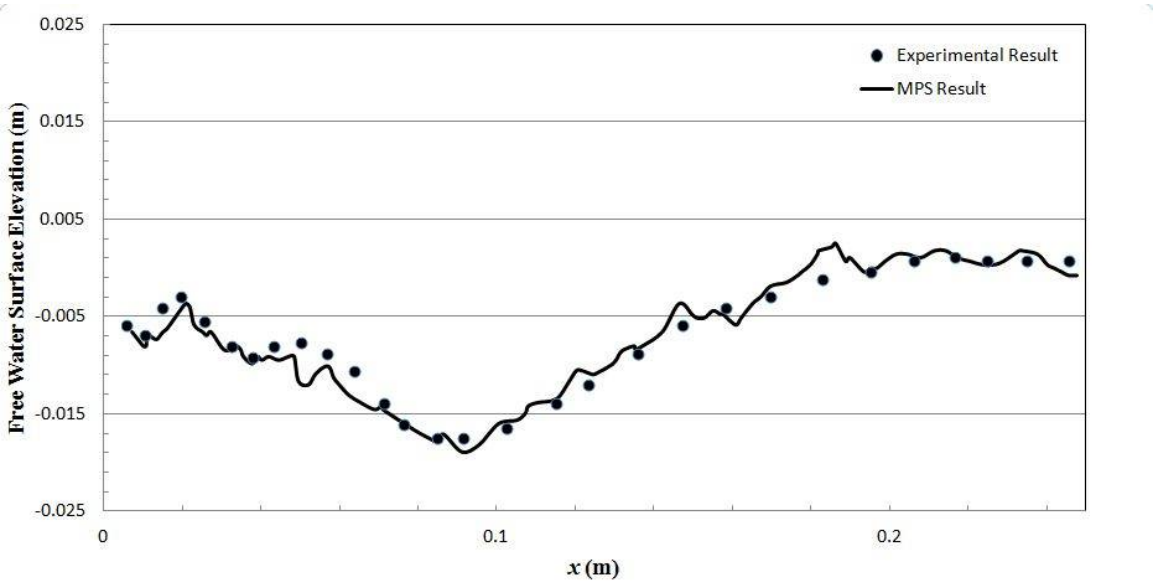
Experimental Result
MPS Result
Free Water Surface Elevation (m)
0.025
0.015
0.005
-0.005
-0.015
-0.025
0
0.1
0.2
x (m)

(d) t=0.4s

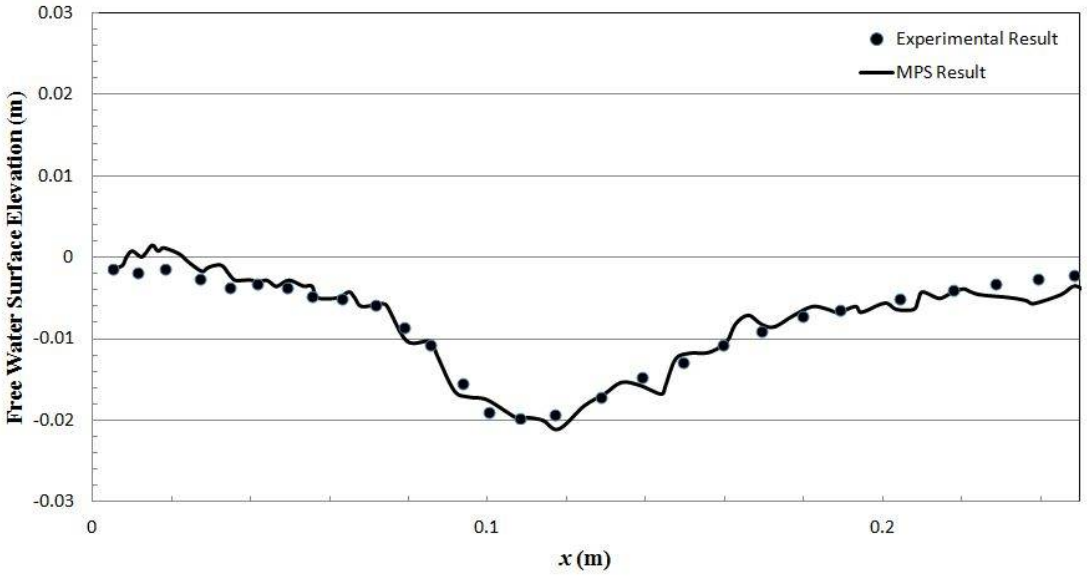
Experimental Result
MPS Result
Free Water Surface Elevation (m)
0.03
0.02
0.01
0
-0.01
-0.02
-0.03
0
0.1
0.2
x (m)

(e) t=0.5s

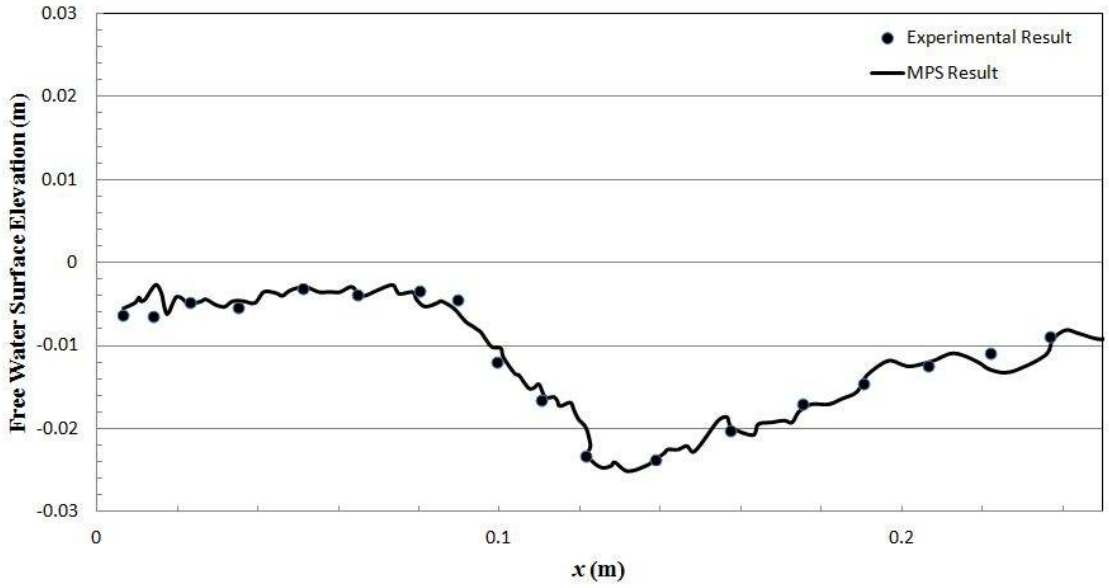
Experimental Result
MPS Result
Free Water Surface Elevation (m)
0.03
0.02
0.01
0
-0.01
-0.02
-0.03
0
0.1
0.2
x (m)

(f) t=0.6s

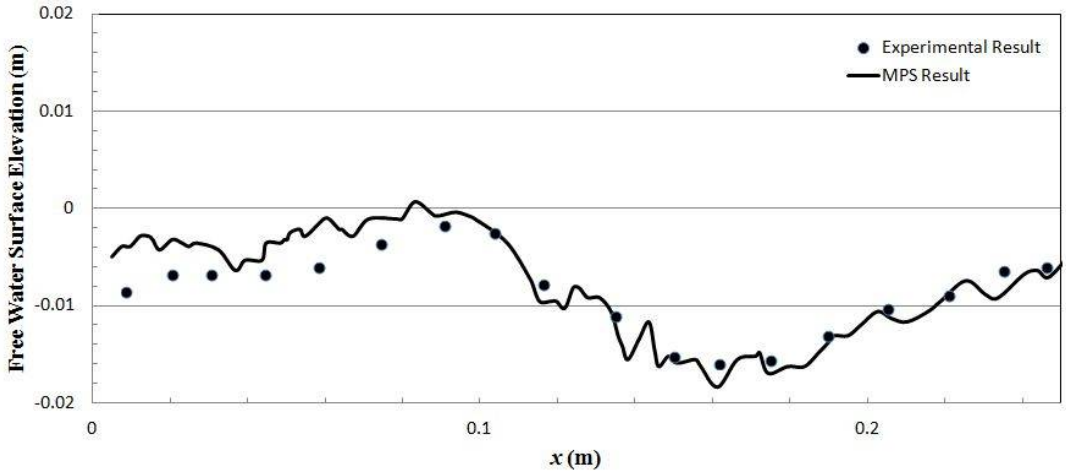
Experimental Result
MPS Result
Free Water Surface Elevation (m)
0.02
0.01
0
-0.01
-0.02
0
0.1
0.2
x (m)

(g) t=0.7s

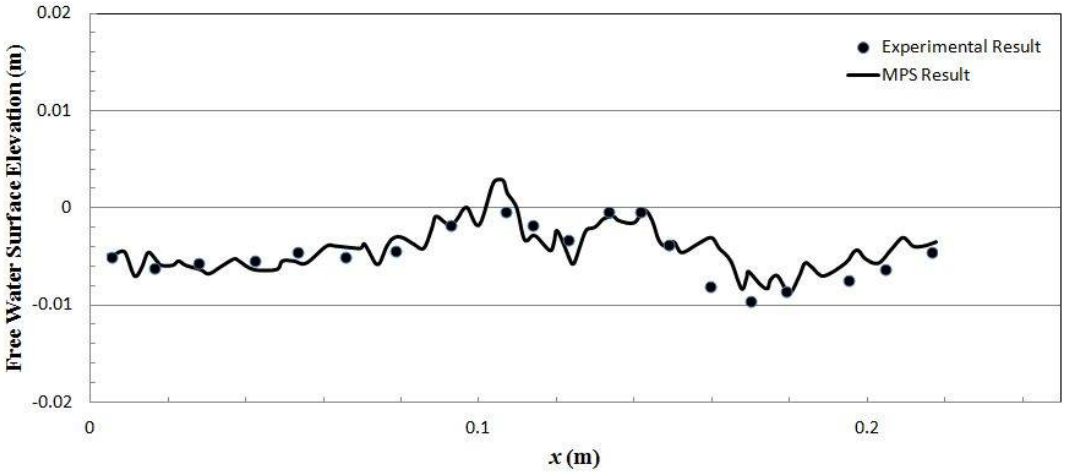
Experimental Result
MPS Result
Free Water Surface Elevation (m)
0.02
0.01
0
-0.01
-0.02
0
0.1
0.2
x (m)

(h) t=0.8s

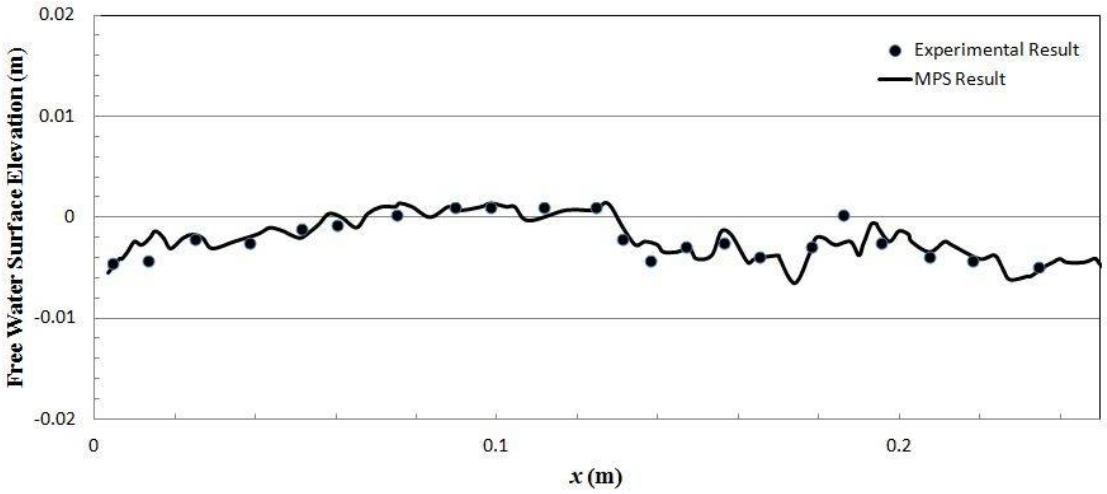

(i) t=0.9s

Figure 5-4. Impulse Wave Comparison for Close to Water Releasing Case at Different Time Steps

Besides the comparison of impulse wave, a detailed water field velocity is also compared. The velocity comparison is mainly focused on the area around the wedge, especially above the wedge. To compare the detailed velocity, another coordinate is introduced in Figure 5-5, and this coordinate is used for all velocity comparisons in the other two cases, which will be discussed later. In this coordinate, X=0 is located at the left top corner of the wedge and changes with the time along the movement of the wedge, and Y=0 located at the initial water surface and remain the same during the whole process of the simulation.

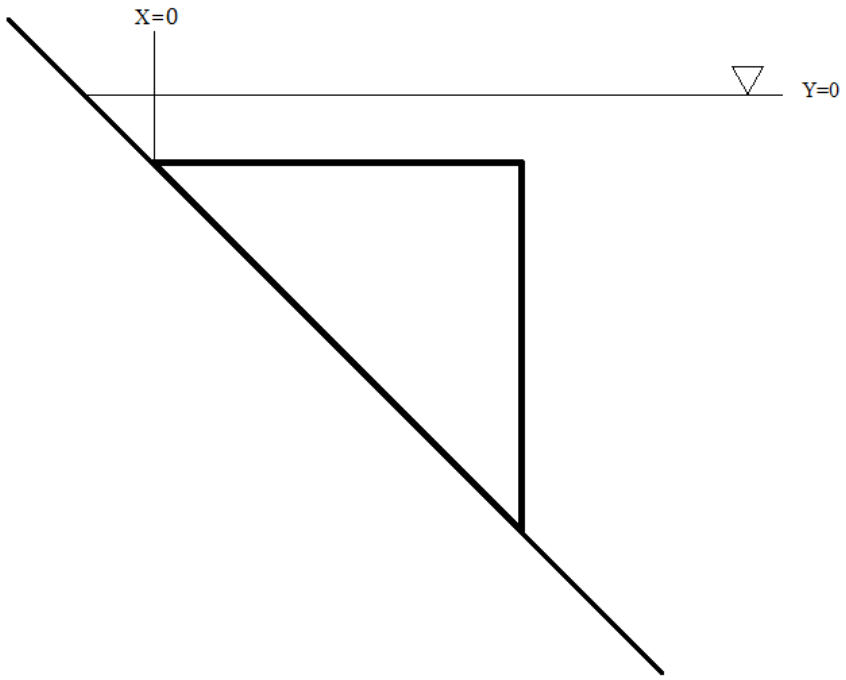

Figure 5-5. Coordinate for Detailed Velocity Comparison

In the comparison, four different locations are considered, which are X=0 (left up corner of the wedge), X=4cm (4cm right to the left up corner of the wedge), X=7cm (7cm right to the left up corner of the wedge), and X=11cm (1cm right to the wedge). The velocity is compared on the cross section at those four locations at 0.1s, 0.3s, and 0.5s with time step of 0.1s. It is worth to be mentioned that the detailed velocity is compared in both X and Y directions separately. The comparison results for both X direction and Y direction at 0.1s are shown in Figure 5-6, and Figure 5-7. As it is mentioned, the detailed velocity comparison is at 0.1s, 0.3s, and 0.5s, the rest comparison results are shown in appendix A.

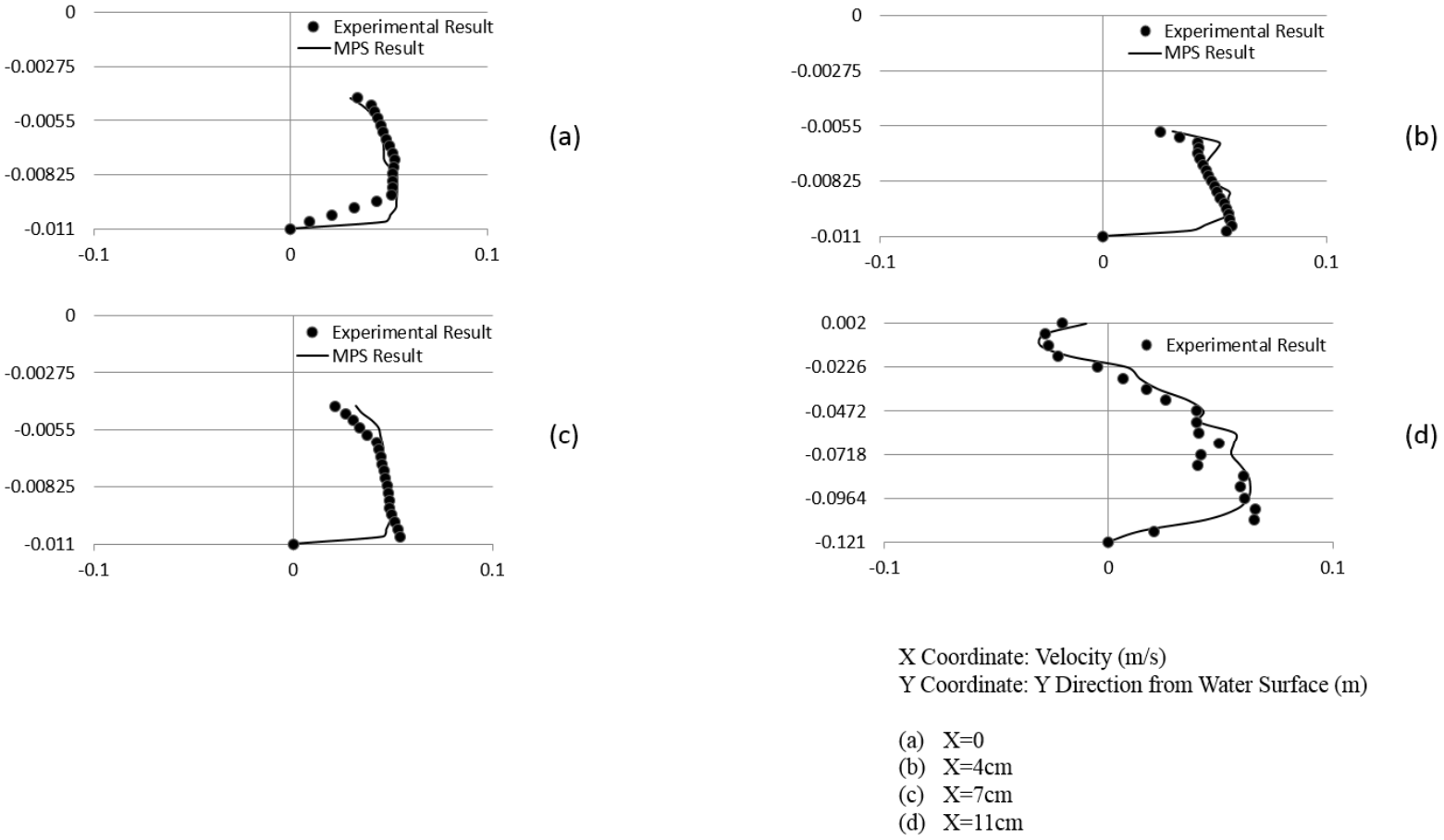

Figure 5-6. Detailed Velocity Comparison of X direction Velocity *u* at 0.1s for Close to Water Releasing Case

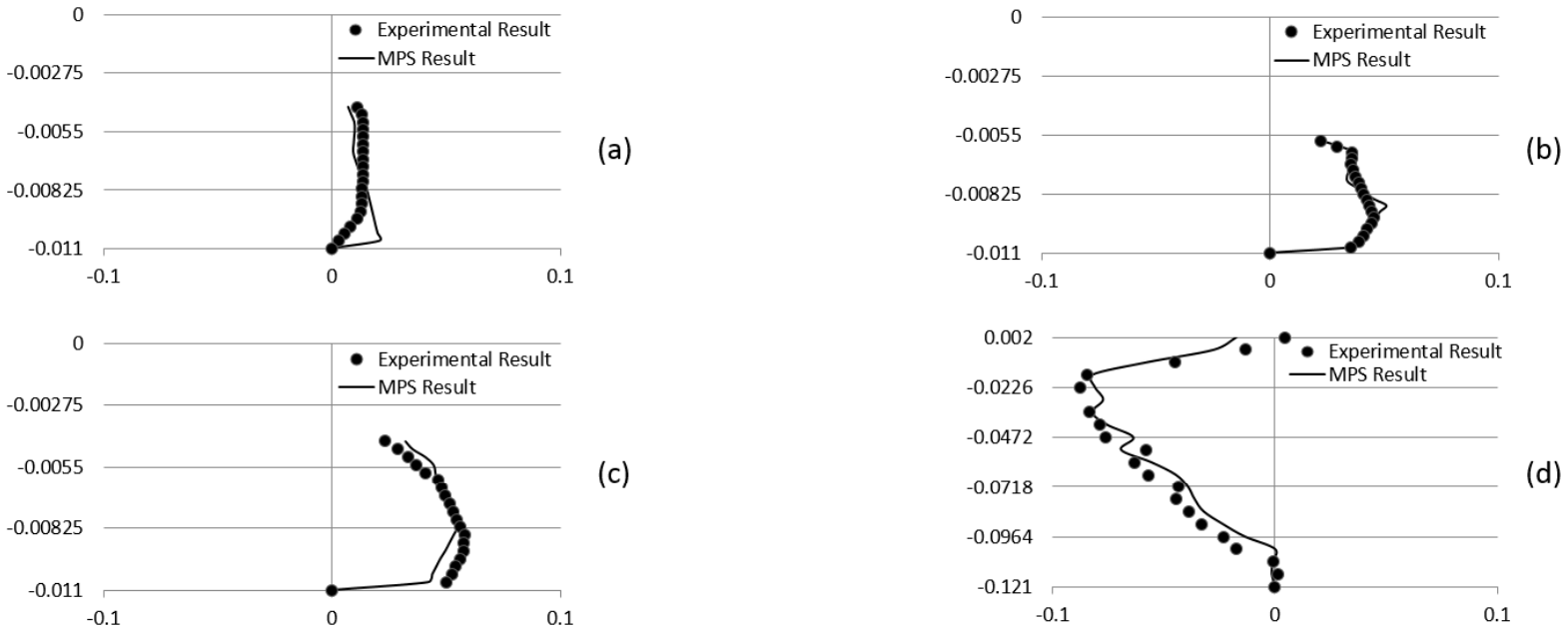

Figure 5-7. Detailed Velocity Comparison of Y Direction Velocity *v* at 0.1s for Close to Water Releasing Case

From the comparison results, both water surface and velocity show a good agreement with the experimental data, also from the velocity profile, it can be found that the circulation of water can also be simulated by MPS method.

5.3.2 Under Water Releasing (Submerged) Case

The experiment setup for this case is described in section 5.2, the MPS simulation is similar to the close to water releasing case. In this case, since the wedge is relatively far from the water surface, the change of water surface is not significant, therefore, this case is focused on the velocity comparison. As it is mentioned above, the coordinate of setting comparison sections is also like Figure 5-5. Different than the close water releasing case, five sections are used to compare the velocity profiles, which are X=0, X=4cm, X=7cm, X=10cm, and X=11cm. The simulation time for this case is extended to 1s, and the velocity is compared every 0.1s for every section. Due to the lack of experimental data, at 1s after releasing the wedge, the velocity at X=11cm is not compared. Similar to the previous case, the used particle size is 0.005m, and total of 187563 particles. The following figures show the velocity comparison results at different time steps. Figure 5-8 shows the vector file around the sliding wedge at 0.4s after releasing, from the figure, the circulation of water at the up right corner of the wedge can be seen clearly.

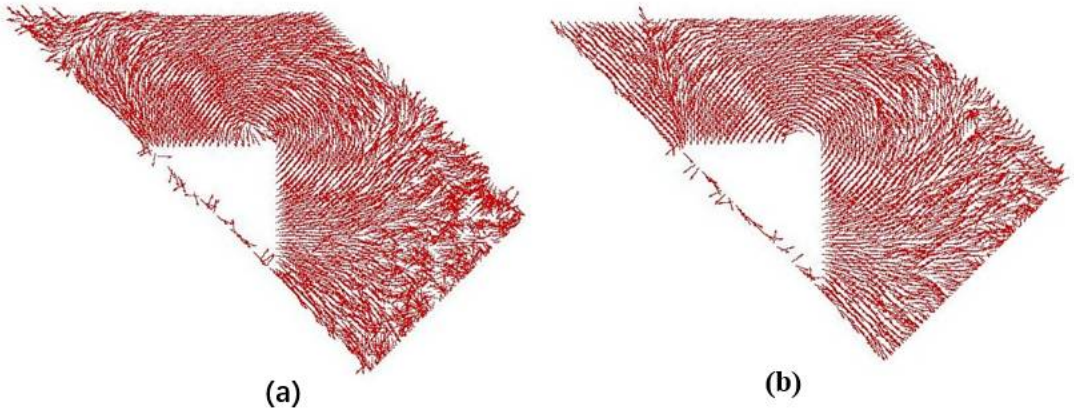

Vector Scale: → 0.5m/s

(a) Vector from MPS Method
(b) Vector from Experimental Result

Figure 5-8. Vector File of Water Field Around the Sliding Wedge at 0.4s for Under Water Releasing Case

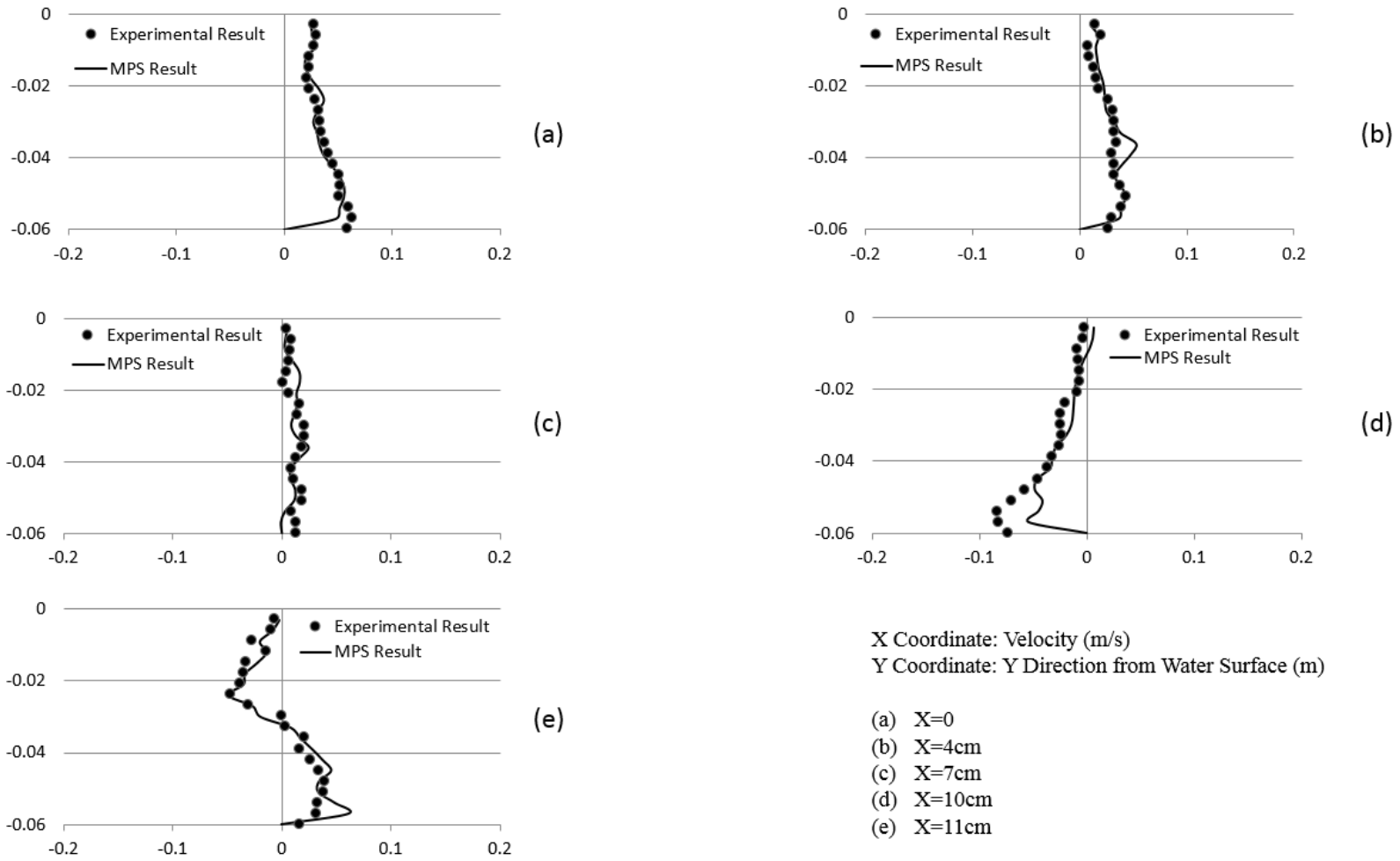

Figure 5-9. Detailed Velocity Comparison of Direction Velocity *u* at 0.1s for Under Water Releasing Case

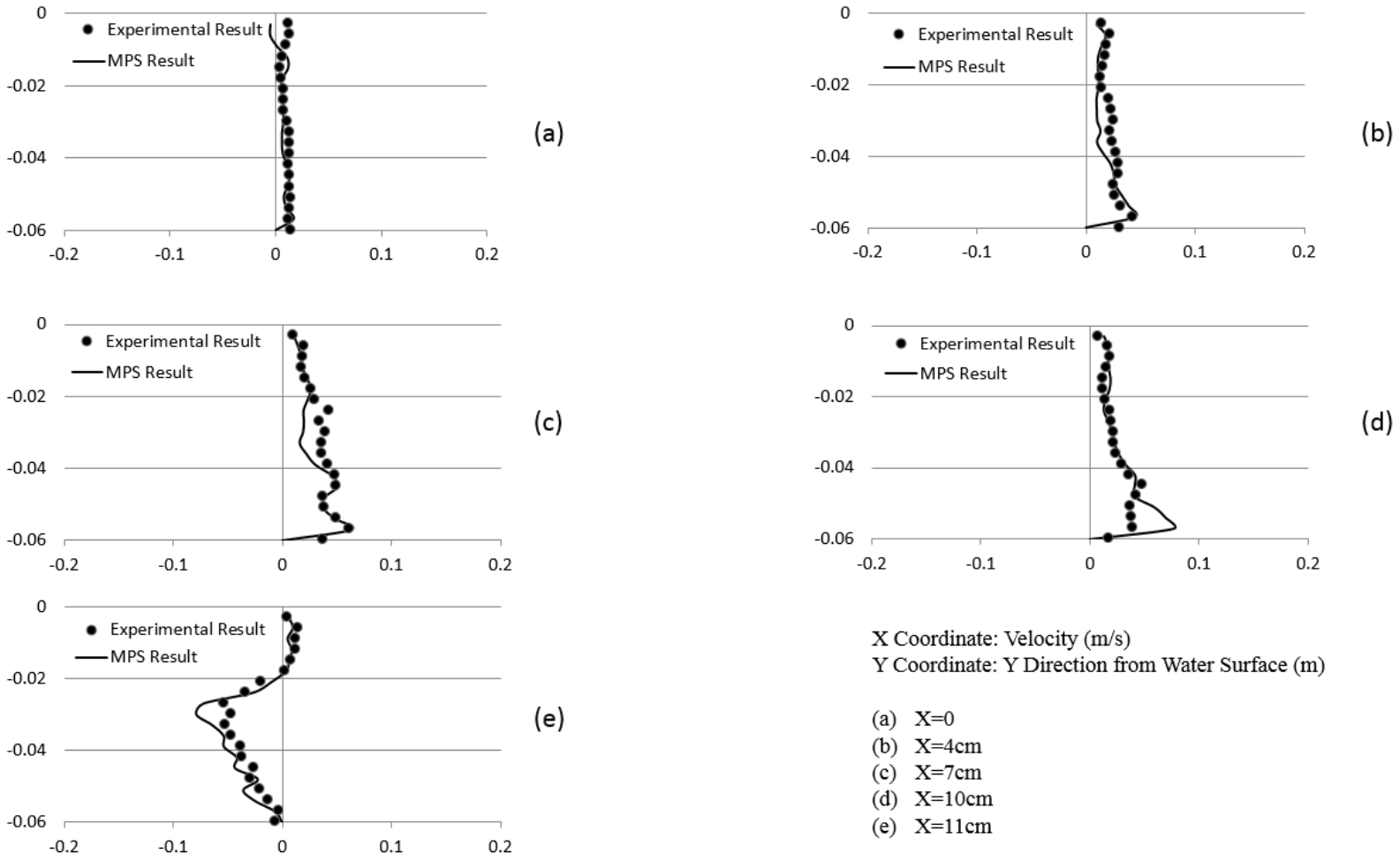

Figure 5-10. Detailed Velocity Comparison of Direction Velocity *v* at 0.1s for Under Water Releasing Case

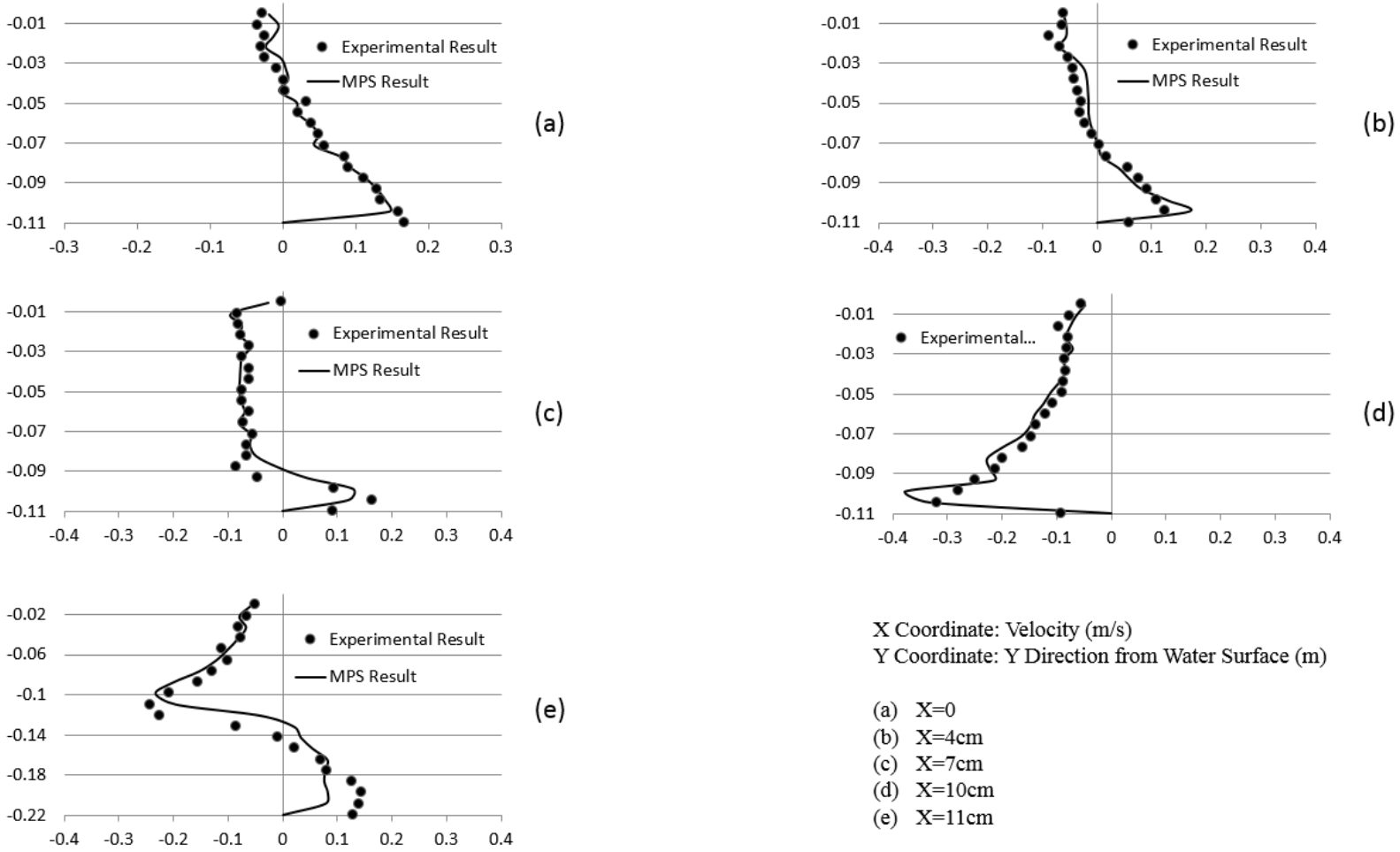

Figure 5-11. Detailed Velocity Comparison of Direction Velocity *u* at 0.5s for Under Water Releasing Case

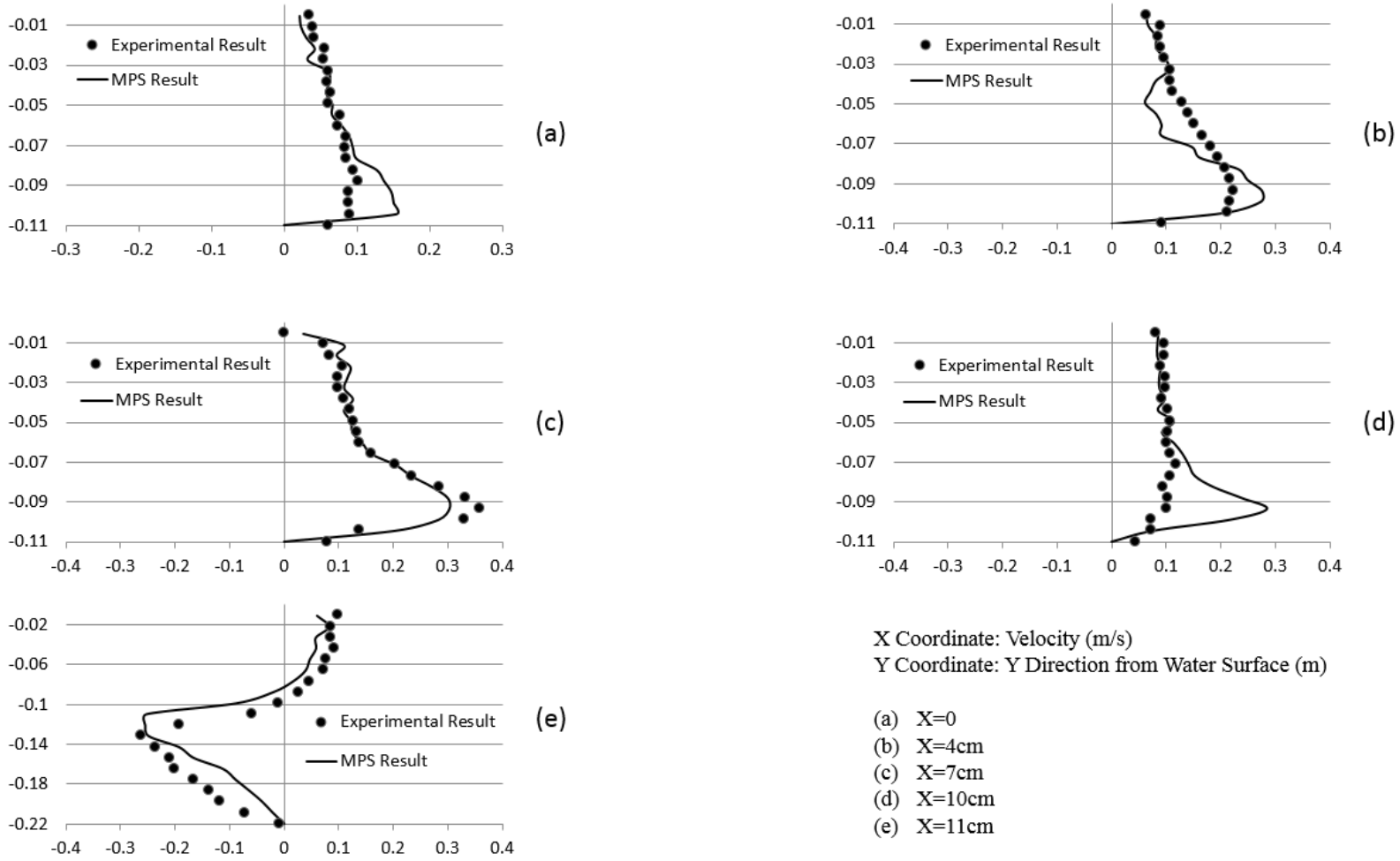

Figure 5-12. Detailed Velocity Comparison of Direction Velocity *v* at 0.5s for Under Water Releasing Case

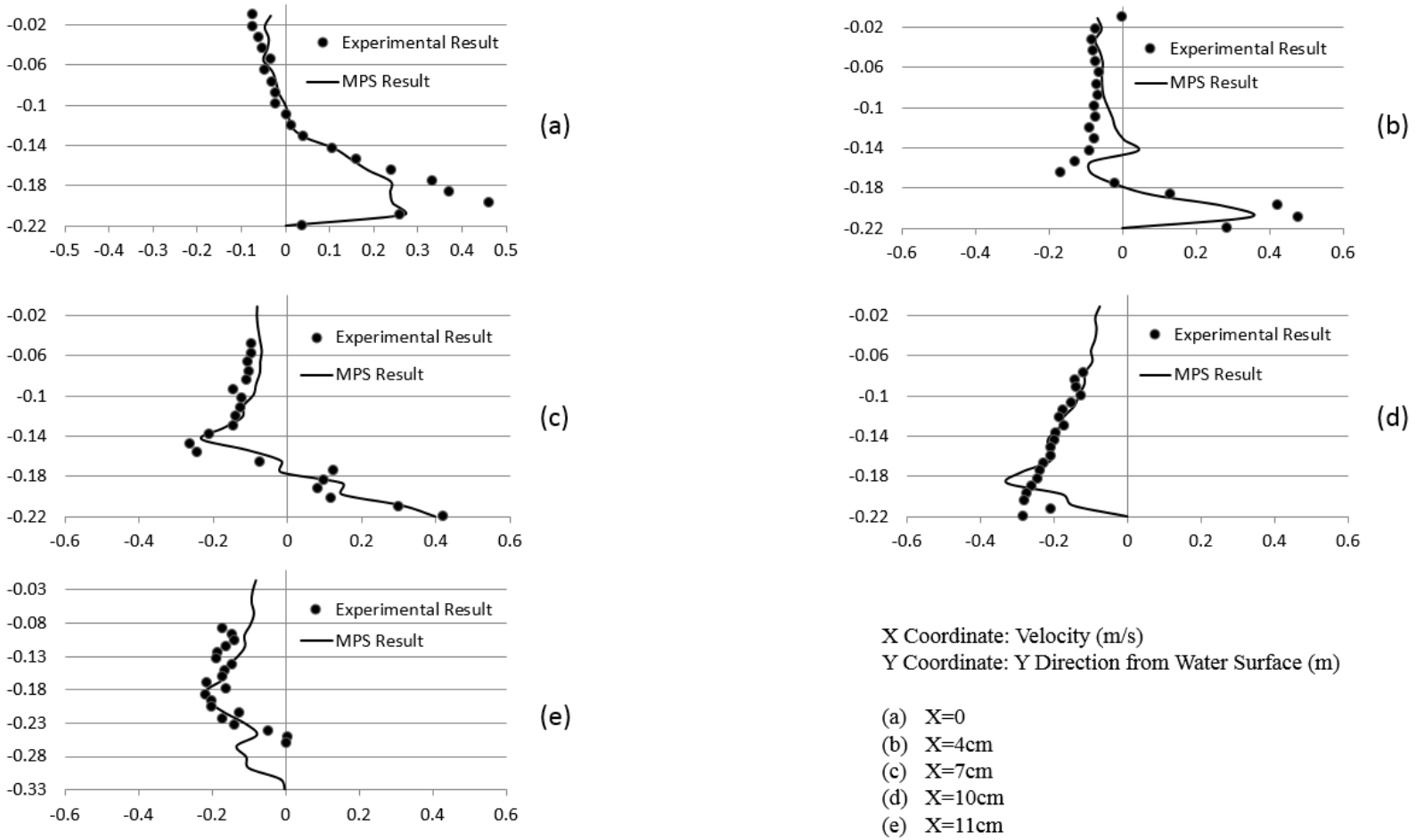

Figure 5-13. Detailed Velocity Comparison of Direction Velocity *u* at 0.9s for Under Water Releasing Case

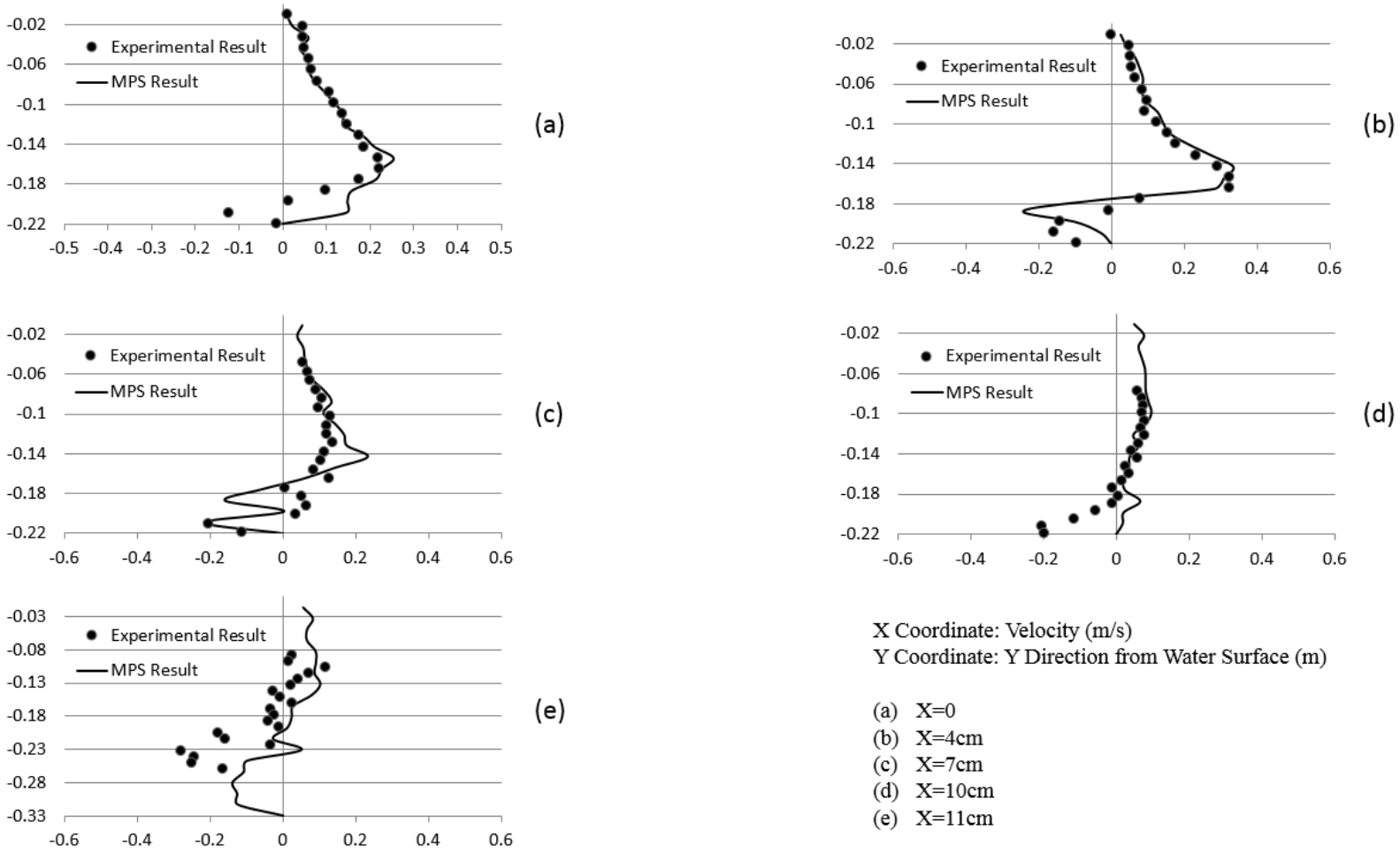

Figure 5-14. Detailed Velocity Comparison of Direction Velocity *v* at 0.9s for Under Water Releasing Case

The velocity comparison results of 0.1s, 0.5s, and 0.9s are shown above, the rest comparison results are provided in Appendix B. As it can be seen from figures, the velocity result simulated by MPS method is similar to the experimental results.

As stated before, landslide cases can be divided into two groups: submerged and un-submerged. To test the capability of simulating impulse wave generated by landslide, the un-submerged landslide case is also need to be studied.

5.3.3 Above Water Releasing (Un-submerged) Case

Compare to submerged landslide, un-submerged landslide will create large deformations and fragmentations on the water surface. The high impact speed will also lead to a severe impact wave, which makes the un-submerged landslide is more difficult to simulate. In this study, a WC-MPS method is created to simulate the experimental case explained in previous section, both impulse wave and water velocity are compared with the real experimental data. In this case, the wedge is placed right above the water surface along the slope bed, once the wedge is released, it will sliding down by its own gravity, and the impact between wedge and water will happen. The particle size for this case is 0.005m, and total particle number is 196562. Some snapshots from the experiment are shown in Figure 5-11. Coordinates from section 5.3.1 are also used in this case.

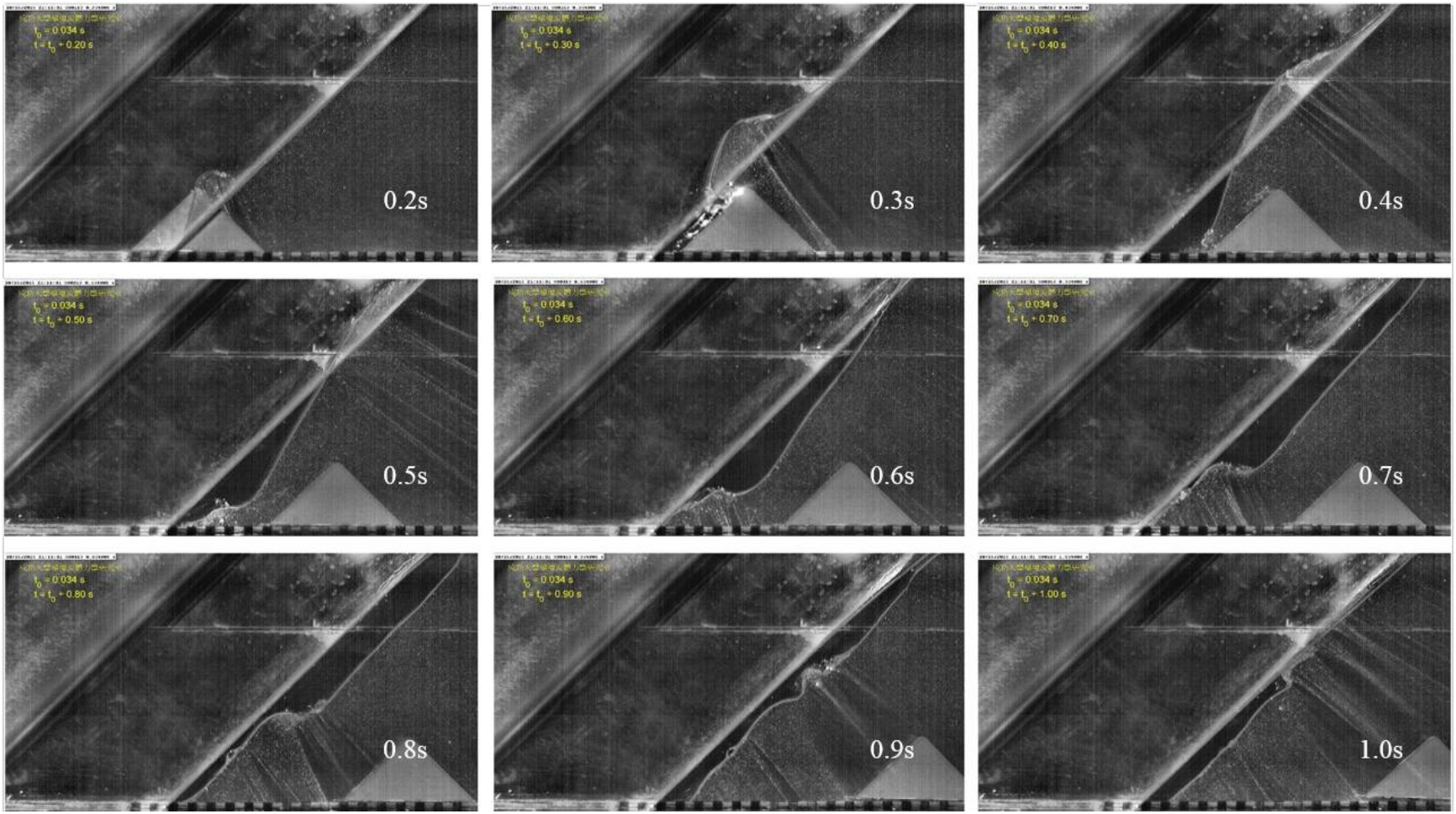

Figure 5-15. Experimental Snapshots of Impulse Wave for Under Water Releasing Case

From the snapshots, fluctuation and large deformation of the water surface can be seen, which is more difficult to be simulated. The simulation result given by WC-MPS method of water surface is compared to the experimental data from 0.2s to 1.1s, and shown in Figure 5-12.

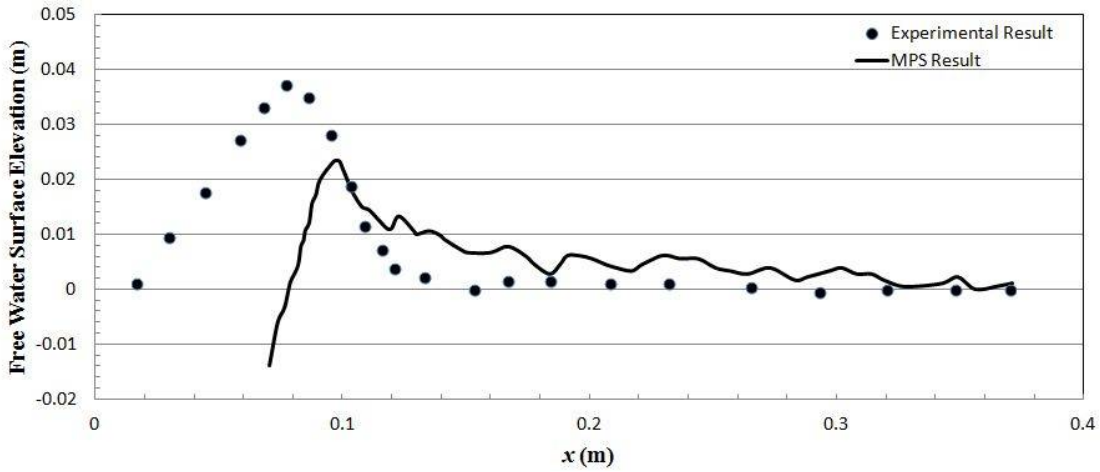

(a) t=0.2s

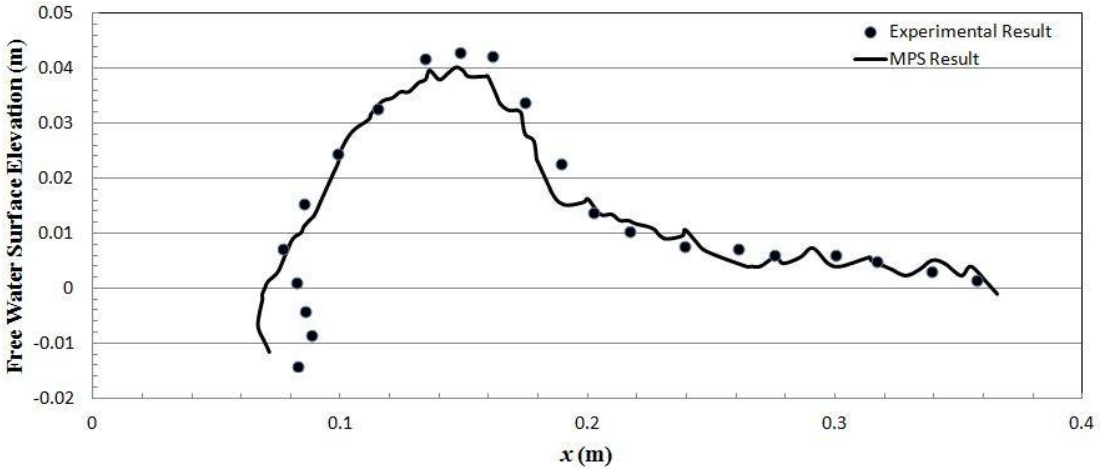

(b) t=0.3s

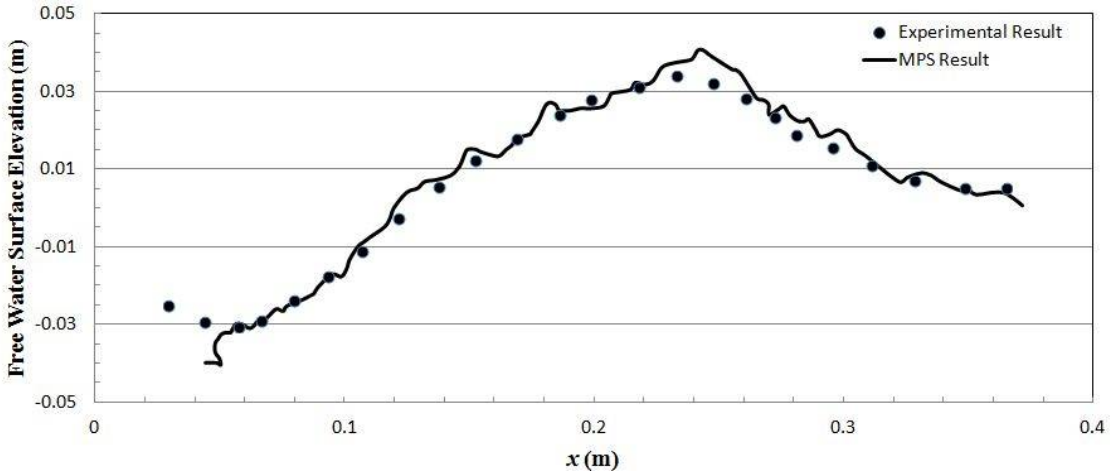
Experimental Result
MPS Result
Free Water Surface Elevation (m)
0.05
0.03
0.01
-0.01
-0.03
-0.05
0
0.1
0.2
0.3
0.4
x (m)

(c) t=0.4s

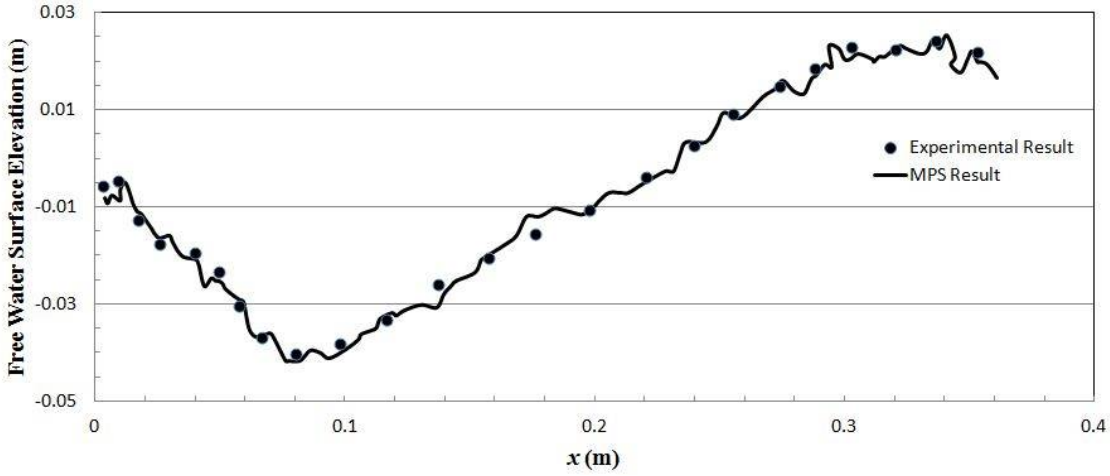
Experimental Result
MPS Result
Free Water Surface Elevation (m)
0.03
0.01
-0.01
-0.03
-0.05
0
0.1
0.2
0.3
0.4
x (m)

(d) t=0.5s

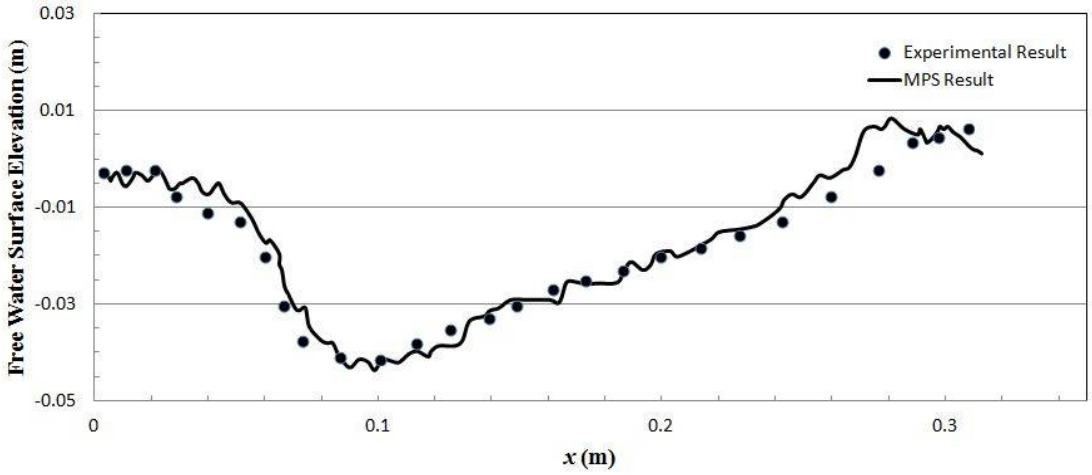
Experimental Result
MPS Result
Free Water Surface Elevation (m)
0.03
0.01
-0.01
-0.03
-0.05
0
0.1
0.2
0.3
x (m)

(e) t=0.6s

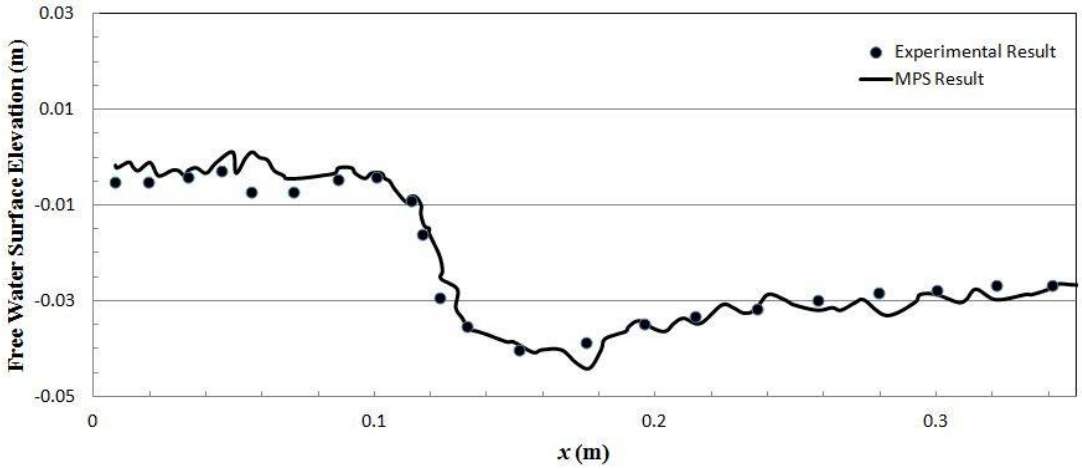
Experimental Result
MPS Result
Free Water Surface Elevation (m)
0.03
0.01
-0.01
-0.03
-0.05
0
0.1
0.2
0.3
x (m)

(f) t=0.7s

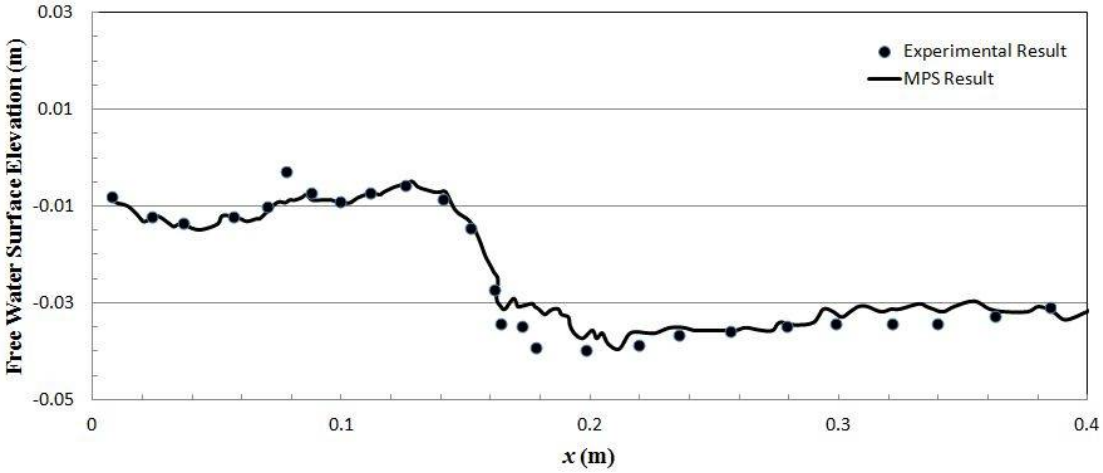
Experimental Result
MPS Result
Free Water Surface Elevation (m)
0.03
0.01
-0.01
-0.03
-0.05
0
0.1
0.2
0.3
0.4
x (m)

(g) t=0.8s

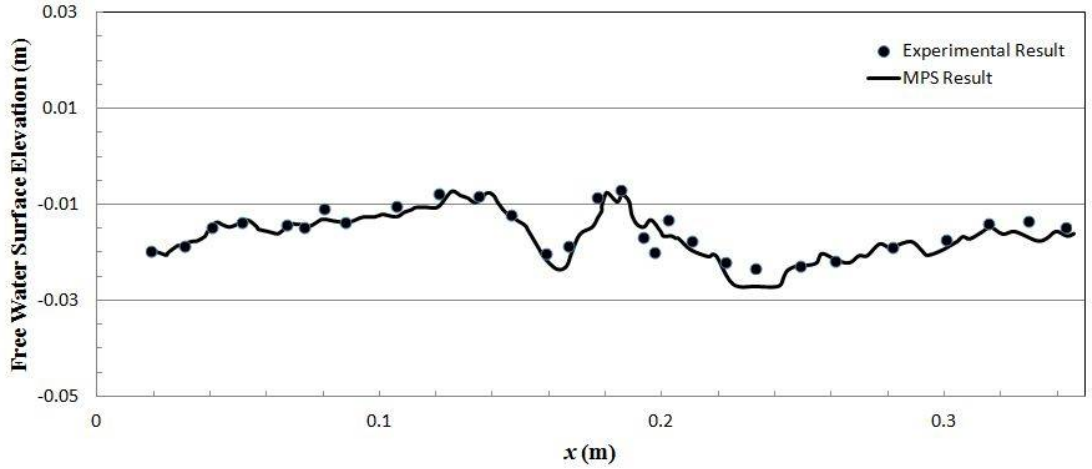
Experimental Result
MPS Result
Free Water Surface Elevation (m)
0.03
0.01
-0.01
-0.03
-0.05
0
0.1
0.2
0.3
x (m)

(h) t=0.9s

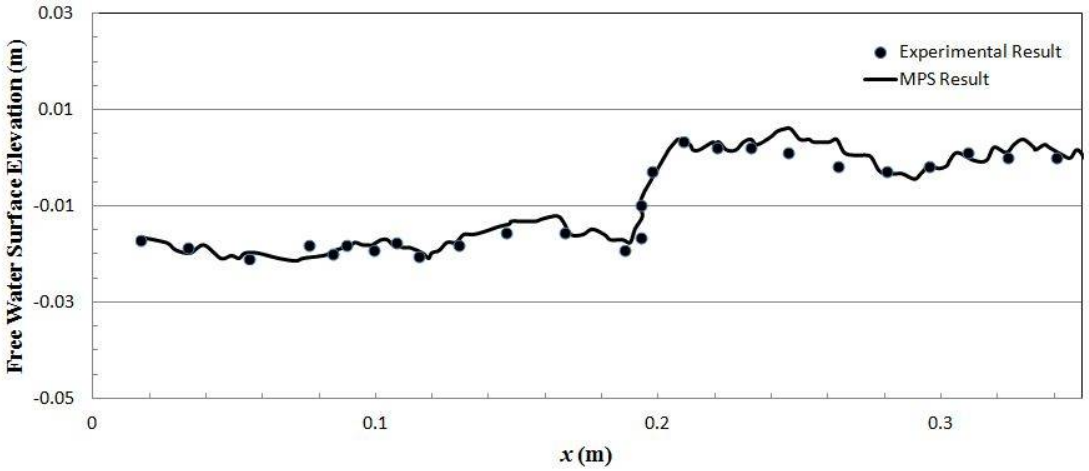

(i) t=1.0s

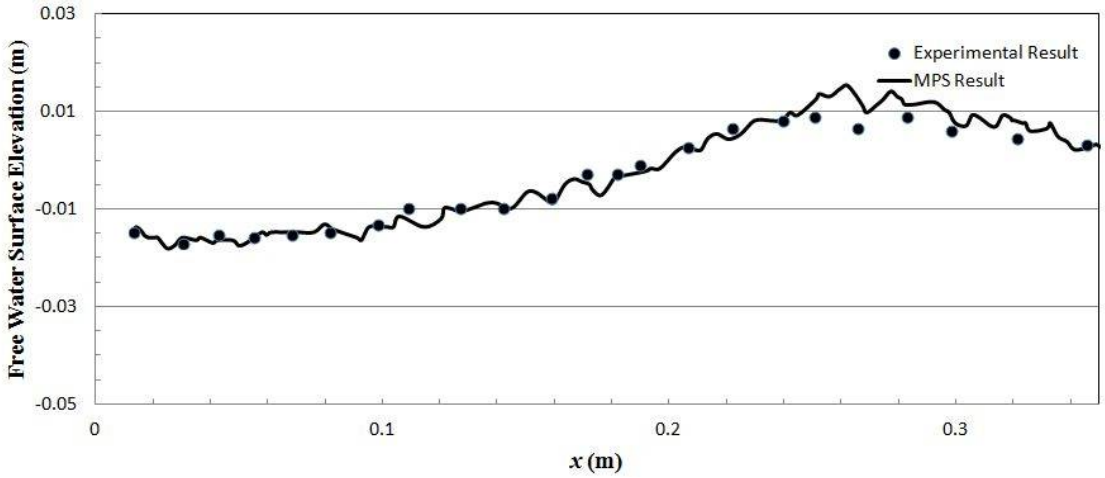

(j) t=1.1s

Figure 5-16. Impulse Wave Comparison for Above Water Releasing Case at Different Time Steps

By comparing the water surface, it is obviously that WC-MPS method is able to simulate the landslide cases with large deformations and fragmentations. For comparison result (a) in Figure 5-16, the difference between simulation result and experimental result between x=0 and x=0.1 is because of the water got into the wedge in the experimental snapshot, which can be seen in Figure 5-15, photo at 0.2s.

For detailed velocity comparison, five different cross section are included, which are X=0, X=4cm, X=7cm, X=11cm, and X=13cm. Also, velocities along X direction and Y direction are compared separately. The compared time steps are 0.1s, 0.2s, 0.4s, and0.5s. Because of the wedge is released above water surface, and it is not fully into the water until 0.4s after releasing, only sections at X=11cm, and X=13cm are compared for 0.1s, and 0.2s. The comparison results are shown in the following figures.

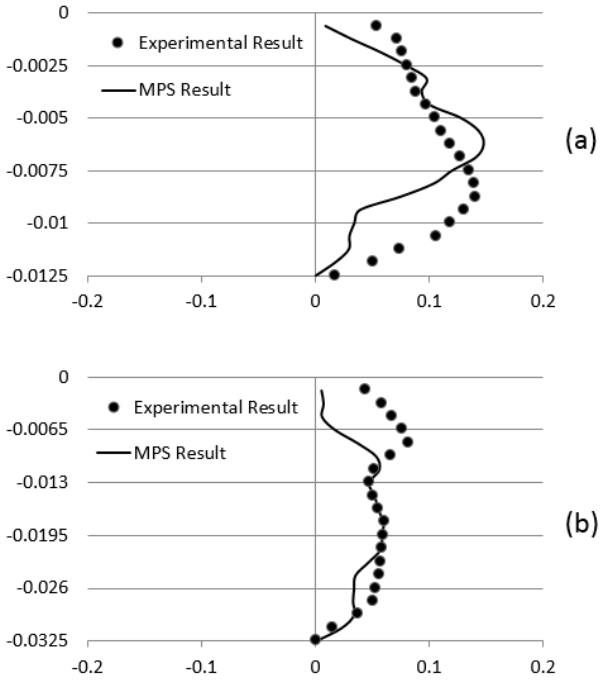

X Coordinate: Velocity (m/s)
Y Coordinate: Y Direction from Water Surface (m)

(a) X=11cm
(b) X=13cm

Figure 5-17. Detailed Velocity Comparison of X Direction Velocity *u* at 0.2s for Above Water Releasing Case

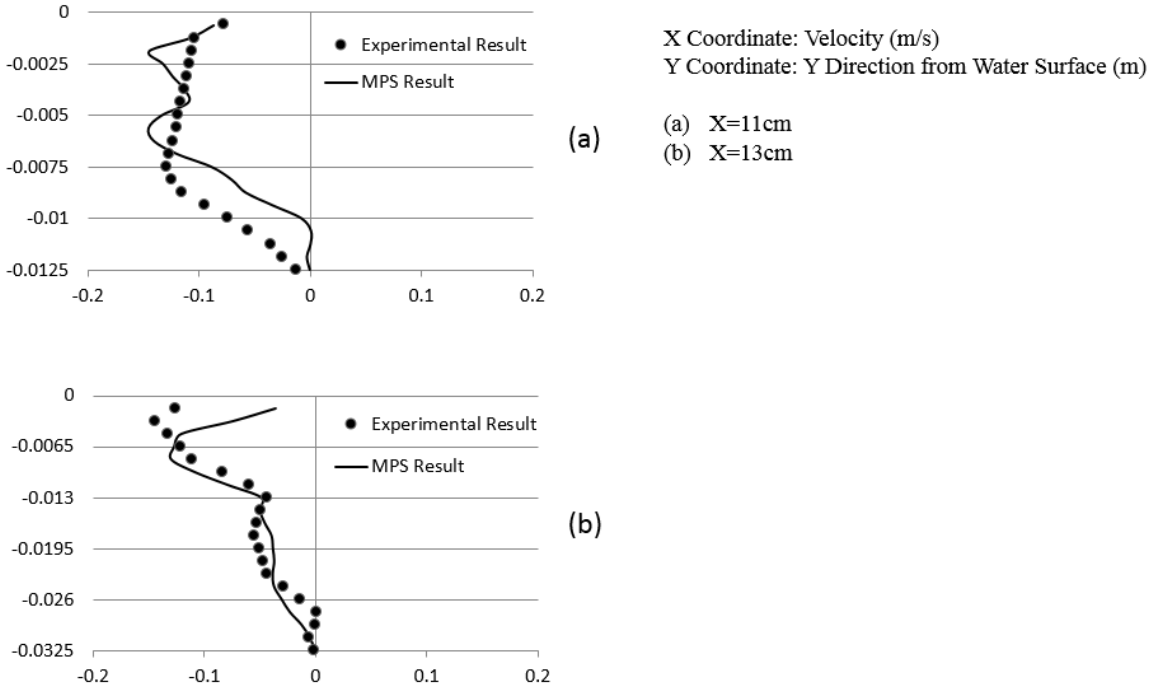

Figure 5-18. Detailed Velocity Comparison of Y Direction Velocity *v* at 0.2s for Above Water Releasing Case

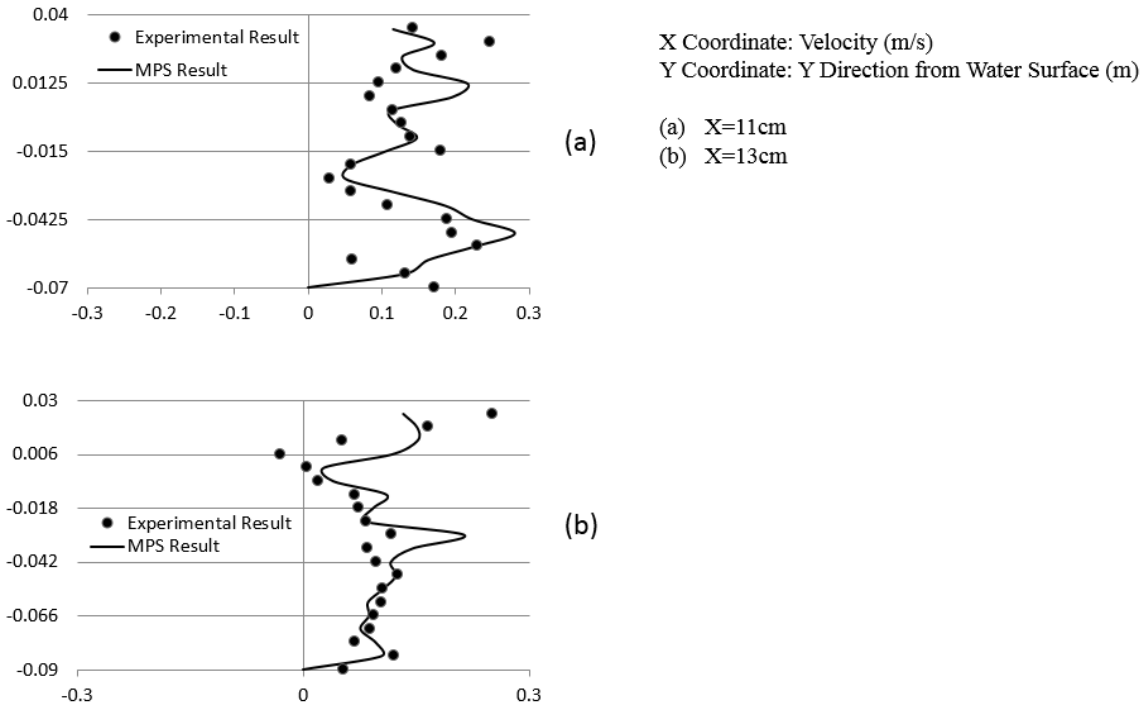

Figure 5-19. Detailed Velocity Comparison of X Direction Velocity *u* at 0.3s for Above Water Releasing Case

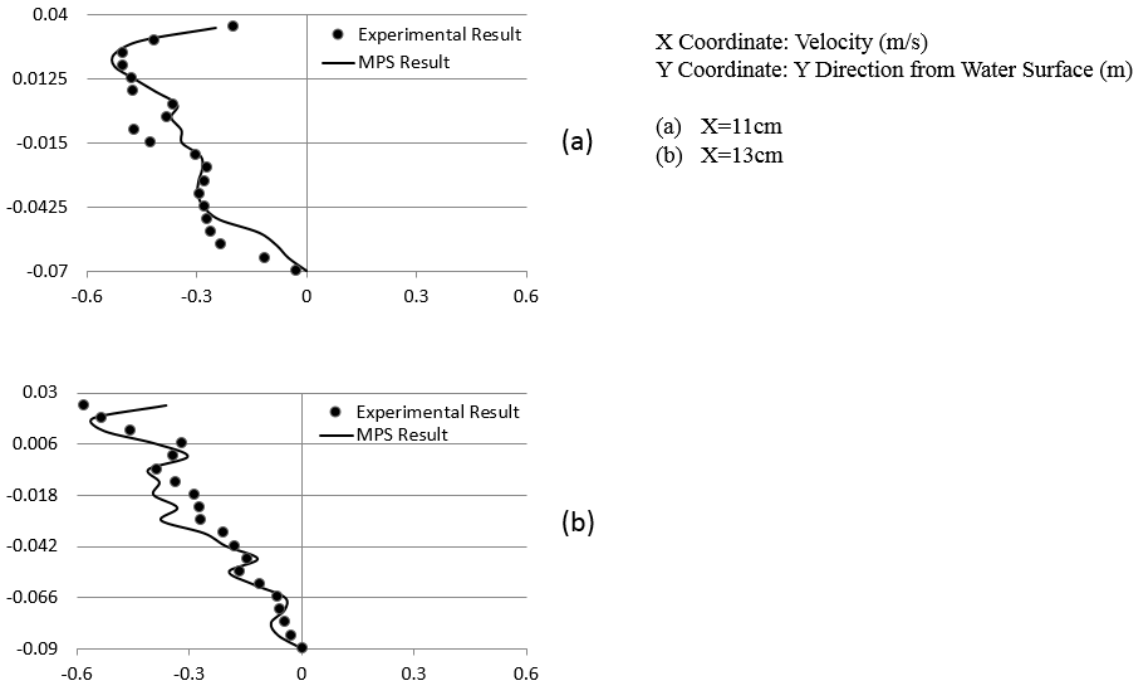

Figure 5-20. Detailed Velocity Comparison of Y Direction Velocity *v* at 0.3s for Above Water Releasing Case

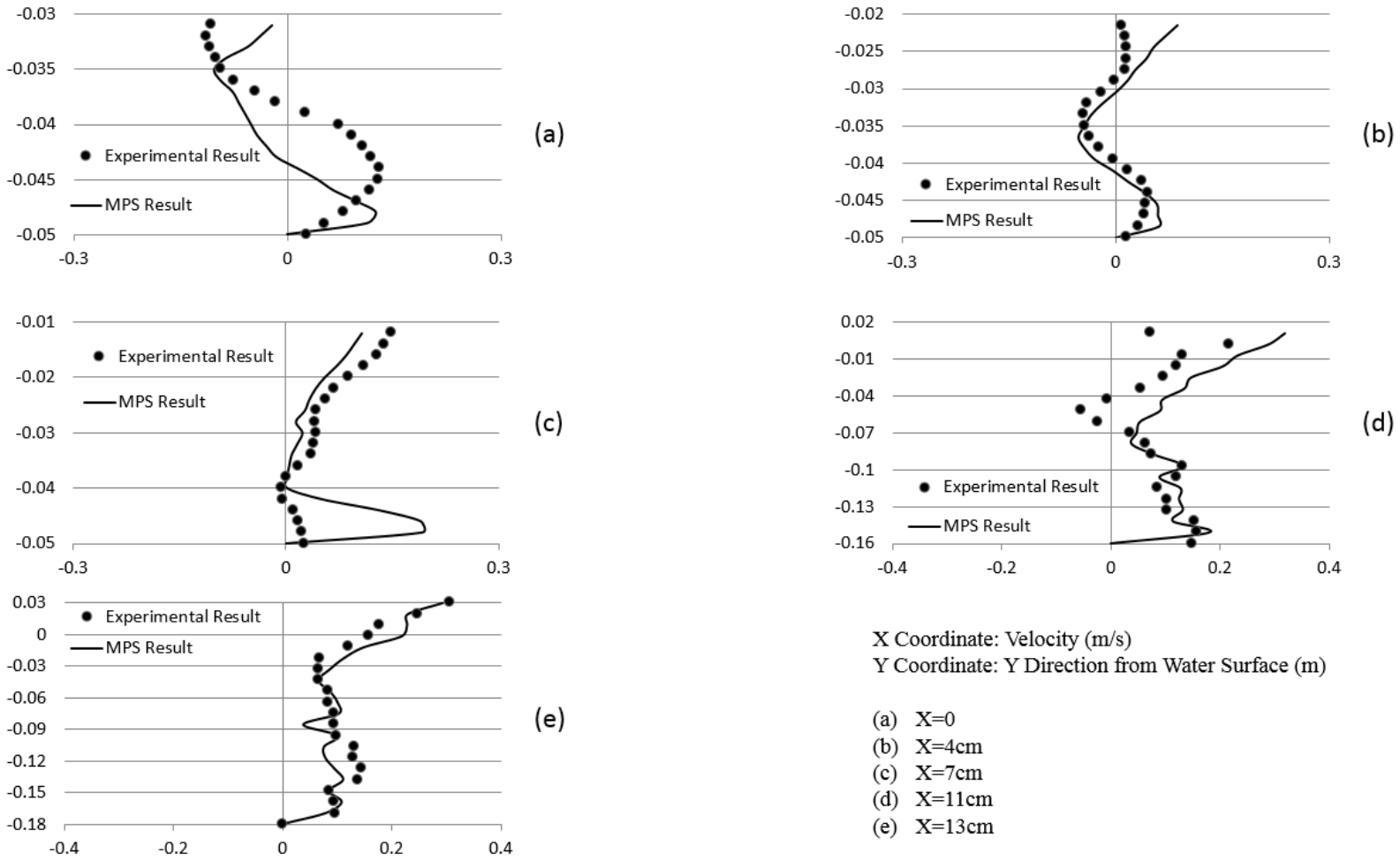

Figure 5-21. Detailed Velocity Comparison of X Direction Velocity *u* at 0.4s for Above Water Releasing Case

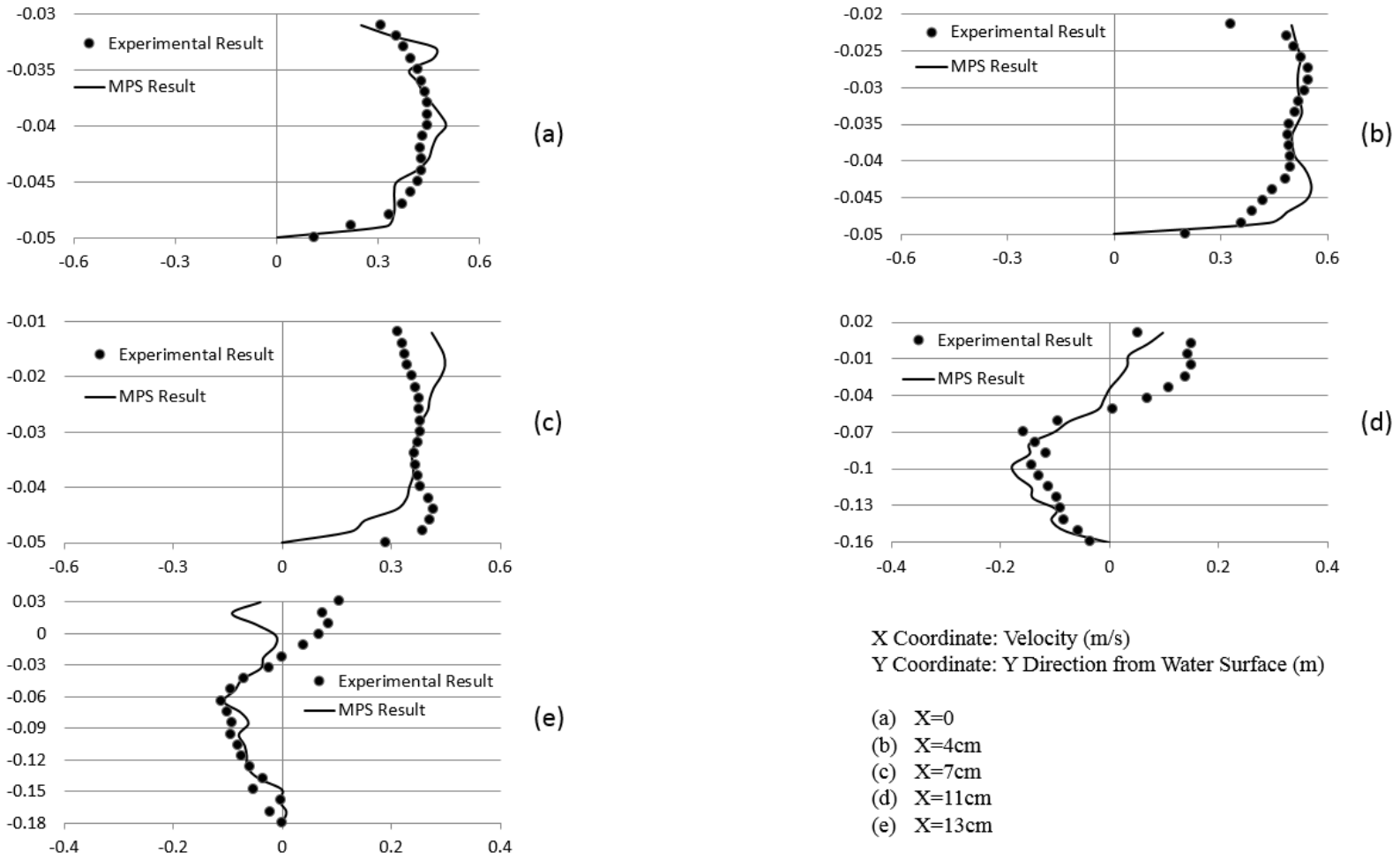

Figure 5-22. Detailed Velocity Comparison of Y Direction Velocity *v* at 0.4s for Above Water Releasing Case

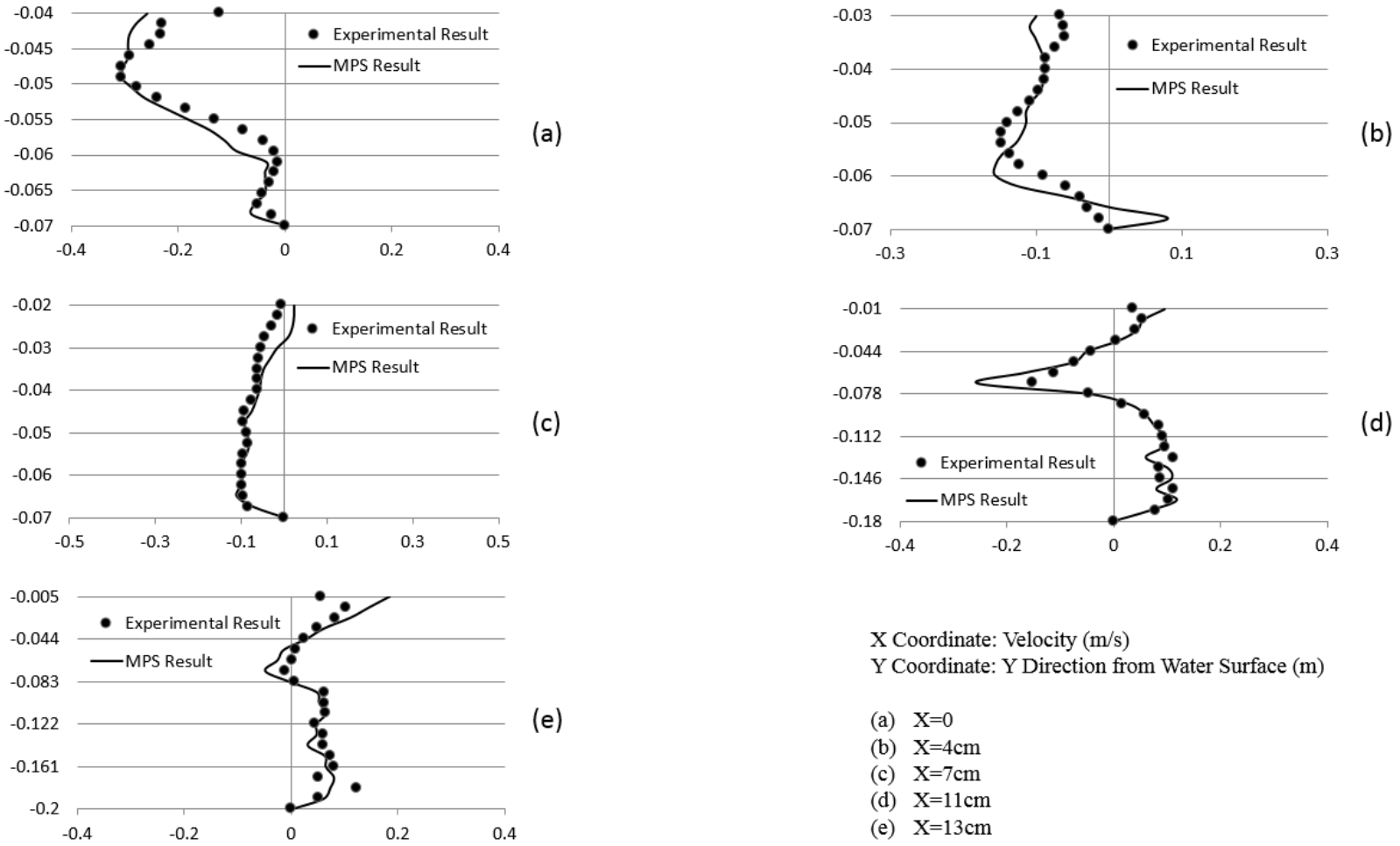

Figure 5-23. Detailed Velocity Comparison of X Direction Velocity *u* at 0.5s for Above Water Releasing Case

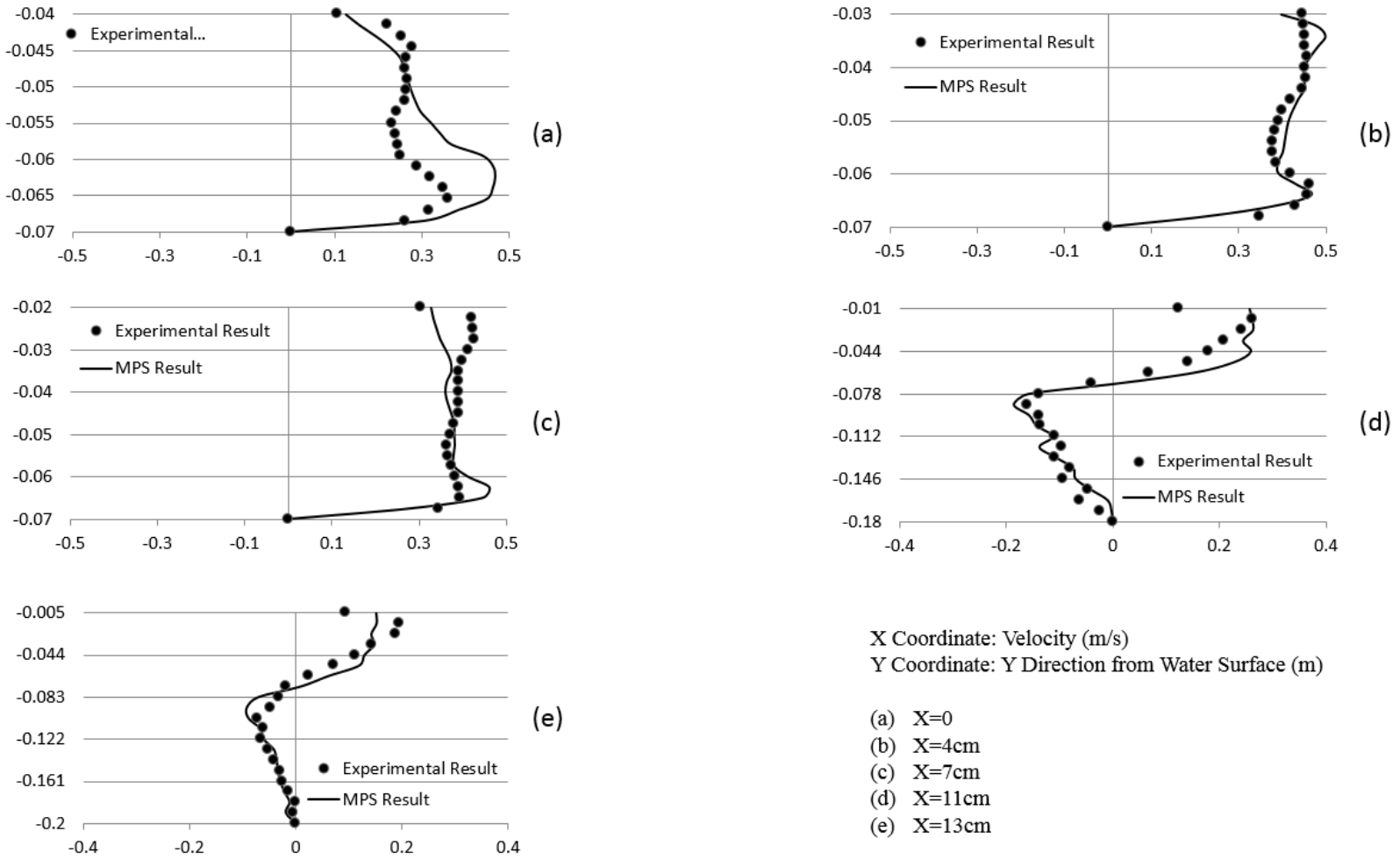

Figure 5-24. Detailed Velocity Comparison of Y Direction Velocity *v* at 0.5s for Above Water Releasing Case

5.4 Discussion

As it is mentioned before, three cases of non-deformable landslide generated impulse waves are tested in this chapter, both water surface and water velocity around the sliding structure are analyzed and compared with the experimental results. Compare to previous studies by other researchers, the simulations are mostly focused on the shape of impulse waves, such as the height of wave. However in this thesis, the simulated velocity is also evaluated and compared with the experimental data.

From the previous sections, it is clearly that the simulation results by using WC-MPS method are close to the experimental results. For water surface comparison, in all three cases, the simulation results show a good agreement to the experimental results, including the height and the shape of the wave and also the location of the head of the wave. Due to the particle method, the fluctuations can be seen from the simulation results, this can be solved by add a surface smooth term into the code or by reduce the particle size. The particle size for these three cases is 5mm, which will provide a relatively good water surface and also efficient on simulation time, by reduce the particle size, the simulation time will be doubled or even tripled, but if the research in mainly focused on the water surface, by reducing particle size, MPS simulation can provide a smoother water surface.

To compare the water surface more in detail, take Figure 5-16 (a) as an example, in this figure, the water surface from MPS simulation (solid line) is different from the experimental result (solid dots) before the location x=0.1m. From the snap shot of the experimental result (Figure 5-15 (a)), it can be seen that there is an overlap solid wedge

and water in the experimental result, which is because of the channel is wider than the sliding wedge. However in MPS simulation, the solid wedge will push all water particles away during its sliding, therefore no overlap of water particles and solid particles will occur in the MPS result. After the wedge is fully submerged, the simulation results are closer to the experimental data (other figures in Figure 5-16). As it is mentioned before, un-submerged landslide will create large deformations and fragmentations, which will bring difficulties to simulate the water surface, and also hard to provide accurate results from the experiment, the water surface results provided in previous sections, shows the similarity between both simulation and experiment results, which means the MPS method is capable of simulating landslide generated impulse waves.

For velocity comparison, because it is difficult to be tested in the experiments, most researchers chose to ignore this part. To successfully simulate the impulse wave generated by landslide, the water velocity is a very important factor. In this thesis, WC-MPS method also provides a similar simulation results compare to the experimental results. Due to the difficulties of testing water velocity, some of the experimental data are not accurate, especially the water surface area, however, the general trend of both results are same, and the average error of velocity for all three cases is less than 10%. In another word, WC-MPS method is capable to simulating the velocity field of water around the sliding wedge. To enhance the results, a better way of testing the water velocity in the experiment can be involved, and also by reducing the particle size, the simulated velocity can be more accurate.

To explain the comparison results, take Figure 5-23 as an example. The figure shows a detailed velocity comparison in X direction at 0.5s for above water releasing case at 5 different locations around the wedge. The Y axis represents the water depth, and X axis represents the velocity in X direction, the positive value means the water particles moving downstream, and the negative value means the water particle moving up stream. From the figure, it can be seen that along the water depth, the flow direction can be suddenly changed (velocity value changes from negative to positive, or from positive to negative), which shows the water circulation. Also from the detailed velocity profiles, the simulated velocity is identical to the experimental result, this proves that MPS method also have the ability of simulating water flow velocities in landslide cases.

In conclusion, the simulation results for both water surface and water velocity are identical to the experimental data, which means the WC-MPS method has a strong capability of simulating any type of the non-deformable landslide generated impulse waves.

CHAPTER 6 CONCLUSION AND RECOMMENDATION

6.1 Conclusion

The objective of this thesis is to simulate the impulse wave generated by landslide with weakly-compressible moving particle semi-implicit method. This study aimed to examine the capability of the WC-MPS method to simulate the free water surface caused by landslide and the velocity of water field around the sliding structure. From the case studies and model applications, the WC-MPS method generates similar results to experiment data, which proves that the WC-MPS method is able to simulate landslide problems, and provide proper results.

In this thesis, the theory of WC-MPS method is discussed, and the method is first evaluated by several case studies. Then, the method is applied to the landslide cases, and the simulation results are compared with the first hand experimental data. Furthermore, the velocity around the sliding structure is also tested, and compared with the experimental data, which will not been done by most of the researchers.

Eventually, the proposed method shows a good capability of simulating all kinds of landslide cases. The major accomplishment of this study can be summarized as follow:

1. Evaluation of the proposed WC-MPS method to simulate impulse wave generated by landslide. The proposed model is used to simulate the water surface for several landslide cases, including not only submerged and un-submerged landslide cases, but also deformable and non-deformable landslide cases. The

capability of simulating impulse wave by proposed WC-MPS method is confirmed.

2. Application of the proposed model to first hand submerged non-deformable landslide experiments. The method is applied into two different cases to test the capability of simulating both water surface and velocity of the water around the sliding structure. The results are close to the experimental data. The method can successfully simulate the velocity, and water surface.

3. The model is further applied into an unsubmerged non-deformable landslide case. The unsubmerged landslide will cause a large deformation and fluctuation of the water surface, which is more difficult to simulate. Also due to the fluctuation, the velocity field of the water around the sliding structure will be more disciplined. As well, the simulation results show a good agreement to the experimental measurements, which means the proposed WC-MPS method is capable of simulating impulse wave and velocity around the sliding structure.

6.2 Recommendations

Based on the current research in this thesis, the following recommendations are conclude:

1. Although the simulation gives aimilar results to the experimental data in all tested cases, the free surface particles need additional processes to consider their characteristics. By improve the treatments of free surface smaller

particles can provide a smoother water surface, and a more accurate simulation result.

2. For solid walls, boundaries, and interfaces between water and sliding structure, the shear stress should be considered if the results needed to be more accurate. An interaction model can be involved in the proposed method to improve the accuracy of the simulation results.

3. More different angles of slope bed, different scales of model, different shapes of sliding structure, and even different material of sliding structures can be used in the simulation.

4. Some more advanced search algorithm (the tree search and the Buchet algorithm) can be introduced in the proposed model. By applying these methods, the computation time will be decreased.

BIBLIOGRAPHY

Abadie, S., Morichon, D., Grilli, S., Glockner, S., 2010. Numerical simulation of waves generated by landslides using a multiple-fluid Navier–Stokes model. Coastal Eng. 57, 779–794.

Alder, B. J., & Wainwright, T. E. 1957. Phase transition for a hard sphere system. The Journal of Chemical Physics, 27(5), 1208–1209.

Anderson J.D. 1995. Computational fluid dynamics: the basics with applications. Mc Graw-Hill.

Ataie-Ashtiani B., and Farhadi L. 2006. A stable moving particle semi-implicit method for free surface flows. Fluid Dynamics Research, 38(4): 241-256.

Ataie-Ashtiani, B; Shobeyri, G., 2008. Numerical simulation of landslide impulsive waves by incompressible smoothed particle hydrodynamics. Int. J. Numer. Methods Fluids. 56, 209–232.

Batchelor G.K. 1967. An introduction to Fluid Dynamics. Cambridge University Press: Cambridge, U.K.

Belytschko T., Krongauz Y., Organ D., Fleming M., and Krysl P. 1996. Meshless methods: an overview and recently developments. Computer Methods in Applied Mechanics and Engineering, 139: 3-47.

Belytschko T., Lu Y.Y., and Gu L. 1994. Element-free Galerkin methods. International Journal for Numerical Methods in Engineering, 37: 229-256.

Belytschko, T., Liu W.K., and Moran B. 2000. Nonlinear finite elements for continua and structures. John Wiley and Sons, New York.

Benson D.J. 1992. Computational methods in Lagrangian and Eulerian hydrocodes. Computer Methods in Applied Mechanics and Engineering, 99: 235-394.

Benz W., 1988. Applications of smoothed particle hydrodynamics (SPH) to astrophysical problems. Computer Physics Communications, 48: 97-105.

Berczik P., and Kolesnik I.G. 1993. Smoothed particle hydrodynamics and its applications to astrophysical problems. Kinematics and Physics of Celestial Bodies, 9: 1-11.

Bird, G. A. 1994. Molecular gas dynamics and the direct simulation of gas flow. Oxford University Press, Oxford, U.K.

Bonet J., and Lok T.S.L. 1999. Variational and momentum preservation aspects of smooth particle hydrodynamics formulations. Computer Methods in Applied Mechanics and Engineering, 180(1-2): 97-115.

Capone, T., Panizzo, A., Monaghan, J.J., 2009. SPH modelling of water waves generated by submarine landslides. J. Hydraul. Res. 48, 80–84.

Courant R., Friedrichs K., and Lewy H. 1967. On the partial difference equations of mathematical physics. IBM Journal, 1967: 215-234. English translation of the 1928 German original.

Cremonesi, M., Frangi, A., Perego, U., 2010. A Lagrangian finite element approach for the analysis of fluid-structure interaction problems. Int. J. Numer. Methods Fluids. 84, 610–630.

Cremonesi, M., Frangi, A., Perego, U., 2011. A Lagrangian finite element approach for the simulation of water-waves induced by landslides. Comput. Struct. 89, 1086–1093.

Cundall P.A. 1987. Distinct element models of rock and soil structure. In Brown (Ed.) Analytical and Computational Methods in Engineering Rock Mechanics, London, 129- 163.

Cundall P.A. 1987. Distinct element models of rock and soil structure. In Brown (Ed.) Analytical and Computational Methods in Engineering Rock Mechanics, London, 129-163.

Dalrymple R.A., and Rogers B.D. 2006. Numerical modeling of water waves with the SPH method. Coastal Engineering Coastal Hydrodynamics and Morphodynamics, 53(23): 141-147.

Daly S.F., and Axelson K.D. 1990. Stability of floating and submerged blocks. Journal of Hydraulic Research, 28(6): 737-752.

Dong, G., Wang, G., Ma, X., Ma, Y., 2010. Harbor resonance induced by subaerial landslidegenerated impact waves. Ocean Eng. 37, 927–934.

Fall, M., Azzam, R., Noubactep, C., 2006. A multi-method approach to study the stability of natural slopes and landslide susceptibility mapping. Engineering Geology 82, 241–263.

Frederic A.R., and James C.L. 1999. Smoothed particle hydrodynamics calculations of stellar interactions. Journal of Computational and Applied Mathematics, 109: 213-230.

Fritz, H.M., Hager, W.H., Minor H.E, 2001. Lituya Bay Case: Rockslide Impact and Wave Run-up. Science of Tsunami Hazard. Vol 19, No.1.

Fritz, H.M., 2002. Initial Phase of Landslide Generated Impulse Waves. (Ph.D. Thesis). ETH, Zürich, Germany.

Gingold, R. A., & Monaghan, J. J. 1977. Smoothed particle hydrodynamics - theory and application to non-spherical stars. Monthly Notices of the Royal Astronomical Society, 181, 375–389.

Gotoh, H., & Fredsøe, J. 2000. Lagrangian two-phase flow model of the settling behavior of fine sediment dumped into water. In Proceeding of ICCE conference, (pp. 3906–3919).

Gotoh, H., & Sakai, T. 2006. Key issues in the particle method for computation of wave breaking. Coastal Engineering, 53(2-3):171–179.

Gotoh, H., Ikari, H., Memita, T., & Sakai, T. 2005. Lagrangian particle method for simulation of wave overtopping on a vertical seawall. Coastal Engineering Journal (CEJ), 47(2-3), 157–181.

Gotoh, H., Shao, S., & Memita, T. 2004. SPH-LES model for numerical investigation of wave interactions with partially immersed breakwater. Coastal Engineering Journal, 46, 39–63.

Gotoh, H., Shibahara, T., & Sakai, T. 2001. Sub-particle-scale turbulence model for the MPS method - Lagrangian flow model for hydraulic engineering. Advanced Methods for Computational Fluid Dynamics, 9-4:339–347.

Gu Y.T., and Liu G.R. 2001. A coupled element free Galerkin/Boundary element method for stress analysis of two-dimensional solids. Computer Methods in Applied Mechanics and Engineering, 190(34): 4405-4419.

Gu Y.T., and Liu G.R. 2001. A local point interpolation method for static and dynamic analysis of thin beams. Computer Methods in Applied Mechanics and Engineering, 190: 5515- 5528.

Gu Y.T., and Liu G.R. 2001. A meshless local Petro-Galerkin (MLPG) method for free and forced vibration analyses for solids. Computational Mechanics, 27(3): 188-198.

Gu Y.T., and Liu G.R. 2001. A meshless local Petrov-Galerkin (MLPG) formulation for static and free vibration analyses of thin plates. Computer Modeling in Engineering and Sciences, 2(4): 463-376.

Hans U Mair 1999. Review: hydrocodes for structure response to underwater explosions. Shock and Vibration, 6(2): 81-96.

Heinrich P. 1992. Nonlinear water waves generated by submarine and aerial landslides. J. Waterw. Port Coast. Ocean Eng. 118(3):249–66.

Heller, V, Spinneken, J., 2013. Improved landslide-tsunami prediction: Effects of block model parameters and slide model. J. Geohys. Res., C. 118, 1489–1507.

Heller, V. and Spinneken, J, 2015. On The Effect of Water Body Geometry on Landslide-tsunamis: Physical Insight from Laboratory Test and 2D to 3D Wave Parameter Transformation. Costal Eng. 104, 113-134.

Heller, V., Hager, W.H., 2011. Wave types of landslide generated impulse waves. Ocean Eng. 38, 630–640.

Huppert, H.E. 1982. Flow and instability of viscous current down a slope. Nature, 300:427–429.

Kamphuis, J.W., Bowering R.J., 1972. Impulse waves generated by landslides. Proc., 12th Coastal Engineering Conference, ASCE, New York, 1, 575–588.

Kessell, T. van, Kranenburg, C., 1996. Gravity current of fluid mud on sloping bed. J. Hydraul. Eng. 122, 710–717.

Khayyer, A., & Gotoh, H. 2009. Modified moving particle semi-implicit methods for the prediction of 2D wave impact pressure. Coastal Engineering, 56(4), 419–440.

Komatina D, Jovanovic M. 1997. Experimental study of steady and unsteady free surface flows with water-clay mixtures. Journal of Hydraulic Research, 35(5): 579-590.

Koshizuka S., Nobe A., and Oka Y. 1998. Numerical analysis of breaking waves using the moving particle semi-implicit method. International Journal for Numerical Methods in Fluids, 26: 751-769.

Koshizuka S., Tamako H., and Oka Y. 1995. A particle method for incompressible viscous flow with fluid fragmentation. Computational Fluid Dynamics Journal, 4: 29-46.

Koshizuka, S., & Oka, Y. 1996. Moving-particle semi-implicit method for fragmentation of incompressible fluid. Nuclear Science Engineering, 123, 421–434.

Lind, S.J., Xu, R., Stansby, P.K., Roger, B.D., 2012. Incompressible Smoothed Perticle Hydrodynamics of Free-surface Flows: A Generalised Diffusion-based Algorithm for Stability and Validations for Impulsive Flows and Propagating Waves. Journal of Computational Physics, 231: 1499-1523.

Liszka T., and Orkisz J. 1980. The finite difference method at arbitrary irregular grids and its applications in applied mechanics. Computers and Structures, 11: 83-95.

Liu G.R., and Gu Y.T. 2003. A meshfree method: meshfree weak-strong (MWS) form method for 2-D solids.

Liu G.R., and Gu Y.T. 2003. A meshfree weak-strong (MWS) form method. 25th World Conference on Boundary Element Methods, 8-10 September, 2003, Split, Crotia.

Liu M.B., and Liu G.R. 2010. Smoothed particle hydradynamics (SPH): an overview and recent developments. Archives of Computational Methods in Engineering, 17: 25-76.

Liu. G.R., and Liu M.B. 2003. Smoothed particle hydrodynamics: a meshfree particle method. Word Scientific.

Monaghan J.J. 1990. Modeling the universe. Proceedings of the Astronomical Society of Australia, 18: 233-237.

Monaghan J.J. 1992. Smoothed particle hydrodynamics. Annual Review of Astronomical and Astrophysics, 30: 543-574.

Monaghan J.J., and Lattanzio J.C. 1991. A simulation of the collapse and fragmentation of cooling molecular clouds. Astrophysical Journal, 375: 177-189.

Monaghan, J, J; Kos, A., 1999. Solitary waves on a cretan beach. J. Waterw. Port Coast. Ocean Eng. 125, 145–154.

Najafi-Jilani, a., Ataie-Ashtiani, B., 2008. Estimation of near-field characteristics of tsunami generation by submarine landslide. Ocean Eng. 35, 545–557.

Ramadan, K.T., Omar, M.A., Allam, A. A., 2014. Modeling of tsunami generation and propagation under the effect of stochastic submarine landslides and slumps spreading in two orthogonal directions. Ocean Eng. 75, 90–111.

Rzadkiewicz, S.A., Marlot, C., Henrich, P., 1997. Numerical simulation of submarine landslides and their hydraulic effects. J. Waterw. Port Coast. Ocean Eng. 123, 149–157.

Shakibaeinia A., and Jin Y.C. 2010. A weakly-compressible MPS method for modeling of open-boundary free-surface flow. International Journal for Numerical Method in Fluids, 63: 1208-1232.

Shao S.D., Lo Y.M. 2003. Incompressible SPH method for simulating Newtonian and non-Newtonian flows with a free surface. Advances in Water Resources, 26: 787-800.

Sue, L.P., Nokes, R.I., Davidson, M.J., 2011. Tsunami generation by submarine landslides: comparison of physical and numerical models. Environ. Fluid Mech. 11, 133–165.

Wang, Q., Zheng, Y., Chen, C., Fujimoto, T., Chiba, N., 2006, Efficient Rendering of Breaking Waves Using MPS Method. Univ. Science A, 7(6): 1018-1025.

Watts, B.P., 1998. Wavemaker curves for tsunamis generated by underwater landslides. J. Waterw. Port Coast. Ocean Eng. 124, 127–137.

Yagawa G., and Yamada T. 1996. Free mesh method: a new meshless finite element method. Computational Mechanics, 18: 383-386.

Yim, S.C., Asce, M., Yuk, D., Panizzo, A., Risio, M. Di., 2008. Numerical Simulations of Wave Generation by a Vertical Plunger Using RANS and SPH Models. J. Waterw. Port Coast. Ocean Eng. 134, 143–159.

Yoon H.Y., Koshizuka S., and Oka Y. 1999. A particle-gridless hybrid method for incompressible flows. International Journal for Numerical Methods in Fluids, 30(4): 407-424.

Zienkiewicz O.C., and Taylor R.L. 2000. The finite element method. 5th Edition, Butterworth Herinemann.

Zweifel, A, Zuccalà, D. Gatti, D., 2007. Comparison between Computed and Experimentally Generated Impulse Waves. J. Hydraul. Eng. 133, 208–216.

Zweifel, A., 2004. Impulswellen: Effekte der Rutschdichte und der Wassertiefe. (Ph.D. Thesis). ETH, Zürich, Germany (in German).

Zweifel, Andreas, Hager, Willi H, Minor, H., 2006. Plane Impulse Waves in Reservoirs. J. Waterw. Port Coast. Ocean Eng. 132, 358–368.

APPENDIX A

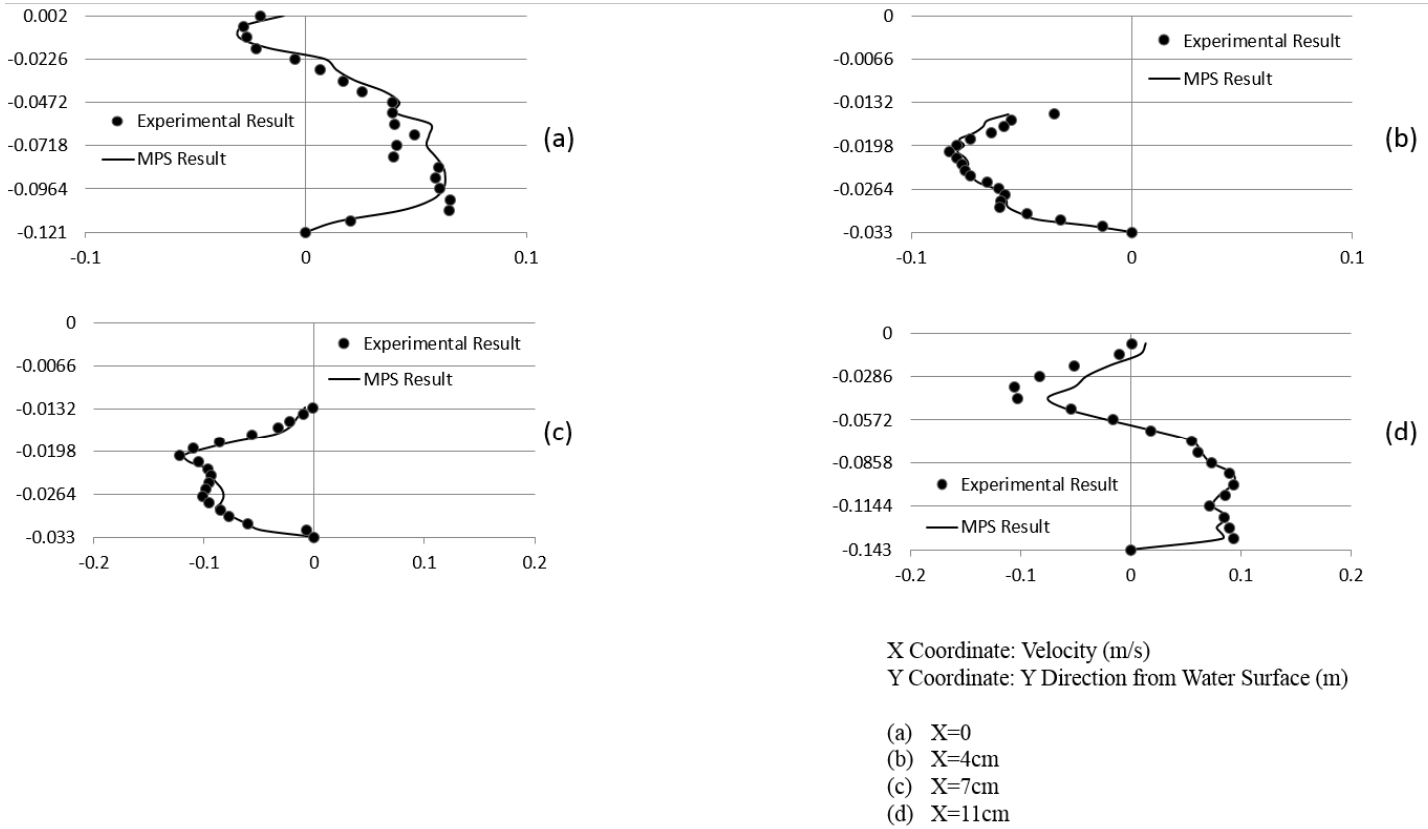

Figure A-0-1. Detailed Velocity Comparison of X direction Velocity *u* at 0.3s for Close to Water Releasing Case

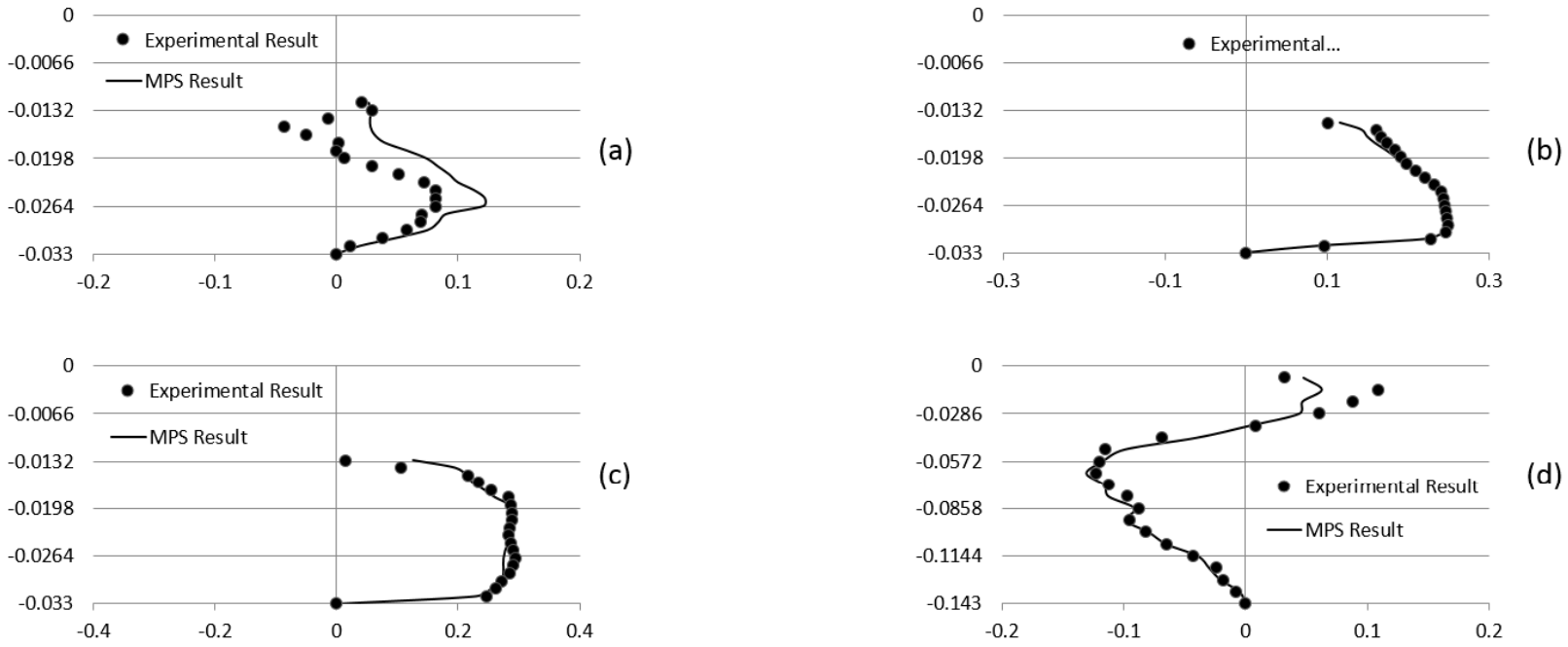

X Coordinate: Velocity (m/s)
Y Coordinate: Y Direction from Water Surface (m)

(a) X=0
(b) X=4cm
(c) X=7cm
(d) X=11cm

Figure A-0-2. Detailed Velocity Comparison of X direction Velocity *u* at 0.3s for Close to Water Releasing Case

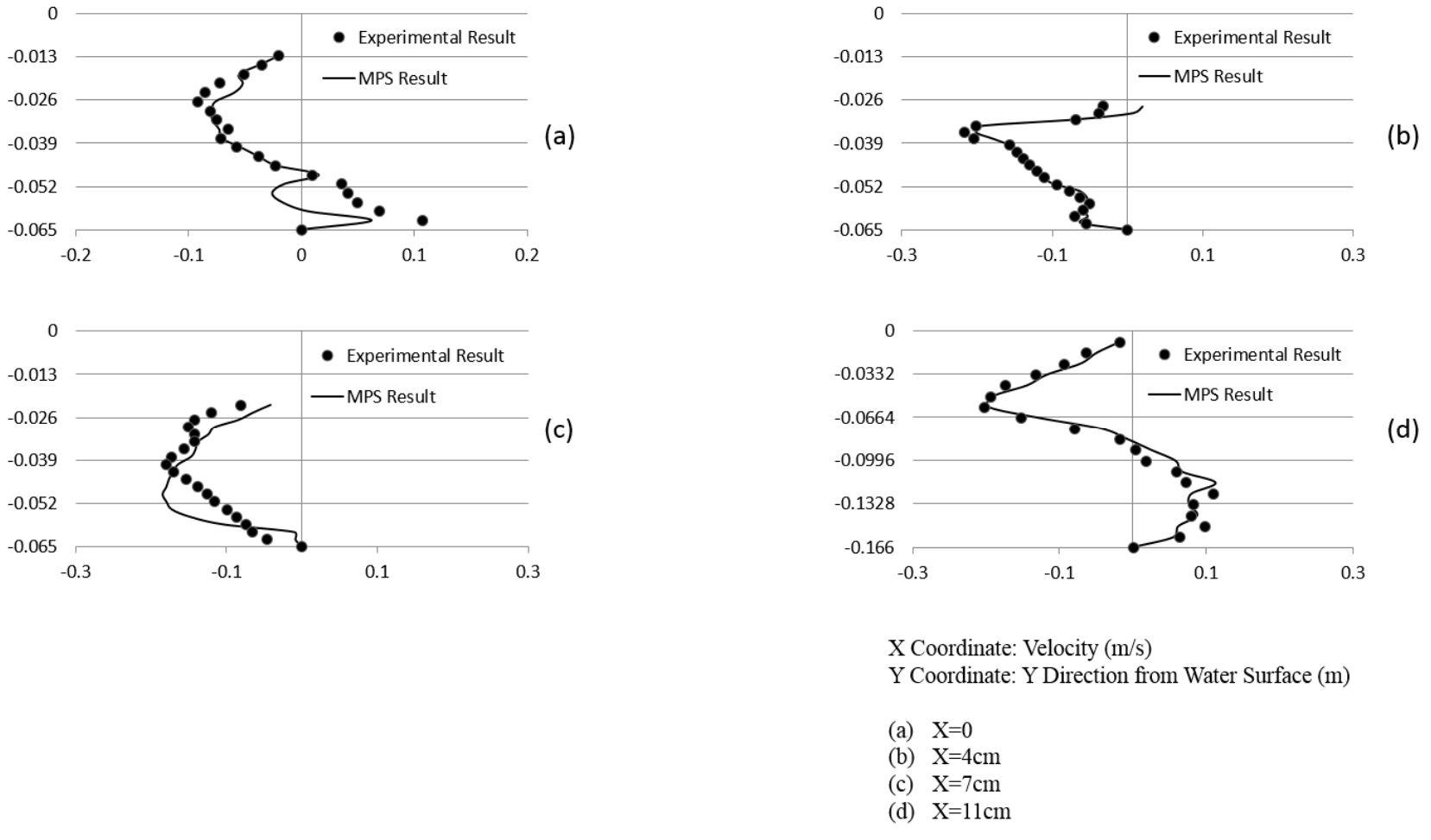

Figure A-0-3. Detailed Velocity Comparison of X direction Velocity *u* at 0.5s for Close to Water Releasing Case

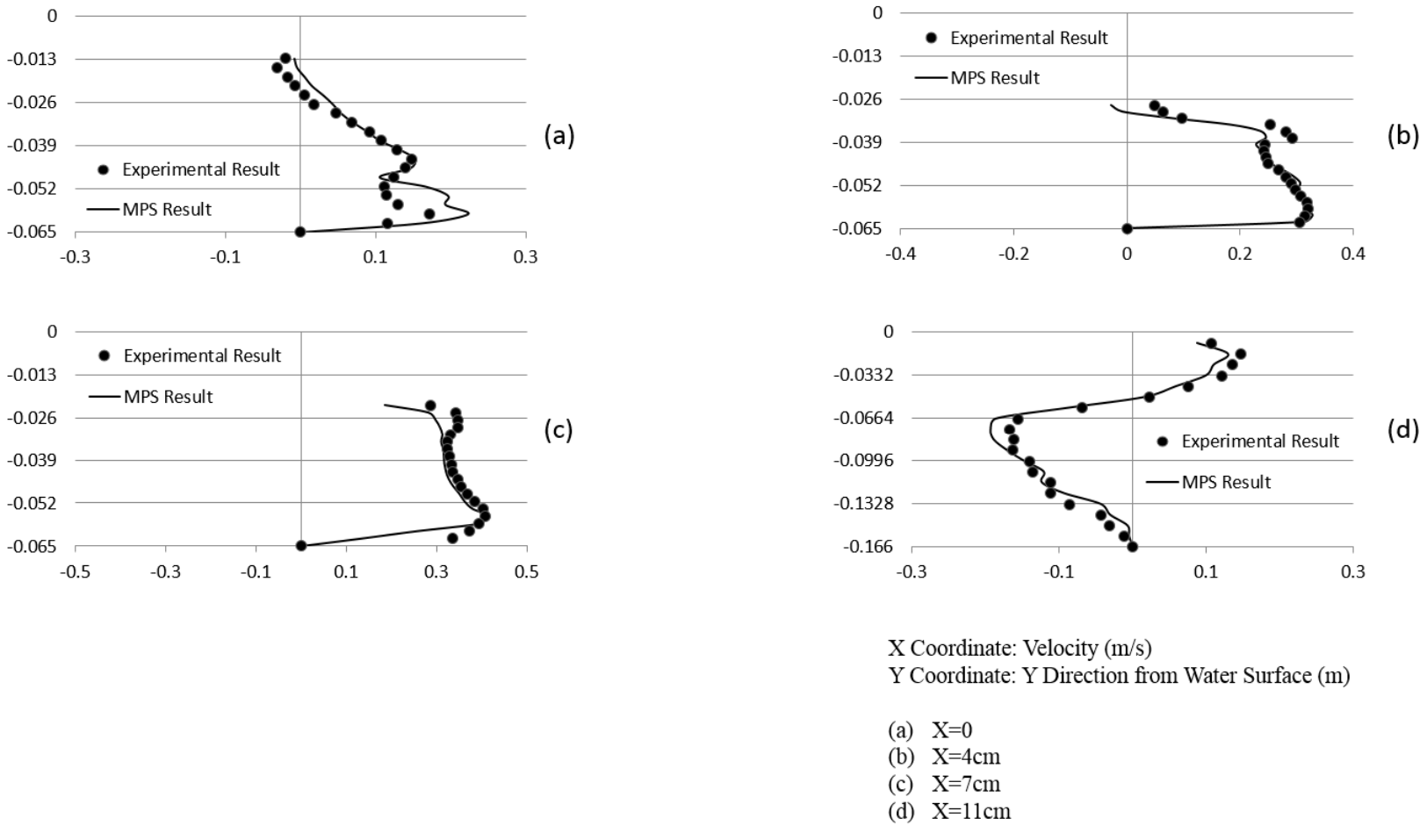

Figure A-0-4. Detailed Velocity Comparison of Y direction Velocity *v* at 0.5s for Close to Water Releasing Case

APPENDIX B

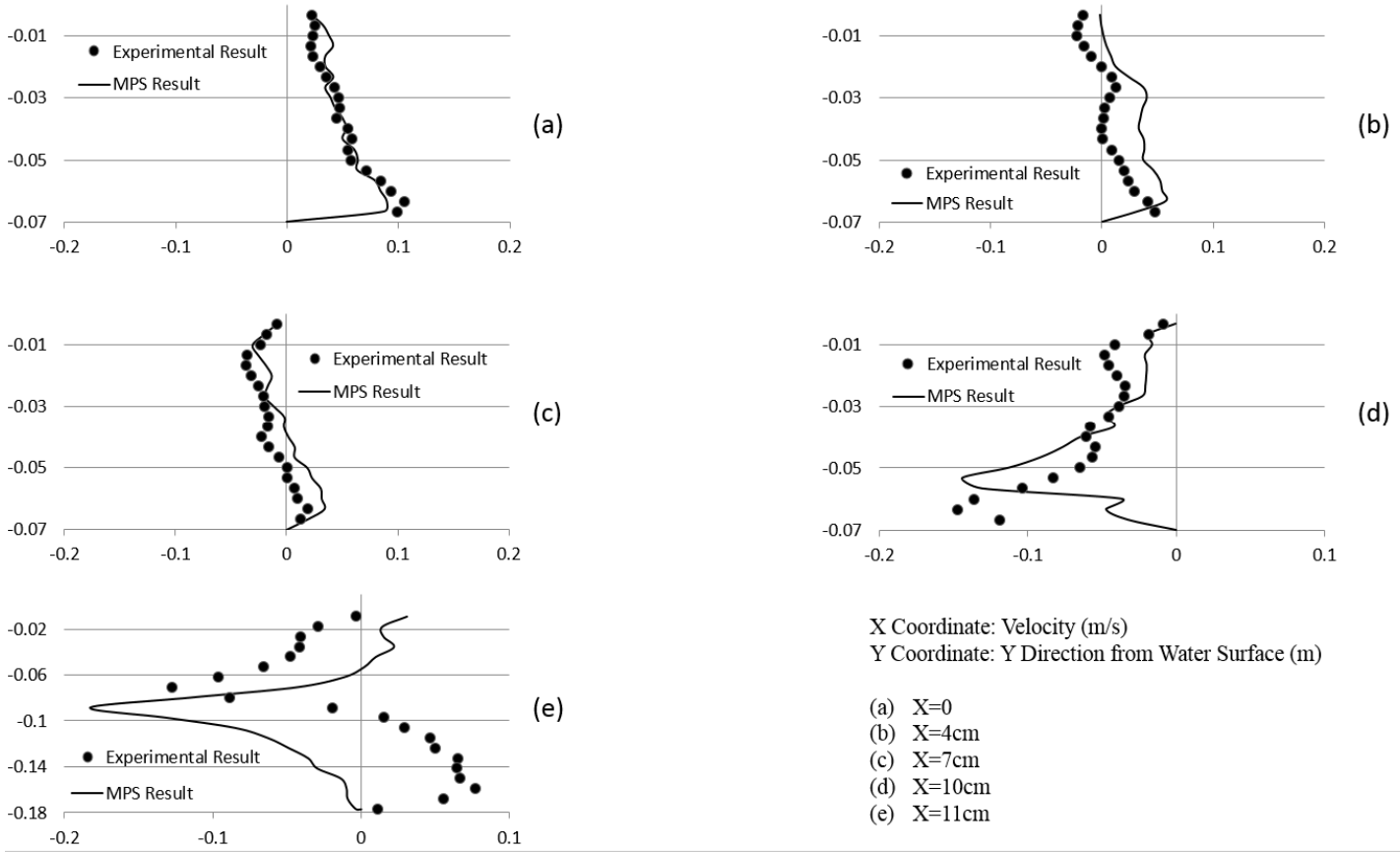

Figure B-0-1. Detailed Velocity Comparison of X direction Velocity *u* at 0.2s for Under Water Releasing Case

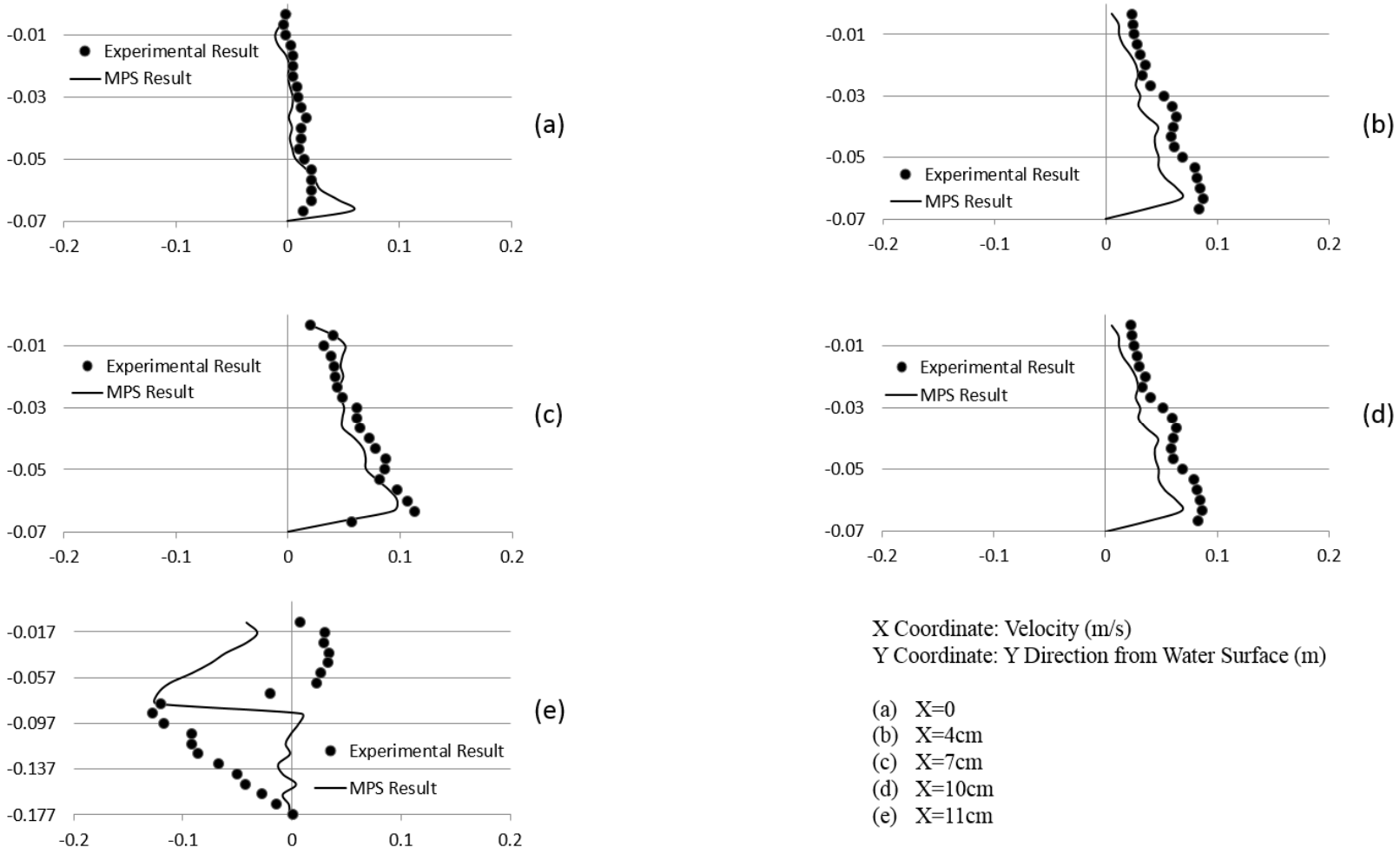

Figure B-0-2. Detailed Velocity Comparison of Y direction Velocity *v* at 0.2s for Under Water Releasing Case

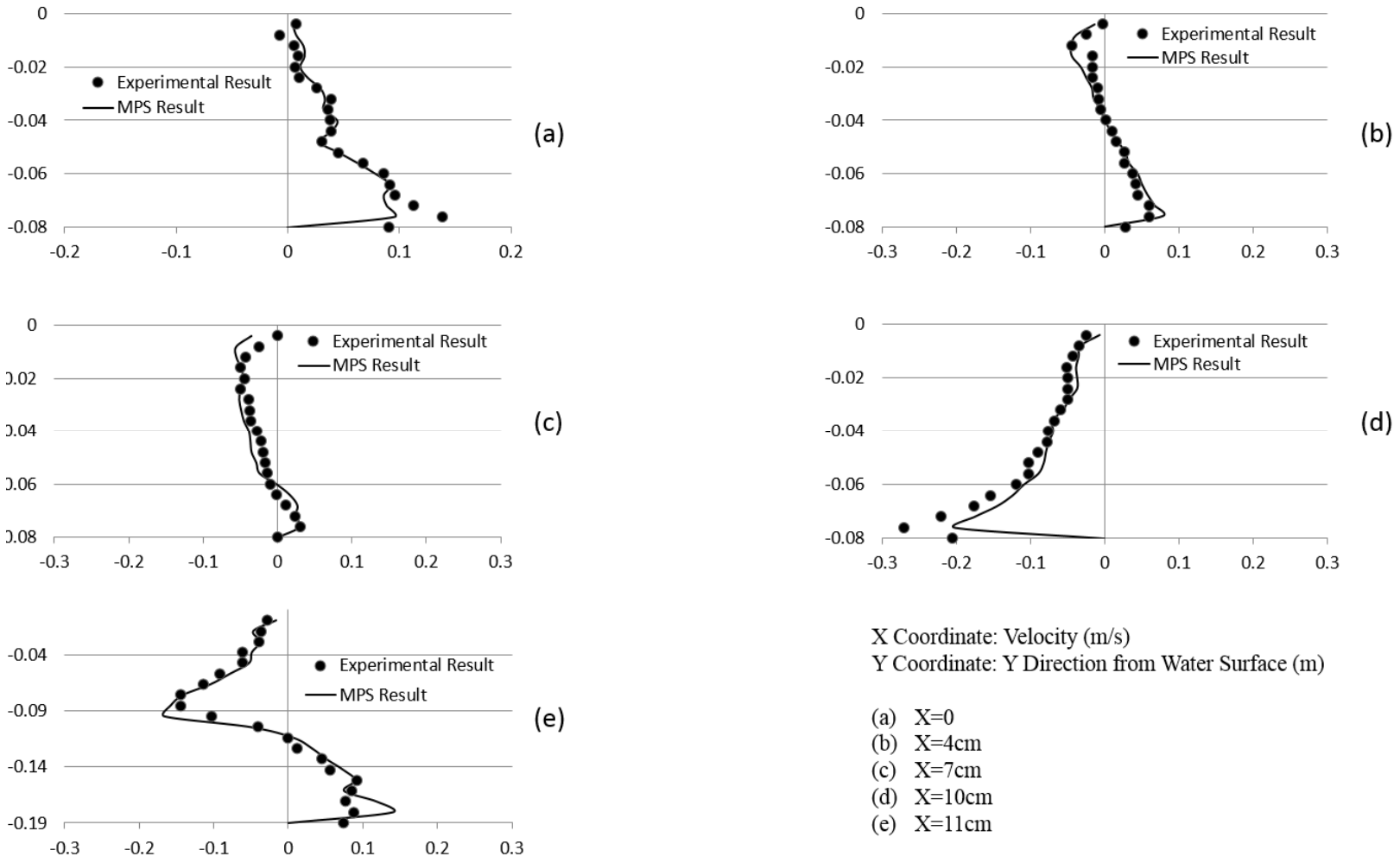

Figure B-0-3. Detailed Velocity Comparison of X direction Velocity *u* at 0.3s for Under Water Releasing Case

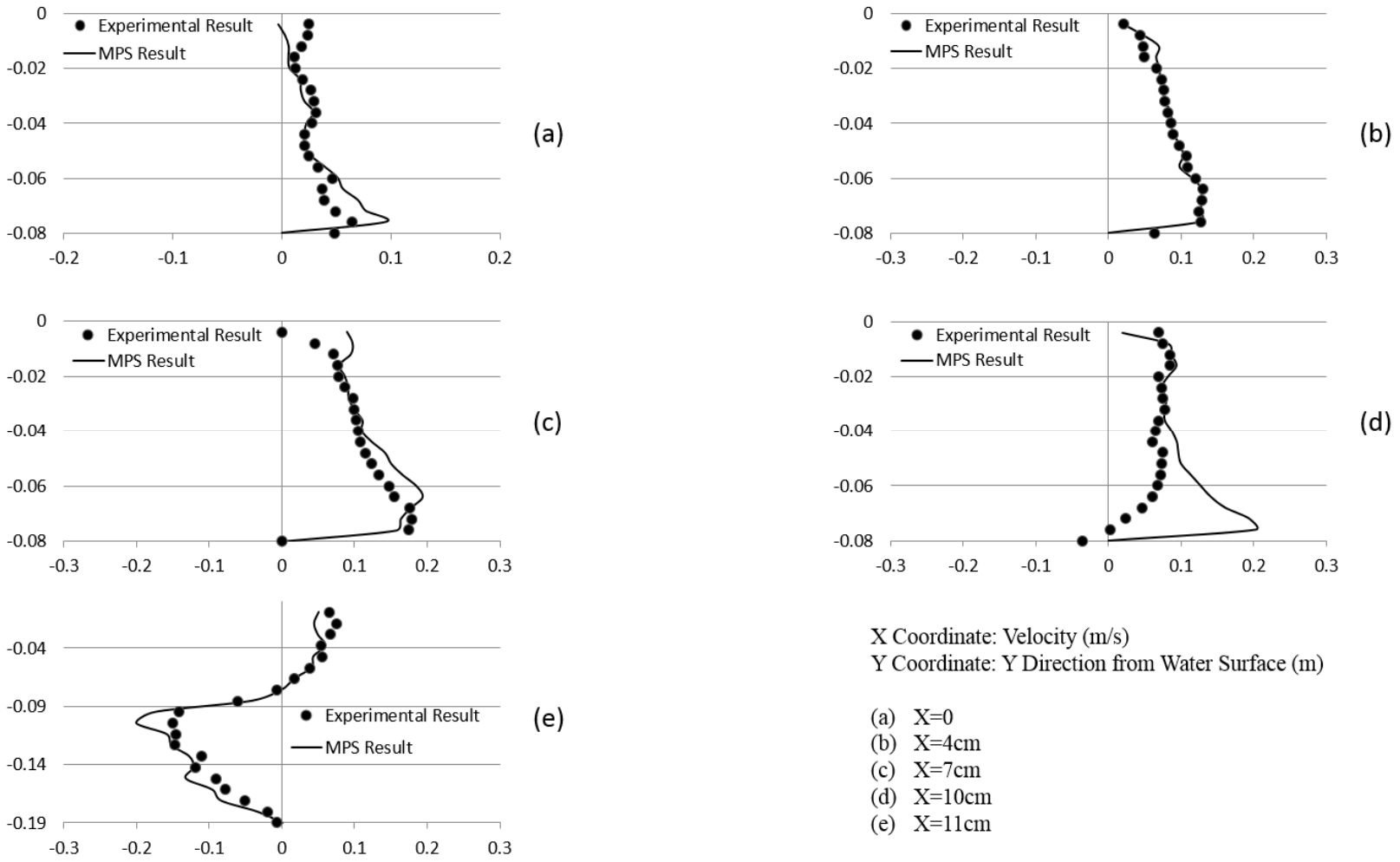

Figure B-0-4. Detailed Velocity Comparison of Y direction Velocity *v* at 0.3s for Under Water Releasing Case

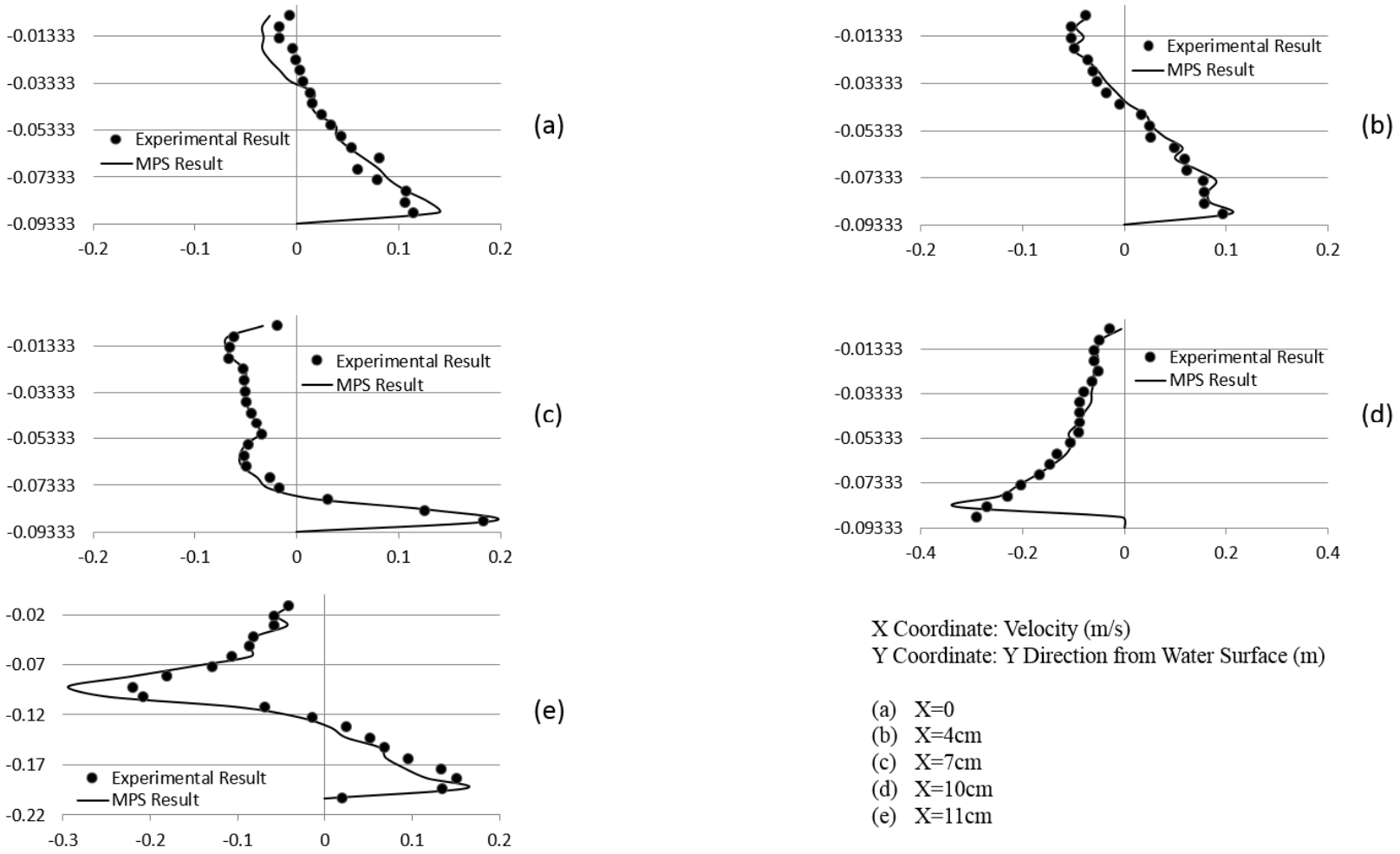

Figure B-0-5. Detailed Velocity Comparison of X direction Velocity *u* at 0.4s for Under Water Releasing Case

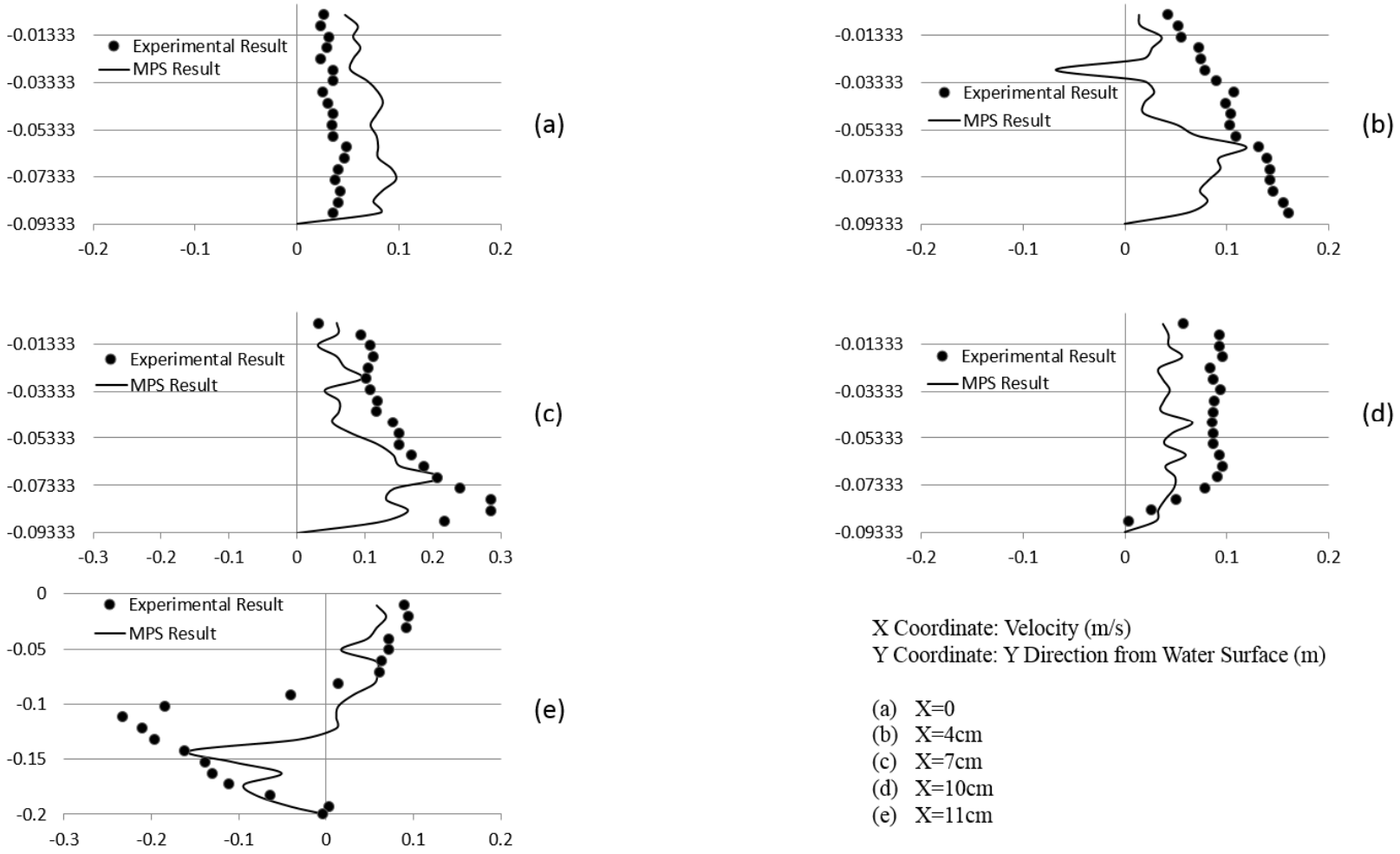

Figure B-0-6. Detailed Velocity Comparison of Y direction Velocity *v* at 0.4s for Under Water Releasing Case

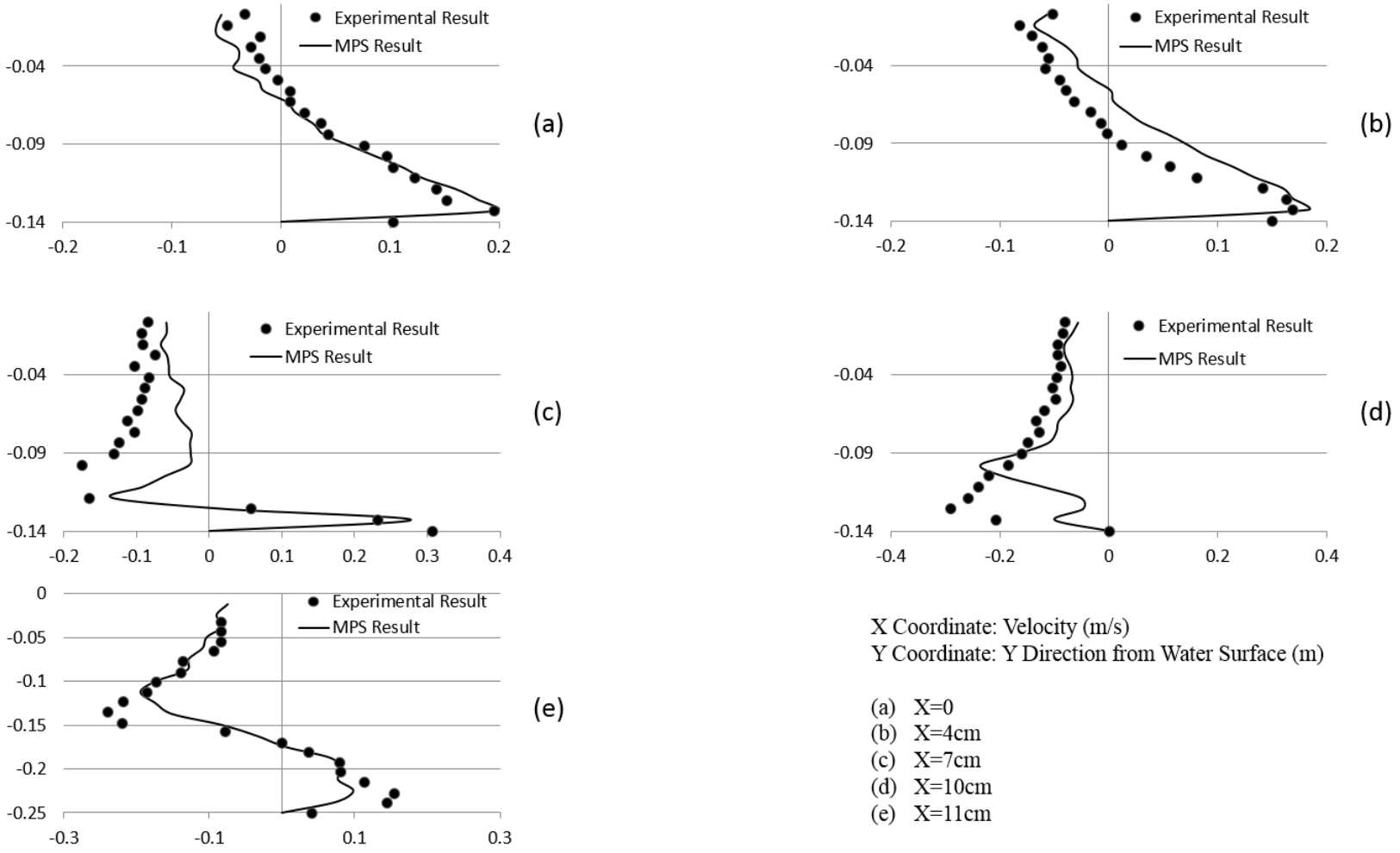

Figure B-0-7. Detailed Velocity Comparison of X direction Velocity *u* at 0.6s for Under Water Releasing Case

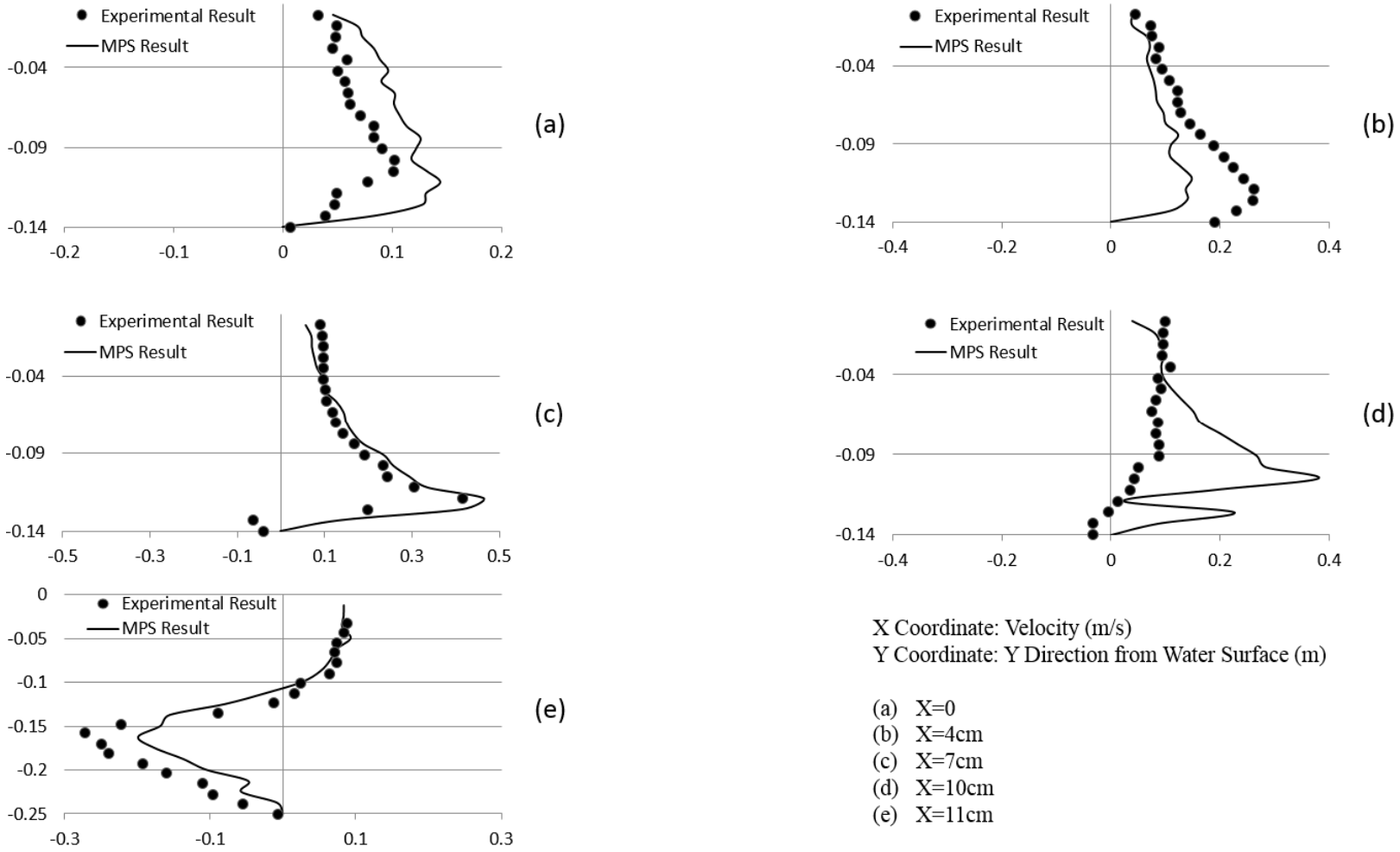

Figure B-0-8. Detailed Velocity Comparison of Y direction Velocity *v* at 0.6s for Under Water Releasing Case

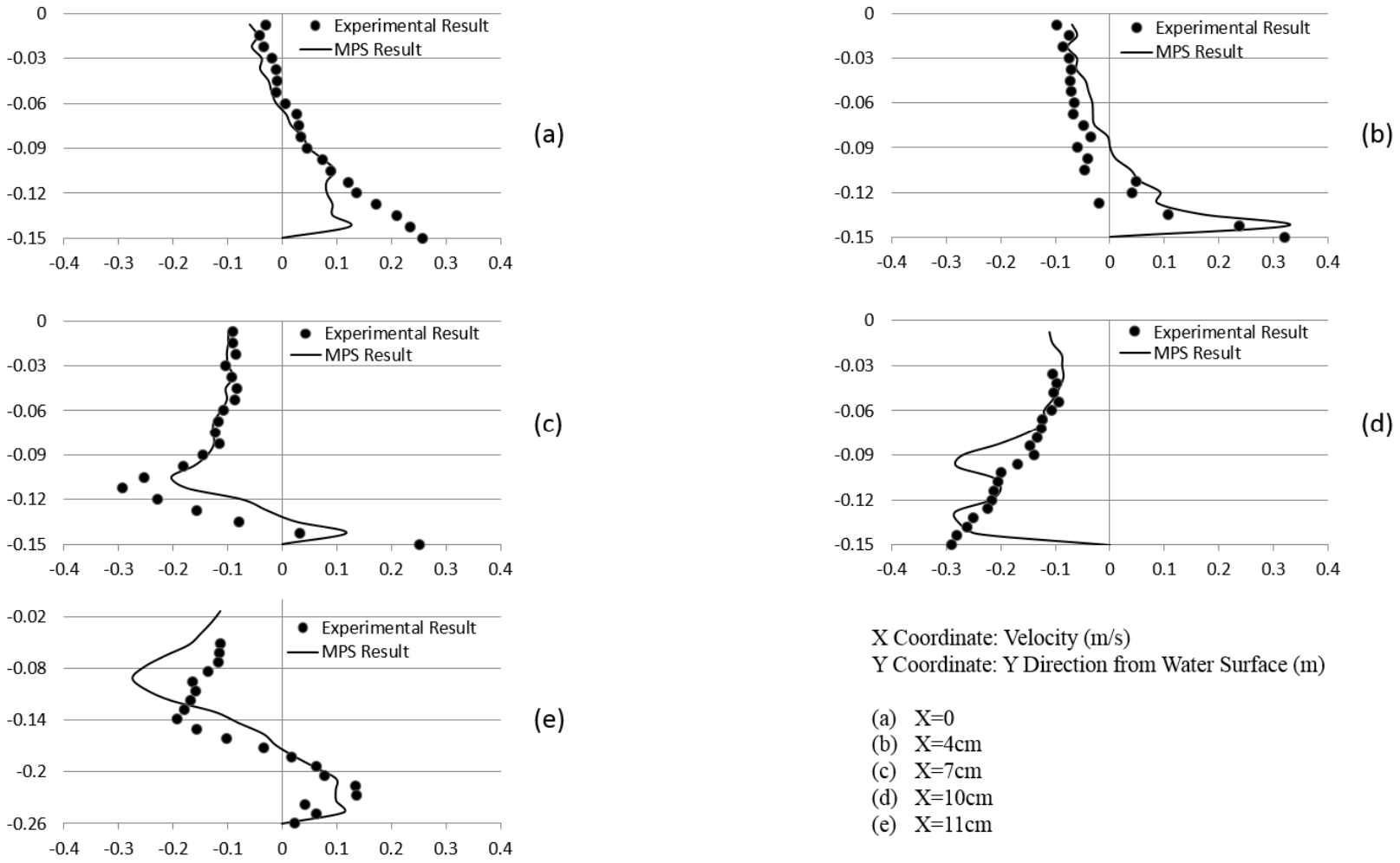

Figure B-0-9. Detailed Velocity Comparison of X direction Velocity *u* at 0.7s for Under Water Releasing Case

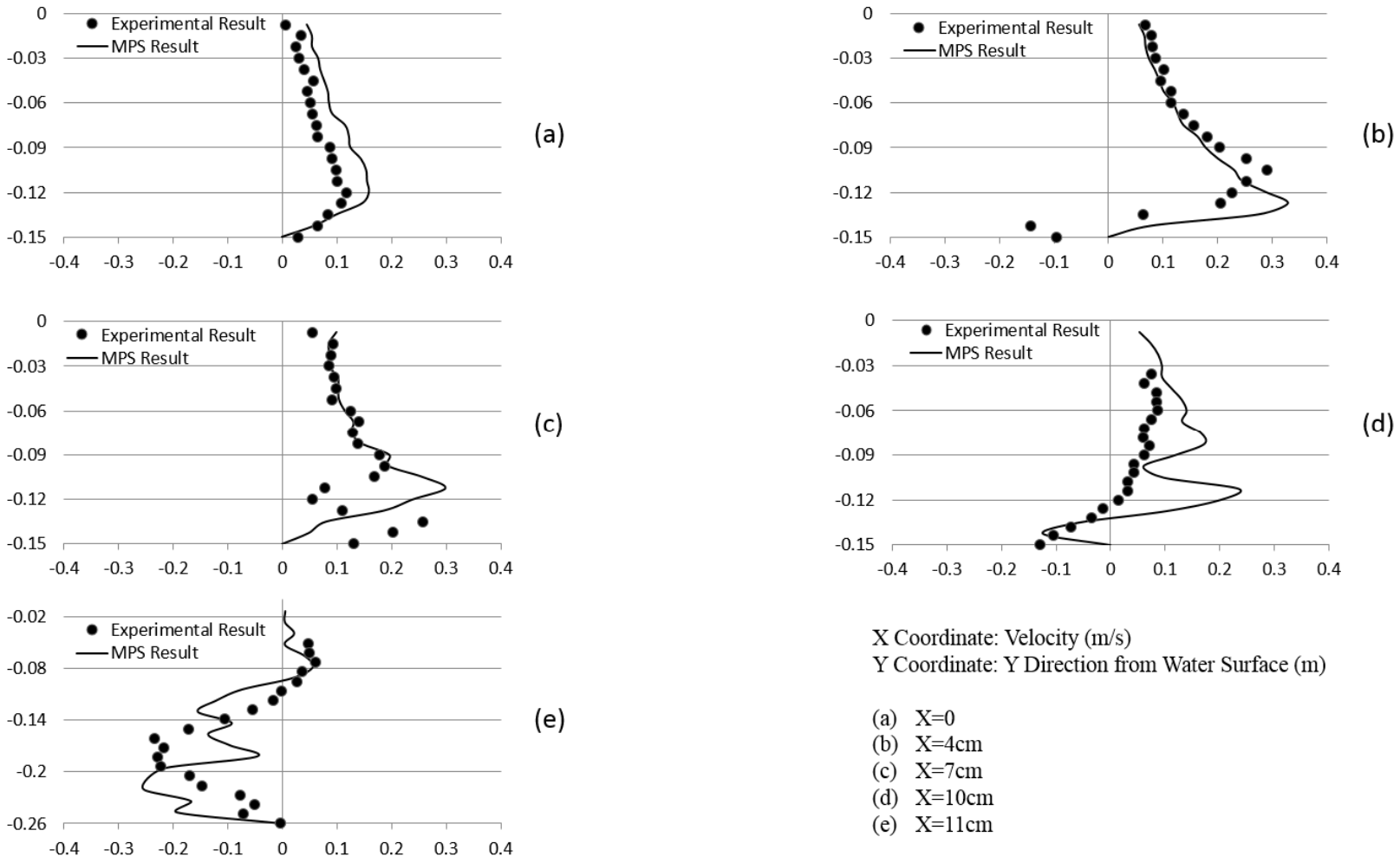

Figure B-0-10. Detailed Velocity Comparison of Y direction Velocity *v* at 0.7s for Under Water Releasing Case

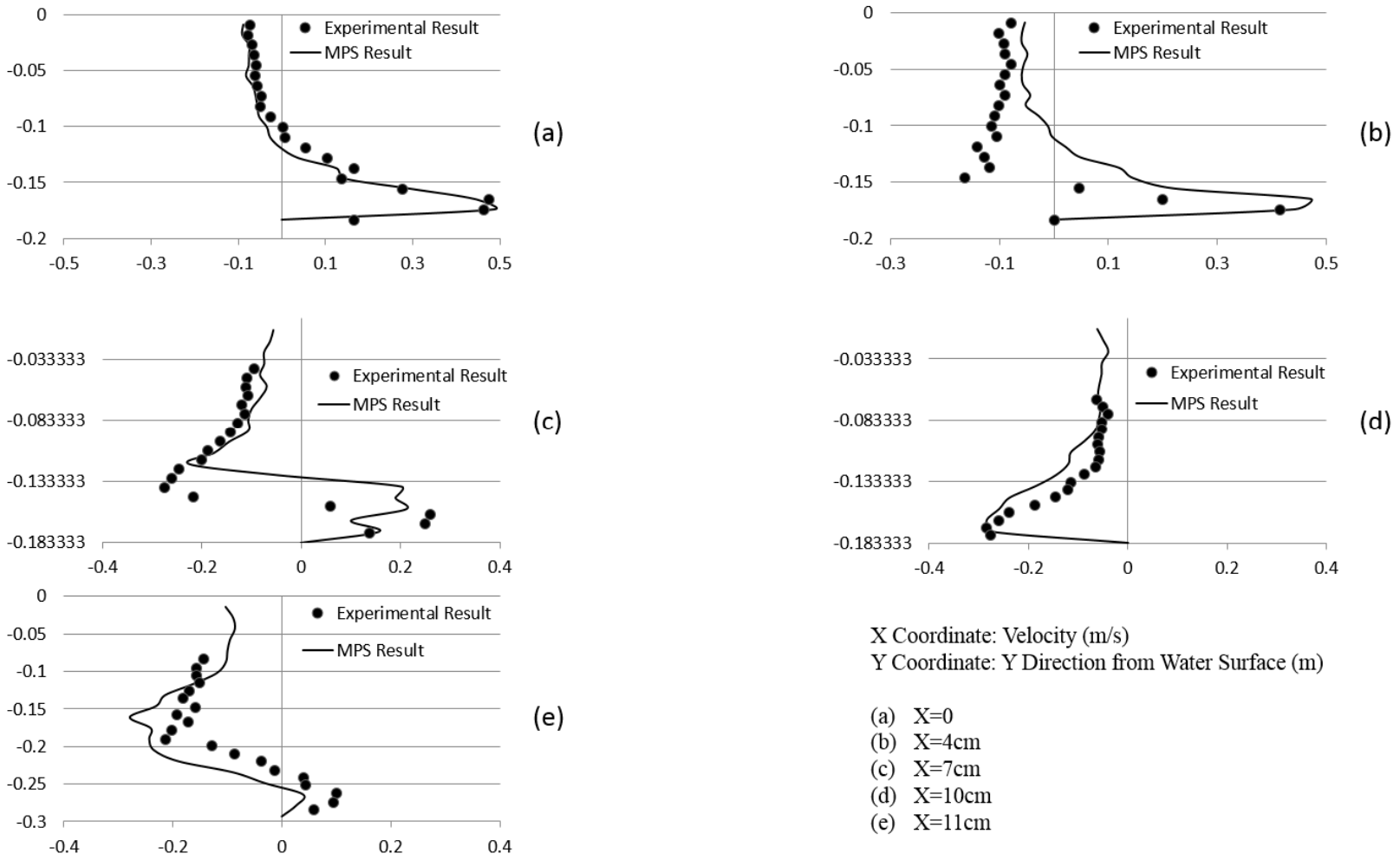

Figure B-0-11. Detailed Velocity Comparison of X direction Velocity *u* at 0.8s for Under Water Releasing Case

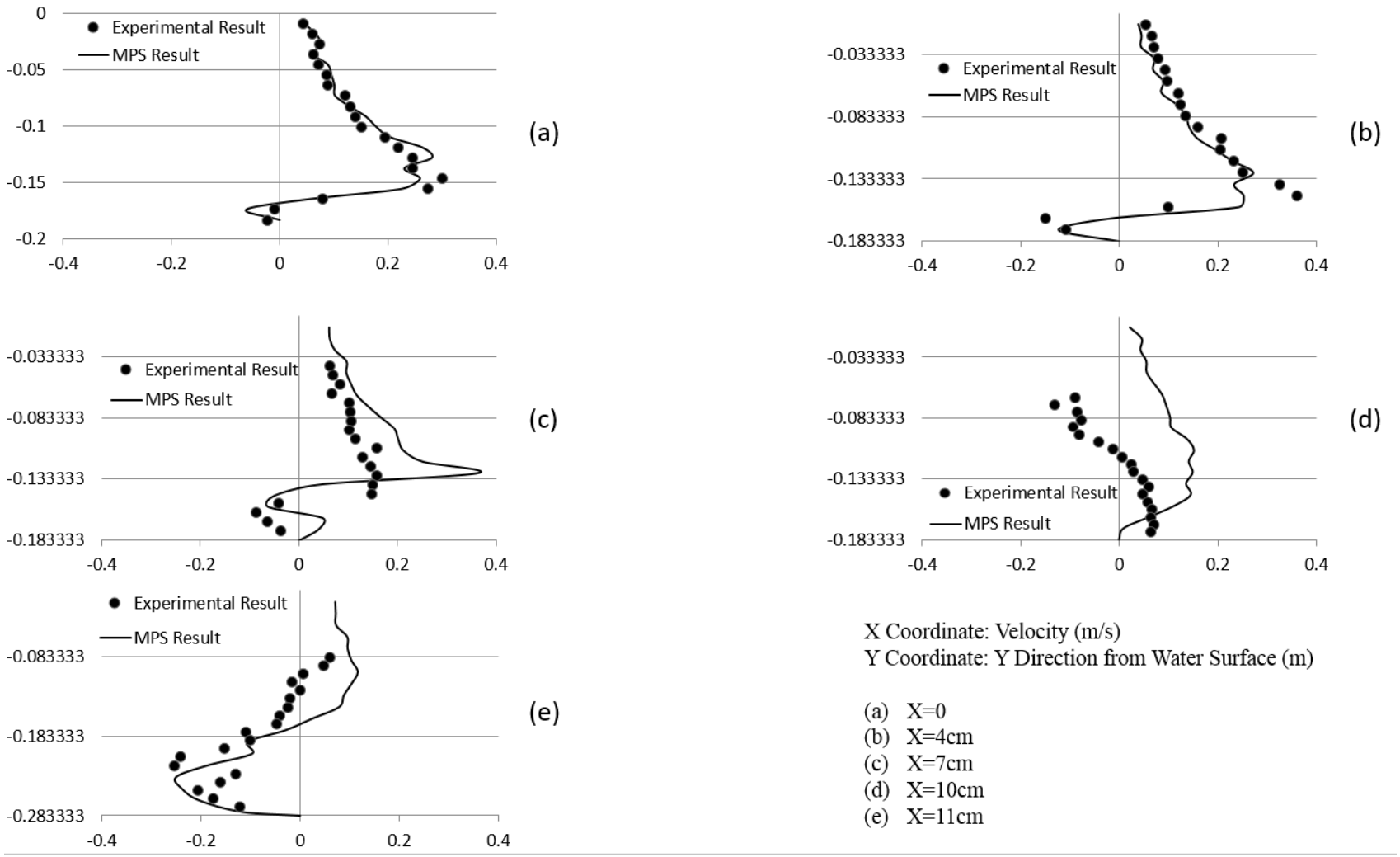

Figure B-0-12. Detailed Velocity Comparison of Y direction Velocity *v* at 0.8s for Under Water Releasing Case